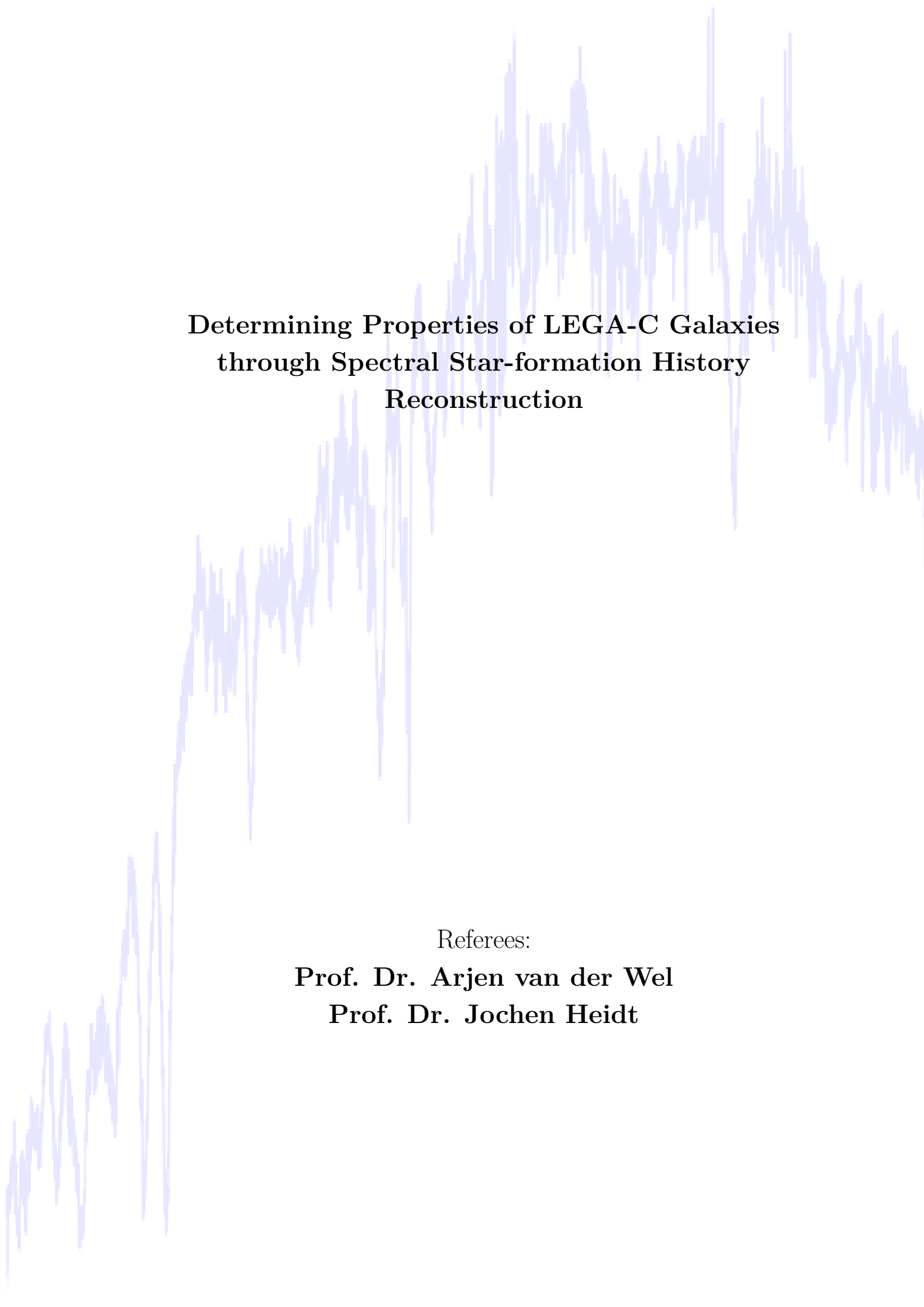


**Determining Properties of LEGA-C Galaxies
through Spectral Star-formation History
Reconstruction**

Priscilla Chauke

Dissertation
submitted
to the
Combined Faculties
for the Natural Sciences and for Mathematics
of the
Ruperto-Carola University of Heidelberg, Germany
for the degree of
Doctor of Natural Sciences

Put forward by
Priscilla Chauke
Born in Giyani, South Africa
Oral Examination: 24 July 2019



**Determining Properties of LEGA-C Galaxies
through Spectral Star-formation History
Reconstruction**

Referees:

Prof. Dr. Arjen van der Wel

Prof. Dr. Jochen Heidt

Va ka hina

**“My work amounts to a drop in a limitless ocean. Yet
what is any ocean, but a multitude of drops?”**

-Adapted from David Mitchell, Cloud Atlas

Acknowledgements

I thank Arjen van der Wel for giving me the opportunity to pursue a PhD at the Max Planck Institut für Astronomy and for being my advisor throughout the years. I thank IMPRS and the DAAD for supporting me financially for the last four years. Lastly, I thank my family and friends for their love, support and encouragement.

Abstract

Over the past decade, photometric and spectroscopic surveys have enabled us to obtain an integrated view of galaxy evolution. We have measured the cosmic star formation history, and we know that about half of the stars we observe formed before the Universe was half of its current age. However, crucial knowledge of individual galaxy evolution has been limited because the detailed stellar population properties that we know about galaxies, such as ages, metallicities and kinematics, have mostly been obtained from nearby galaxies, which contain mostly old stellar populations. To advance our understanding of galaxy evolution, measurements have to be extended to more distant galaxies, which have a wider variation in age and star formation (SF) activity. In this thesis, I investigate the stellar population properties of a galaxy population at half the Universe's current age (redshift $z \sim 1$), using high quality, high resolution spectra from the (recent) LEGA-C Survey. I present an algorithm that uses full-spectrum fitting to reconstruct the star formation histories (SFHs) of LEGA-C galaxies. First, I investigate the dependence of individual SFHs on stellar mass, stellar velocity dispersion and SF activity. The individual SFHs of high-mass (velocity dispersion) quiescent and star-forming populations are increasingly divergent towards lower redshifts, which indicates a strong correlation between current SF activity and past SF activity. Second, I trace the stellar mass evolution of LEGA-C galaxies between redshifts $z \sim 1$ and $z = 3$ (when the Universe was a sixth of its age). Galaxies that are similar in stellar mass at one redshift, have diverse evolutionary paths that lead to a wide range of stellar masses at another redshift, whether they are being traced backward or forward in time. Last, I investigate rejuvenation in quiescent galaxies, that is, when galaxies that are quiescent, re-ignite their SF before becoming quiescent again. Although, rejuvenation events do not contribute significantly to the growth of quiescent galaxies, a majority of rejuvenated galaxies lie in the 'green valley', where galaxies are thought to be in the (one-way) transition phase from the blue cloud to the red sequence. Reconstructing SFHs has allowed us to trace the individual pathways along which galaxies evolve, and investigate the physical processes that drive them. Measurements from this work, as well as other LEGA-C studies, will be important for future studies at even higher redshifts because they will act as a benchmark to connect populations at higher redshifts to the nearby Universe.

Zusammenfassung

Das letzte Jahrzehnt über haben photometrische und spektroskopische Untersuchungen uns erlaubt, ein ganzheitliches Bild über die Entstehung der Galaxie zu erhalten. Wir haben den Verlauf der kosmischen Sterneneinstellung gemessen und wissen, dass ungefähr die Hälfte der Sterne, die wir beobachten, entstanden, bevor das Universum halb so alt war wie jetzt. Allerdings war wichtiges Wissen über die Entstehung individueller Galaxien beschränkt, da die detaillierten Sternpopulationseigenschaften, die wir über Galaxien kennen, zum Beispiel Alter, Metalizität und Kinematik, hauptsächlich von nahen Galaxien beobachtet wurden, welche überwiegend alte Sternpopulationen enthalten. Um unser Verständnis der Entstehung der Galaxie voranzutreiben, müssen Messungen auf weiter entfernte Galaxien, die eine größere Variation in Alter und Aktivität bei Sternbildung (SF) haben, ausgeweitet werden. In dieser Arbeit untersuche ich die Sternpopulationseigenschaften einer Galaxienpopulation als das Universum halb so alt war, wie jetzt (Rotverschiebung $z \sim 1$), indem ich hochwertige, hochauflösende Spektren der (jüngsten) LEGA-C-Untersuchung verwende. Ich präsentiere einen Algorithmus, der Vollspektrumanpassung verwendet, um die Sternentstehungsgeschichten (SFHs) von LEGA-C-Galaxien zu rekonstruieren. Zunächst untersuche ich die Abhängigkeit individueller SFHs von Sternmasse, Sternengeschwindigkeit, Geschwindigkeitsstreuung und SF-Aktivität. Die individuellen SFH von inaktiven und sternbildenden Populationen mit großer Masse (Geschwindigkeitsstreuung) gehen in Richtung niedriger Rotverschiebungen zunehmend auseinander, was auf eine starke Korrelation zwischen aktueller SF-Aktivität und vergangener SF-Aktivität hinweist. Zweitens verfolge ich die Entwicklung der Sternmassen von LEGA-C-Galaxien zwischen Rotverschiebungen $z \sim 1$ und $z = 3$ (als das Universum ein Sechstel seines jetzigen Alters alt war). Galaxien, deren Sternmasse bei einer Rotverschiebung ähnlich ist, haben unterschiedliche evolutionäre Pfade, die zu einer großen Reichweite an Sternmassen bei einer anderen Rotverschiebung führen, egal ob sie zeitlich zurück- oder vorausverfolgt werden. Abschließend untersuche ich Verjüngung in inaktiven Galaxien, also wenn Galaxien, die inaktiv sind, ihre SF wiederentzünden, bevor sie wieder ruhen. Obwohl Verjüngungsereignisse nicht wesentlich zum Wachstum inaktiver Galaxien beitragen, liegt ein Großteil der verjüngten Galaxien im "grünen Tal", von dem man annimmt, dass Galaxien hier in der (Einweg-)Übergangsphase von der blauen Wolke zur roten Sequenz sind. SFHs zu rekonstruieren hat uns ermöglicht, die individuellen Bahnen, entlang derer Galaxien entstehen, zu verfolgen und die physikalischen Prozesse, die sie antreiben, zu untersuchen. Messungen dieser Arbeit, sowie andere LEGA-C-Untersuchungen, werden für zukünftige Untersuchungen bei noch höheren Rotverschiebungen wichtig sein, da sie als Maßstab dienen werden, um Populationen bei höheren Rotverschiebungen mit dem nahegelegenen Universum zu verbinden.

Contents

List of Figures	v
List of Tables	ix
Acronyms	xi
1 Introduction	1
1.1 Insights from Galaxy Evolution Studies	1
1.1.1 Star Formation History of the Universe	2
1.1.2 Stellar Mass Growth	3
1.1.3 How do Galaxies Quench?	3
1.1.4 Do Galaxies Rejuvenate?	5
1.2 Stellar populations in galaxies	5
1.2.1 Stellar Population Synthesis Models	6
1.2.2 Star Formation Histories of Individual Galaxies	9
1.3 Spectroscopic Surveys	11
1.3.1 Local Universe	12
1.3.2 Beyond the Local Universe	13
1.3.3 LEGA-C Survey	13
1.4 Thesis Outline	15
2 STAR FORMATION HISTORIES OF $Z \sim 1$ GALAXIES IN LEGA-C	17
2.1 Introduction	17
2.2 Data	20
2.3 Spectral Fitting Technique	21
2.3.1 Stellar Population Model	21
2.3.2 Fitting Algorithm	23
2.3.3 Robustness of Fitting Results	24
2.4 Fitting Results	26
2.4.1 Model Outputs	26

2.4.2	Sample SFHs	27
2.4.3	General Trends	27
2.5	SFHs of the Galaxy Population	32
2.5.1	Correlations between Age, $M_{*,spec}$ and σ_*	32
2.5.2	Evolution of the average SFHs	34
2.5.3	The variety of SFHs	36
2.5.4	Comparisons to Literature Measurements	37
2.6	Summary	38
3	STELLAR MASS EVOLUTION AND RANKING OF $z \sim 0.8$ GALAXIES IN LEGA-C	41
3.1	Introduction	41
3.2	Data	43
3.2.1	Star Formation Histories	44
3.3	Evolution of the Galaxy Population from $z \sim 0.8$ backward to $z = 3$	45
3.3.1	Stellar mass evolution and SF activity	45
3.3.2	Evolution as a function of current stellar mass	46
3.3.3	Stellar mass evolution, velocity dispersion and central mass density	48
3.4	Stellar mass evolutionary tracks	48
3.4.1	Individual galaxy evolutionary tracks	48
3.4.2	Tracing the galaxy population forward and backward in time	50
3.5	Summary	51
4	REJUVENATION IN $z \sim 0.8$ QUIESCENT GALAXIES IN LEGA-C	53
4.1	Introduction	53
4.2	Data	56
4.2.1	Star Formation Histories	57
4.2.2	Identifying Rejuvenated Galaxies	57
4.2.3	Determining the Rejuvenation Fraction	60
4.3	Properties of Rejuvenated population	61
4.3.1	The Green Valley	61
4.3.2	SFHs and rejuvenation timescales	62
4.3.3	SFR-Mass relation during rejuvenation	64
4.3.4	Stellar mass and local environmental density dependence . .	66
4.3.5	Contribution to the Cosmic Star-formation Rate Density . .	68
4.4	Summary	69
5	Summary and Outlook	71
5.1	Summary	71
5.2	Outlook	73
5.2.1	Quenching	73
5.2.2	SFH and Galaxy Structure	73

5.2.3	Comparing Reconstructed SFHs to Simulations	74
5.3	Concluding Remarks	74
6	First Author Publications of P. Chauke	77
	Bibliography	79

List of Figures

1.1	Cosmic star formation history	2
1.2	Overview of the stellar population synthesis technique	7
1.3	Example of reconstructed SFHs from full-spectrum fitting	10
1.4	Simulated spectrum of a typical galaxy in the LEGA-C sample	14
2.1	Template CSP spectra used to fit LEGA-C galaxies. They were generated from <i>FSPS</i> , using the time intervals listed in Table 2.1, with solar metallicity and arbitrary velocity dispersion; and they have been normalised and shifted here for comparison purposes.	22
2.2	Reconstructed SFH (black) of a synthetic galaxy (green) with $S/N = 10\text{\AA}^{-1}$ (left) and $S/N = 30\text{\AA}^{-1}$ (right). The converged walkers are shown in grey and the upper and lower uncertainties are based on the 16 th and 84 th percentiles, respectively, as explained in Section 2.3.2. By $S/N = 30\text{\AA}^{-1}$, the recovered SFHs predict the stellar mass, age and luminosity with precision $\leq 0.1\text{dex}$	24
2.3	Distributions of $M_{*,spec}$ (left), $a_{<MW>}$ (middle) and $a_{<LW>}$ (right) of the LEGA-C sample. The quiescent and star-forming populations (as defined in Section 2.5.1) are shown in red and blue, respectively. The distribution of the uncertainties for each parameter are shown at the top of each figure.	26
2.4	Sample of emission line subtracted spectra of 12 LEGA-C galaxies with the best fitting model obtained from combining the 12 template spectra using MCMC. The bottom-right figure, in each plot, is the reconstructed star formation history (the converged walkers are shown in grey). The MCMC resultant mass, luminosity, mass-weighted age and dust reddening values are shown in red. The spectra are ordered by $a_{<MW>}$	28
2.4 (Continued)	29
2.4 (Continued)	30
2.4 (Continued)	31

2.5	EW(H δ) versus D $_n$ 4000 (upper panel) and U-V colour versus V-J colour (lower panel) colour-coded by the time after which the final 10% of stars were formed (left), the mean light-weighted age (middle), and the mean mass-weighted age (right). Typical error bars are indicated in grey. . . .	32
2.6	a $_{\langle MW \rangle}$ as a function of M $_{*,spec}$ (left) and σ_* (right). The star-forming and quiescent populations are indicated in blue and red, respectively, and typical error bars are indicated in grey. Galaxies with $\sigma_* \gtrsim 200\text{km s}^{-1}$ are almost exclusively old ($> 4\text{Gyrs}$) and quiescent, which indicates that σ_* is a stronger predictor of age and SF activity.	33
2.7	σ_* versus M $_{*,spec}$, colour-coded by a $_{\langle MW \rangle}$. The star-forming and quiescent populations are shown in the middle and right panels, respectively. Typical error bars are indicated in grey. The clear separation between young and old galaxies at $\sigma_* \sim 170\text{km s}^{-1}$ shows a stronger correlation between a $_{\langle MW \rangle}$ and σ_* over M $_{*,spec}$, which also depends on the current SF activity.	33
2.8	Ensemble-averaged SFHs of LEGA-C galaxies, normalised by stellar mass and separated into various σ_* (top) and M $_{*,spec}$, bins (bottom). The histories are divided into the star-forming and quiescent populations in the middle and right panels, respectively. The stellar content in massive galaxies formed earlier and faster, regardless of current SF activity. . . .	35
2.9	SFHs of the LEGA-C sample (normalised by stellar mass) as a function of the age of the Universe separated into four σ_* bins indicated by the labels. The colours differentiate between the star-forming and quiescent populations at the observed redshift.	36
3.1	SFR as a function of M $_{*,spec}$ of the LEGA-C sample at the observed redshift. Star-forming and quiescent populations are indicated in blue and red, respectively.	44
3.2	Stellar mass evolution of LEGA-C galaxies from their observed redshift back to redshifts 1.5, 2 and 3. Galaxies that are star-forming and quiescent at the observed redshift are indicated in blue and red, respectively.	45
3.3	Stellar mass evolution of M $_{*,spec}$ selected galaxies (shown in black) from the redshift of observation backward to redshifts 1.5, 2 and 3. The star-forming and quiescent populations from Figure 3.2 are shown in the background for comparison.	46
3.4	Stellar mass evolution of σ_* (a) and lMcen $_*$ (b) selected galaxies (shown in black) that have a median stellar mass $\sim 10^{10.7}M_{\odot}$ from the redshift of observation backward to redshifts 1.5, 2 and 3. The star-forming and quiescent populations from Figure 3.2 are shown in the background for comparison.	47

3.5	Stellar mass evolution of selected galaxies (10 in each of the 3 stellar mass bin) from $z = 1$ backward to $z = 3$. In some cases, the stellar mass growth of less massive galaxies at $z = 3$ surpasses that of more massive galaxies by $z = 1$, in contrast with constant number density assumptions.	49
3.6	Stellar mass evolution of galaxy populations between $z = 1$ and $z = 3$. The left panel shows selected masses at $z = 1$ traced backward in time to $z = 3$ and the right panel shows selected masses at $z = 3$ traced forward in time to $z = 1$. The solid lines indicate the median mass evolution of each population and the shaded regions indicate the 16 th and 84 th percentiles of the distributions.	50
4.1	sSFR _{UV+IR} as a function of $M_{*,spec}$ (left) and the rest-frame UVJ diagram (right) of the LEGA-C population. The dashed line distinguishes the star-forming and quiescent populations. The rejuvenated quiescent population is color-coded by sSFR _{UV+IR} for comparison. Typical error bars are indicated in dark gray.	56
4.2	Average spectrum (LEGA-C as well as best-fit model) of rejuvenated galaxies (black) compared to the average spectrum of stellar mass and H _δ matched quiescent galaxies that do not show evidence of rejuvenation (gray). The PSB spectrum is shown for comparison. The spectra have been normalised and shifted for comparison purposes.	59
4.3	Rest-frame U-V color versus $M_{*,spec}$ of the quiescent (filled gray circles) and star-forming (open gray circles) populations in the LEGA-C sample. The black points represent rejuvenated quiescent galaxies, while the green band and the blue and red lines indicate the green valley, star-forming and quiescent regions, respectively. Typical error bars are indicated in dark gray.	62
4.4	The reconstructed star formation histories of rejuvenated galaxies obtained from MCMC full-spectrum fitting (the walkers are shown in gray, Chauke et al., 2018). The fraction of stellar mass formed from the rejuvenation episode and the redshift of the peak SFR of the event are shown in black.	63
4.4	(Continued)	64
4.5	Spectra of rejuvenated galaxies along with the resulting spectra obtained from MCMC full-spectrum fitting. Their IDs and redshifts are shown in black and the resultant normalised χ^2 values and stellar masses are shown in gray.	65
4.5	(Continued)	66

4.6	The peak SFR versus the stellar mass during the rejuvenation event (black) compared to the SFR- M_* relation of the same sample at the redshift of observation (red). The gray connecting lines track the evolution of each galaxy in SFR and stellar mass. The blue dashed lines represent the Speagle et al. (2014) SFMS at $z = 1$ with a 0.3dex scatter and the black dashed line distinguishes the star-forming sequence from the quiescent sequence. Typical error bars are indicated in dark gray. . . .	67
4.7	Stellar mass of rejuvenated galaxies versus the fraction of stellar mass from the rejuvenation event. The upper and lower uncertainties are based on the 16 th and 84 th percentiles of the walkers (see Section 4.2.1). The median trend is indicated in red.	67
4.8	Local overdensity versus the stellar mass of quiescent LEGA-C galaxies. The large black points represent galaxies that were rejuvenated. Distributions of the stellar mass and local overdensity are shown on the top and right, respectively.	68

List of Tables

2.1 Properties of the *FSPS* template spectra. 21

Acronyms

AGN	active galactic nuclei
BH	black hole
CH	carbon-hydrogen molecule
CSP	composite stellar population
EW	equivalent widths
FSPS	Flexible Stellar Population Synthesis package
H I	Neutral hydrogen gas
IMF	initial mass function
IR	Infrared
K	Potassium
CDM	Cold Dark Matter
LEGA-C	Large Early Galaxy Astrophysics Census
MCMC	Markov Chain Monte Carlo
SDSS	Sloan Digital Sky Survey
SED	spectral energy distributions
SF	star formation
SFH	star-formation history
SFMS	star-forming main sequence
SFR	star-formation rate

SFRD star-formation rate density

SSP simple stellar population

sSFR specific star-formation

SPS stellar population synthesis

S/N signal-to-noise

PSB post star burst galaxy

UV Ultraviolet

Introduction

Most of us are unaware that when we look up at the night sky, we ‘see’ the history of the formation of the Universe. In awe, we stare at the twinkling stars, once clouds of cold and dense gas, as they illuminate the vast skies and, together with enormous quantities of dust and gas, encapsulate our own galaxy, the Milky Way. Further still, with the aid of telescopes, we see billions of distant ‘island universes’: galaxies, much like our own, with varying shape, size and stellar content.

It’s no surprise that the mystery of the formation of the Universe consumes some. A picture has been built, piece by piece, over the past several decades by observing stars in distant galaxies at different distances. Although most of the matter in the Universe is non-baryonic ‘dark matter’ which interacts only gravitationally, studying luminous matter provides clues about all matter, and allows us to understand the physical processes related to the conversion of gas into stars, as well as the formation and evolution of galaxies in general. A galaxy’s formation and evolution history are contained in its various populations of stars, shape, dynamics and its dust and gas properties. Most of this information is contained in the integrated light we see from its collection of stars.

1.1 Insights from Galaxy Evolution Studies

The goal of astronomy is to understand how structures in the Universe formed and how they evolve. This is done by comparing developed theories/models to data collected from observations. In the following sections, I give a brief overview of insights, which pertain to this thesis, that we have gained from galaxy evolution studies.

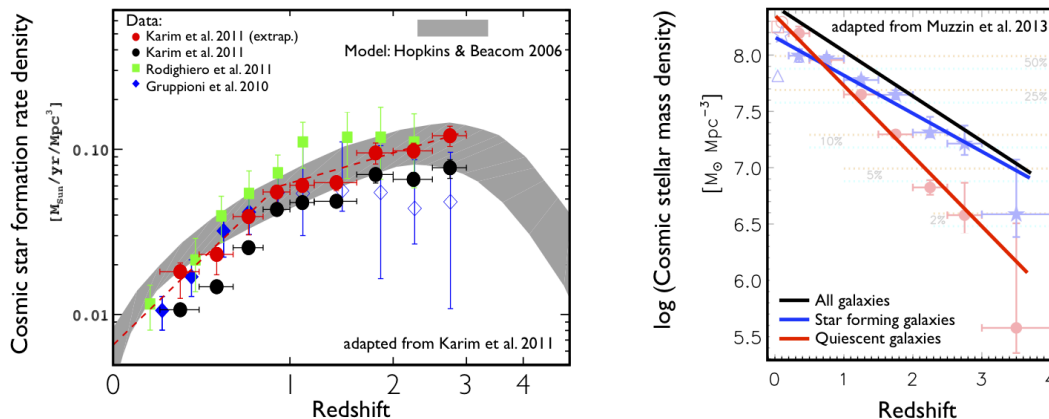


Figure 1.1: The left panel shows the cosmic star formation history adapted from Karim et al. (2011) and the right panel shows the number density evolution of galaxies adapted from Muzzin et al. (2013a).

1.1.1 Star Formation History of the Universe

Mapping the cosmic history of star formation (SF) is crucial to our understanding of how structure in the Universe forms and evolves, and it requires the study of the evolution of galaxies. Observations in this field have been accumulated over the past two decades. On one hand, multi-wavelength imaging surveys with the Hubble and Spitzer space telescopes and ground-based telescopes, have resulted in several discoveries. This includes the confirmation that SF activity was significantly higher in the past (e.g. Lilly et al., 1996) and the discovery of galaxies at redshifts (distances) as large as $z = 11.1$ (Oesch et al., 2016). Redshift is related to distance via $z \approx \frac{D}{c}H$ (for small distances), where D is the proper distance, the distance between two regions of space at a constant cosmological time; c is the speed of light; and H is the Hubble constant, a parameter that describes the expansion of the Universe. On the other hand, spectroscopic surveys, which measure galaxies' light intensity as a function wavelength or frequency, such as the Sloan Digital Sky Survey, have found that various galaxy properties like the star-formation rate (SFR) and colour (ratio of a source's brightness in different filters), are bimodal (e.g. Kauffmann et al., 2003). That is, they show a clear division between galaxies that are actively forming stars and those that have stopped forming stars (quiescent galaxies).

With these observations, we have drawn a consistent picture of the star formation rate density (SFRD) of the Universe by modelling all the stars that formed from the present to higher redshifts. Figure 1.1 shows the cosmic SFRD as a function of redshift from Karim et al. (2011, left panel) and the number density evolution of galaxies adapted from Muzzin et al. (2013a, right panel). We have found that the SFRD peaked at $z \sim 2$ and declined exponentially at later times, and that about

50% of stars formed before $z \sim 1$. This makes probing the redshift range $1 < z < 2$ a crucial component of understanding galaxy evolution. This is the aim of current surveys such as the Large Early Galaxy Astrophysics Census (see Section 1.3.3) and future surveys that will use the James Webb Space Telescope.

1.1.2 Stellar Mass Growth

Galaxy stellar masses have mostly been computed from multi-wavelength photometric surveys, using models that require an assumed star-formation history (SFH) and an initial mass function, which describes how stellar masses are distributed in a stellar population (e.g. Brammer et al., 2011). Modelling the mass evolution of a galaxy from observational data has typically involved linking galaxy populations at different epochs, in an attempt to connect the progenitors of galaxies to their descendants at lower redshifts. A common method that recovers the median stellar mass evolution of a galaxy population to within a factor ~ 2 -3 (e.g. Torrey et al., 2015), is the constant number density approach, where galaxies are assumed to be ordered by some property such as stellar mass (e.g. van Dokkum et al., 2010; Papovich et al., 2011). This method assumes that the most massive galaxies at higher redshifts evolve to be the most massive galaxies at lower redshifts, and that galaxy mergers are negligible.

However, observations of massive quiescent galaxies suggest that they are formed through major mergers, where two galaxies of the same size collide, which drives away most of their gas (e.g. van der Wel et al., 2009b). Additionally, quiescent galaxies at higher redshifts are observationally smaller in size compared to those at lower redshifts (e.g. van der Wel et al., 2008). This indicates that quiescent galaxies may grow through minor mergers, where smaller stellar systems are accreted, or gas-poor mergers, as these processes increase galaxies' sizes without igniting SF. Furthermore, galaxy evolution simulations and semi-analytical models have found that the factor of $\sim 2 - 3$ error in median stellar masses measured from the constant number density approach is mainly due to scatter in stellar mass growth rates and mergers (e.g. Leja et al., 2013; Torrey et al., 2015). This means that galaxy populations do not evolve along constant number density tracks, and that galaxies that have similar stellar masses at one redshift, have diverse evolutionary paths that lead them to have various stellar masses.

1.1.3 How do Galaxies Quench?

Galaxies are typically divided into two populations: the 'blue cloud', which contains galaxies that are actively forming stars; and the 'red sequence', which contains galaxies that are no longer forming stars (passive or quiescent galaxies). It is believed

that red quiescent galaxies evolve from blue star forming ones because several studies have shown that quiescent galaxies have been increasingly dominant since $z = 1$ (e.g. Brammer et al., 2011; Moustakas et al., 2013; Muzzin et al., 2013a, see Figure 1.1). This underscores the importance of galaxy ‘quenching’ (cessation of SF) in the context of galaxy evolution. The processes that cause galaxies to quench are not well understood and have been a matter of debate in the study of the evolution of galaxies. The processes could be internal, and dependent on the galaxy itself, or they could be driven by the galaxy’s surrounding environment. Several external and internal mechanisms with different quenching timescales have been proposed, however, there is not as of yet an accepted mode of thought.

SF quenching may be a natural occurrence, caused by the consumption of the cold gas reservoir of field galaxies, or by the growth of galaxy halos/bulges which stabilise gas reservoirs, making SF inefficient (e.g. Martig et al., 2009; Dekel and Burkert, 2014). Simulations, however, have shown that halo quenching alone does not reproduce the observed red sequence (e.g. Gabor et al., 2010). Alternately, quenching could be caused by environmental effects, especially in high-density group and cluster regions, where in-falling galaxies are stripped of their gas reservoir, preventing them from forming new stars (e.g. McCarthy et al., 2008; Bahé and McCarthy, 2015). However, quenched galaxies are observed outside of these high-density environments, which means that there are at least other processes at work. Stellar feedback plays a role: massive stars transfer momentum and energy to their surroundings. This blows away some of the surrounding gas and heats up and ionises the remainder, which prevents the gas from turning into stars. However, this type of quenching is a gradual process, with star formation declining over several gigayears (e.g. Zolotov et al., 2015). It is, therefore, by itself not enough to explain the fraction of early type galaxies that are formed by much more rapid quenching. It is instead believed that stellar feedback regulates star formation, otherwise galaxies would have much higher SFRs and stellar masses than we observe.

Many studies suggest that quenching is linked to active galactic nuclei (AGN) powered by supermassive black holes (BHs), which are believed to be at the centre of every large galaxy. An AGN is believed to be the result of matter (gas and dust) that is accreted by the BH, it forms an accretion disc around the BH and generates radiation when the disc is compressed by the BH’s force of gravity. If the accretion rate is high, i.e. ‘quasar’ mode feedback, the generated radiation is strong and drives gas outflows, expelling gas from the galaxy. If the accretion rate is low, i.e. ‘maintenance’ mode feedback (considered to be the dominant mode), the generated radiation is weak but it prevents the gas in galaxies’ halos from cooling, suppressing further SF. Studies find a correlation between BH mass and stellar mass in galaxies’ bulges (tightly packed group of stars surrounding the centres of spiral galaxies; e.g. Kormendy and Ho, 2013) as well as SF activity (e.g., Terrazas et al., 2016). This could mean that feedback from BHs regulate the SFR. However, AGN activity has

also been observed in highly star-forming galaxies (e.g. Carniani et al., 2016), which suggests that we do not know the precise role that BHs play. Alternatively, both internal and external processes could be at work, but they are relevant in different redshift regimes. Darvish et al. (2016) found that external processes (galaxy interactions and the density of the surrounding environment) cause quenching at lower redshifts ($z \lesssim 1$) and internal processes (presence of a BH and stellar feedback) are relevant at earlier cosmic times ($1 \lesssim z \lesssim 3$).

1.1.4 Do Galaxies Rejuvenate?

Although number density evolution studies indicate that galaxies evolve from being star-forming to quiescent, multiple studies have measured secondary SF in galaxies, where galaxies that stopped forming stars at some earlier time, show evidence of recent SF. The fraction of galaxies that show evidence of recent SF is between 10 and 30% (Schawinski et al., 2007; Donas et al., 2007; Behroozi et al., 2019) and is found to be higher in low-density environments (e.g., Schawinski et al., 2007; Thomas et al., 2010). Secondary SF episodes are linked to either gas accretion or galaxy mergers which bring in gas, because this often results in the formation of a small population of young stars (e.g. Kaviraj et al., 2009; Marino et al., 2009). Multiple secondary SF studies exist, however, there are still open questions on secondary SF processes. We still need to determine whether any galaxies that have secondary SF episodes actually rejuvenate, i.e. transition back to the blue cloud from the red sequence, and how often this occurs. We also need to determine if the stellar mass formed from these events is a significant portion of the SFRD of the Universe, and on what timescale they occur.

Many studies on secondary SF, quenching, and stellar mass growth in general are based on photometric measurements, data from the local Universe, or low quality data at higher redshifts. To advance our current understanding of galaxy evolution, we should obtain high quality stellar population data across different redshifts.

1.2 Stellar populations in galaxies

When we observe galaxies today, we see the result of the various stellar populations that formed and evolved over the galaxies' lifetimes. Therefore, contained in a galaxy's integrated light, is its star formation history as well as its chemical evolution. There has been considerable effort that has been devoted to understanding the stellar content of galaxies at high and low redshift over the past several decades. However, much of this work has been limited to the local Universe, because it is not as time consuming to obtain stellar content information of nearby galaxies.

Stellar content information is extracted from a galaxy spectrum or spectral energy distributions (SEDs). A galaxy spectrum can reveal many of its properties, such as its age (SFH), chemical composition, mass, luminosity and distance. We are able to measure these parameters because of the shape of the spectrum (continuum) as well as the several absorption and emission features it contains. The stars, gas and dust in a galaxy contain elements that interact with the light particles that we see when we observe galaxies. The interaction either causes an excess or deficit of light particles at certain wavelengths, and this results in emission or absorption lines, respectively. Different spectral features allow us to constrain different stellar population properties. For example, the presence of strong Balmer lines (Hydrogen absorption and emission lines) indicates that a galaxy is young and star-forming, and the presence of Magnesium (Mg) absorption lines indicates that a galaxy has a high metal content, i.e. contains elements that are heavier than Hydrogen and helium. However, it is difficult to disentangle age from metal content for older stellar populations without very high quality spectra.

To extract meaningful information from observed integrated light, the data needs to be compared to predictions from stellar population synthesis (SPS) models. SPS modelling refers to the generation of spectra or SEDs of groups of stars or galaxies. It relies heavily on stellar evolution theory to constrain the range of possible outputs. SPS models provide the fundamental link between galaxy formation theory/models and observations, and much effort has gone into their development.

1.2.1 Stellar Population Synthesis Models

SPS models rely on advancements made in stellar evolution theory because stellar evolution theory allows us to describe a star's stellar mass, effective temperature, luminosity and metal abundance as a function of time. In this theory, stars are formed from the gravitational collapse of dense molecular clouds, which fragment into smaller regions that contract to form stellar cores. When the temperature becomes high enough for nuclear reactions to begin, the stars start to burn Hydrogen into Helium in their cores and they enter the 'main sequence' phase of their evolution. A star's mass determines how it evolves throughout time. The least massive stars eventually turn into white dwarfs, and the most massive stars eventually collapse into black holes, ejecting gases with elements which were synthesised during the star's lifetime into the interstellar medium. For an intermediate mass star like our sun, its core eventually forms a white dwarf, which cools throughout its lifetime, and its outer layers are ejected into the interstellar medium creating a planetary nebula. These supernovae and planetary nebulae are the chemical distribution centres of the Universe: they enrich the interstellar medium with elements that are heavier than Hydrogen and this increases the metal content (metallicity) of subsequent generations of stars. The evolution of stars with varying stellar masses is usually shown

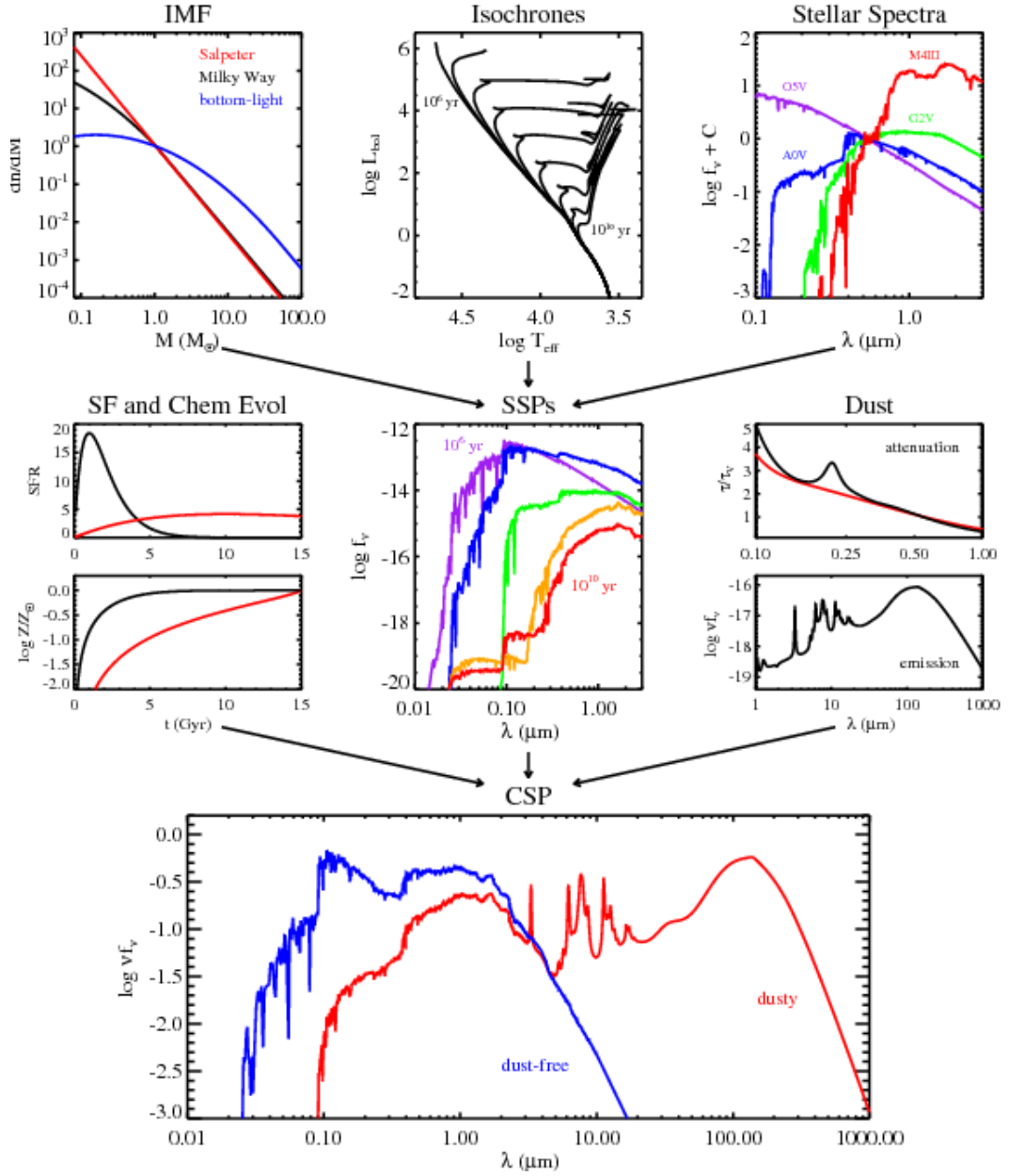


Figure 1.2: Overview of the stellar population synthesis technique from Conroy (2013). The upper panels represent what is necessary to construct simple stellar populations: an IMF, isochrones for a range of ages and metallicities, and stellar spectra for a range of effective temperatures, luminosities and metallicities. The middle panels represent the models needed (i.e. SFH, chemical evolution and dust attenuation and emission) to compute the final composite stellar population (bottom panel).

in a Hertzsprung-Russell (HR) diagram, a scatter plot which shows the relationship between luminosity and stellar mass or effective temperature.

Equipped with stellar evolution theory, we can synthesise a simple stellar population (SSP) which describes the spectrum or SED as a function of time, of a single population of stars which are identical in age and metallicity. For this, isochrones, stellar spectral libraries and an initial mass function are required as inputs. Isochrones specify the location in the HR diagram of stars, with a common age and metallicity, as well as their remnants (e.g. white dwarfs, neutron stars, black holes, etc.). Stellar spectral libraries are required to compute stellar evolution outputs as a function of metallicity into SEDs. These are either obtained from observations (e.g. *MILES*: Sánchez-Blázquez et al., 2006), which vary in quality, or they are constructed from theoretical calculations (e.g. *BaSeL*: Lejeune et al., 1997, 1998; Westera et al., 2002), which have the advantage of producing spectra that are not subject to observational constraints such as spectral resolution or flux calibration, for example. However, they are only as good as the input parameters and assumptions made in the computation of the model. The initial mass function (IMF) is an empirical function that describes the initial distribution of stellar masses for a population of stars entering the main sequence. We do not have a complete theoretical understanding of what determines the exact mass of a star, so we cannot as yet determine the exact distribution of a population of stars' stellar masses. The IMF is a representation of this distribution, and it is currently based on an average from observations of stars in our Milky Way. The form of the IMF was initially introduced by Salpeter (1955) and has since been extended to accommodate the range of stellar masses (e.g. Kroupa et al., 2001; Chabrier, 2003). However, it is not clear if the IMF has the same form in all stellar systems, as some studies have suggested that the IMF varies in different environments (e.g. Conroy and van Dokkum, 2012; Geha et al., 2013).

However, a galaxy consists of billions of stars which formed at different times and have a range of metallicities, along with gas and dust. Therefore, one requires more than just SSPs to synthesise the spectrum of a galaxy. SSPs are the building blocks of more complicated stellar systems, viz. composite stellar populations (CSPs), which are a group of stars which range in age (given by their SFH) and metallicity (given by their chemical evolution), and they contain dust. The SFH can have a variety of forms. It can be as straightforward as having constant SF over time, or have multiple bursts of SF. It can be an exponentially decreasing function, viz. the τ -model, where $SFR \propto e^{-t/\tau}$. This form has been found to occur naturally when SFR is linearly dependent on gas density (Schmidt, 1959). The SFH can also increase with time, which is thought to be the case in the high-redshift regime for galaxies which evolve in a hierarchical universe (e.g. Finlator et al., 2007; Papovich et al., 2011). In many cases, the SFH is a combination of multiple simpler forms (e.g. Simha et al., 2014; Ciesla et al., 2017). A single metallicity is usually chosen for a CSP, however, if very high quality spectra are at hand, non-parametric metallicity histories can be modelled (e.g. Cid Fernandes et al., 2005; Tojeiro et al., 2009). Disentangling age from metallicity is notoriously difficult because old stellar populations cannot be distinguished from another population that is 3 times older and has half the

metallicity (Worthey, 1994). It is only with very high quality spectra that one can use spectral features that are more sensitive to metallicity, or age, to lift the age-metallicity degeneracy. Dust is made of carbon and silicates, the products of stellar evolution. It has been observed in almost all galaxies, especially those that are actively forming stars. Dust particles preferentially absorb and scatter Ultraviolet (UV) light compared to radiation at longer wavelengths, and re-radiate this light in the Infrared (IR). This can have a significant effect on observed spectra (dust attenuation) which in turn affects the ability to derive accurate SFR measurements as a young, dust attenuated population can resemble an older, dust-free population. The effect of dust on stellar populations makes it an essential component of SPS models. There are multiple dust attenuation laws that have been developed to correct for dust, but the empirically derived (from a sample of starburst galaxies) Calzetti law is widely used (Calzetti et al., 2000). This correction is most important for star-forming galaxies, as these galaxies require significant corrections.

Figure 1.2 shows an overview of the process of synthesising stellar populations (Conroy, 2013). The upper panels show what is required to construct SSPs, viz. an IMF, isochrones for a range of ages and metallicities as well as stellar spectra for a range of effective temperatures, luminosities and metallicities. The middle panels show what is necessary to construct CSPs, viz. SSPs, models for the SFH, chemical evolution and dust attenuation of the population; and the lower panel shows the final CSPs. Once CSPs are constructed, they or a combination of them are fit to galaxy spectra in order to determine their SFH and measure galaxy parameters like stellar mass, age, metallicity, etc. Fitting procedures differ, some studies use χ^2 minimisation, but Markov Chain Monte Carlo (MCMC) fitting techniques have become popular over the last few years (e.g. Conroy and van Dokkum, 2012; Choi et al., 2014).

There have been several Stellar Population Synthesis packages developed over the years. In this thesis, I will make use of the Flexible Stellar Population Synthesis package (*FSPS v3.0*; Conroy et al., 2009; Conroy and Gunn, 2010). *FSPS v3.0* is a collection of fortran routines to compute SSPs for a variety of IMFs and metallicities, as well as CSPs for a variety of SFHs, metallicity histories and dust attenuation prescriptions. The routine outputs spectra and magnitudes of the SSPs and CSPs at arbitrary redshift.

1.2.2 Star Formation Histories of Individual Galaxies

Recovering the SFH of a galaxy from its spectrum is notoriously difficult. It not only requires high quality SPS models, but also high quality, high resolution spectra and a wide wavelength coverage. Individual stars would preferably be resolved, however, for most galaxies, we have to rely on their observed integrated stellar light. This leads to several challenges, for example, it is difficult to measure accurate metallicities

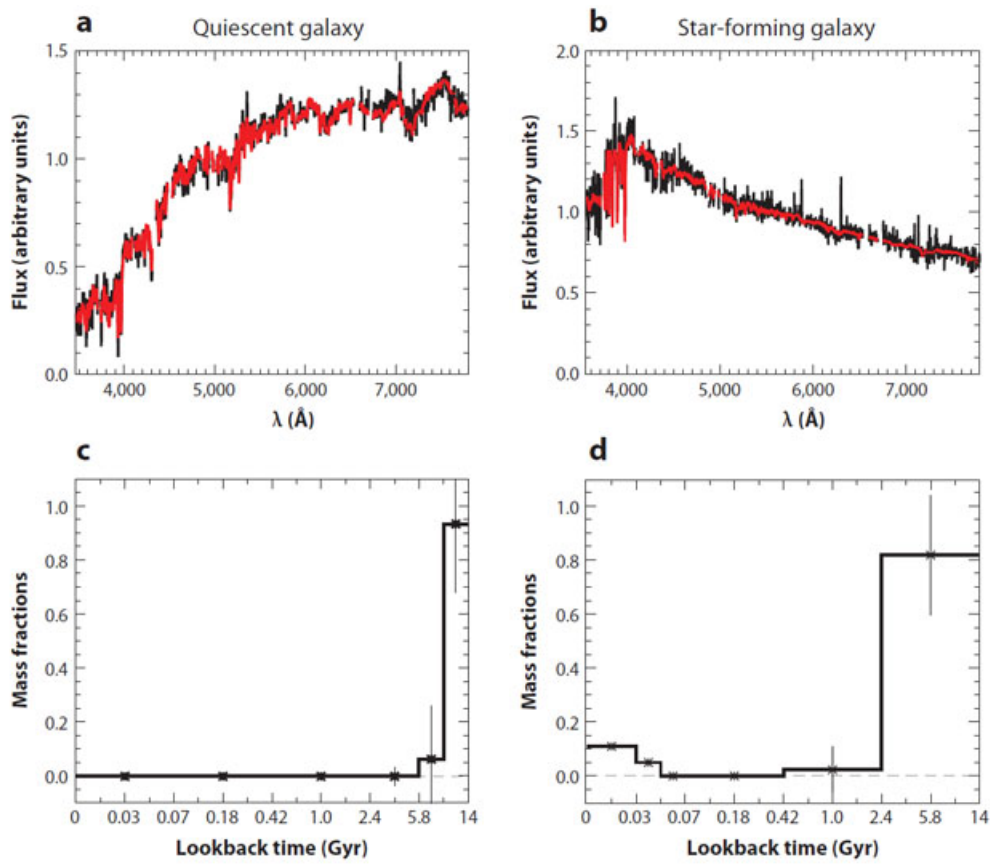


Figure 1.3: Example of full-spectrum fitting (top panels) resulting in the reconstructed SFHs (bottom panels) of a quiescent (left) and star-forming galaxy (right) from Tojeiro et al. (2009).

and SFRs (hence ages) because of the degeneracy between age, metallicity and dust, unless very high quality data are available. Additionally, young, high mass stars are so luminous that they dominate the integrated stellar light in star-forming galaxies, ‘outshining’ the numerous low-mass stars, which leads to under-estimated galaxy ages.

Because of the lack of knowledge of the parameter space, model assumptions (prior probabilities) can lead to biased results. This means that parameters that are under-constrained should not be fixed to certain values, or chosen based on minimum χ^2 estimation techniques, which aim to find parameter values that result in the smallest difference between the model and the data. This is because the likelihood function, the probability distribution that describes how likely different parameter values are, given the data, may contain multiple peaks and valleys. Therefore, priors need to be carefully considered, especially when the number of parameters is large. These challenges make MCMC fitting techniques appealing because they explore the parameter space efficiently, even with a large number of parameters, and can additionally use the full spectrum, not just a few spectral indices (e.g.

Conroy and van Dokkum, 2012; Choi et al., 2014). MCMC techniques sample the probability distribution by exploring the parameter space in order to find the most likely parameter values.

The choice of a SFH model can also lead to biased results. As stated earlier, the SFH can be parametrised in different ways; it can be constant, rising, declining, or it can incorporate an early phase with a late-time delay, where the SFR initially rises then falls exponentially at a later time ($SFR \propto te^{-t/\tau}$). The data can be fit to multiple forms of the SFH, which means that one has to ensure that the data is fit to a wide variety of SFH types, if one wants to accurately recover the SFH. However, parametrised SFHs can only have so many forms. This makes modelling spectra with non-parametric SFHs desirable because one can simply generate a set of CSPs with fixed (or adaptive) age bins and then fit for the fraction of mass formed within each bin. This method of fitting has been tested and found to be capable of recovering complex SFHs (e.g. Ocvirk et al., 2006; Tojeiro et al., 2007). As a result, there have been several algorithms that have been developed over the past decade that use this technique to recover SFHs, viz. *MOPED*, *STARLIGHT*, *STECMAP*, *VESPA*, *ULYSS* and *FIREFLY* (Heavens et al., 2000; Cid Fernandes et al., 2005; Ocvirk et al., 2006; Tojeiro et al., 2007; Koleva et al., 2009; Wilkinson et al., 2015). Figure 1.3 shows reconstructed SFHs of a quiescent (left) and star-forming galaxy (right) using non-parametric full-spectrum fitting (Tojeiro et al., 2009).

In any case, even if we limit uncertainties and biases by using the best models and the best fitting techniques, accurate recovery of SFHs is still limited to the quality of spectra obtained from surveys. These are expensive to obtain, increasingly so at higher redshifts (see the following section).

1.3 Spectroscopic Surveys

Advancements in redshift surveys have propelled our understanding of structure formation and galaxy evolution. Since these spectroscopic surveys began in the 80's (e.g. Huchra et al., 1983), they have been instrumental in measuring distances of astronomical objects to obtain the 3D distribution of matter in the Universe, as well as in placing strong constraints on cosmological parameters such as the Hubble constant, allowing us to estimate the size and age of the Universe.

The large sample sizes of these surveys has meant that the quality of the acquired spectra has had to be compromised. Fortunately, local ($z \sim 0$) galaxies require an integration time of only a few hours to reach a high signal-to-noise ratio (S/N). However, the integration time is increasingly large the higher the redshift. Galaxies at $z \sim 1$, for example, require ~ 20 hours to reach the same S/N . To be able to accurately reconstruct a galaxy's SFH and measure its stellar population properties,

one does not only require high quality SPS models, but also high resolution, high quality stellar continuum spectra. Since it is relatively inexpensive to obtain high- S/N spectra of nearby galaxies, detailed studies of stellar properties such as ages, metallicities and kinematics, which are obtained through accurate measurements of continuum emission and absorption lines, are few and mostly based on nearby galaxies.

There have been a plethora of high resolution spectra of local galaxies which have been obtained from surveys such as the Sloan Digital Sky Survey (SDSS), but the high redshift regime has had, until recently, limited sample sizes. The Large Early Galaxy Astrophysics Census (LEGA-C) survey has recently collected a few thousand high resolution spectra of $z \sim 1$ galaxies. It has been designed to provide both the quality and sample size required to make analogous measurements to those made by SDSS studies. Below, I give a brief overview of some spectroscopic surveys of galaxies in the local Universe, and beyond. This thesis is based on spectra of $z \sim 1$ galaxies from the LEGA-C survey, however, it is important to address surveys at different redshifts to obtain a consistent picture of galaxy formation and galaxy evolution.

1.3.1 Local Universe

The Sloan Digital Sky Survey (SDSS; York et al., 2000) is the largest and most detailed spectroscopic survey of the Universe that has ever been made. It has not only captured imaging of a third of the sky, but it has also collected high signal-to-noise (S/N) spectra of millions of astronomical objects, including galaxies, quasars and intergalactic gas. It has been active for over two decades and studies that have used the dataset have made significant steps towards understanding the formation and evolution of individual galaxies. These studies have constrained the ages and metallicities of stellar populations (e.g. Gallazzi et al., 2005); the structures, sizes as well as SFHs of galaxies (e.g. Kauffmann et al., 2003; van der Wel et al., 2009a); and many other parameters, including their scaling relations. Studies based on SDSS spectra of present-day galaxies have shown that low-mass galaxies have more extended SFHs that peak at later cosmic times compared to high-mass galaxies (e.g. Thomas et al., 2005; Cid Fernandes et al., 2007; McDermid et al., 2015; Ibarra-Medel et al., 2016). However, most $z \sim 0$ galaxies are old (> 5 Gyrs, Gallazzi et al., 2005); therefore, it is difficult to resolve their SFHs due to the similarity of stellar spectra in the age range > 5 Gyrs.

The latest phase, SDSS-IV (APOGEE-2, eBOSS and MaNGA; 2014-), aims to push our current knowledge even further. The surveys aim to explore the assembly history and evolution of our own galaxy by mapping the dynamical and chemical patterns of Milky Way stars (APOGEE-2); measure the expansion history of the Universe

by observing galaxies and quasars at different redshifts (eBOSS); and understand the SFH, merger history and quenching of $\sim 10,000$ nearby galaxies by making spectral measurements across the face of each galaxy (MaNGA; Bundy et al., 2015). The results from SDSS studies have undoubtedly pushed the envelop, however, the SDSS is mainly confined to the local universe, the survey's main sample has a median redshift of $z \sim 0.1$. To obtain a full picture of galaxy formation and evolution, we need to extend the properties of present-day galaxies to higher redshifts by making analogous measurements at larger lookback times.

1.3.2 Beyond the Local Universe

There have been a number of spectroscopic surveys beyond the local Universe. Surveys such as zCOSMOS (Lilly et al., 2007), DEEP2 (Newman et al., 2013), VVDS (Le Fèvre et al., 2013), VIPERS (Guzzo et al., 2014), KBSS (Steidel et al., 2014) and MOSDEF (Kriek et al., 2015) have collected thousands of galaxy spectra out to $z \sim 3$. They have been useful in measuring redshifts and studying star-formation and interstellar medium properties with emission lines. However, the quality of their spectra is not adequate to constrain the ages and metallicities of the stellar populations in individual galaxies. Stellar population measurements beyond the local Universe have been limited to either stacked spectra (e.g. Whitaker et al., 2013; Choi et al., 2014; Onodera et al., 2015), where spectra are added together in bins of mass and redshift; or small sample sizes ranging from single objects to a handful (e.g. van Dokkum and Brammer, 2010; Toft et al., 2012; van de Sande et al., 2013; Kriek et al., 2016), which do not represent the full galaxy population at their redshift. Stacking spectra effectively increases the signal of spectral features, enabling average measurements to be made. We know from photometric surveys that about 50% of stars formed since $z \sim 1$ (e.g. Muzzin et al., 2013a; Madau and Dickinson, 2014). This makes connecting galaxy populations between $z \sim 1$ and the present an important step towards understanding galaxy evolution. For this reason, the LEGA-C survey was carried out (see the following section), designed to provide both the required S/N and sample size to characterise the stellar population properties of a representative sample of $z \sim 1$ galaxies.

1.3.3 LEGA-C Survey

Recently, the Large Early Galaxy Astrophysics Census (LEGA-C, 2014-2018; van der Wel et al., 2016; Straatman et al., 2018) survey collected high S/N spectra of ~ 3000 galaxies in the COSMOS field ($R.A. = 10^h00^m$; $Dec. = +2^\circ12'$) with redshifts in the range of $0.6 < z < 1$ using the Very Large Telescope/VIMOS. The galaxies were K -band selected from the Ultra-VISTA catalog (Muzzin et al., 2013b). Selecting galaxies by their K -band magnitude is close to a stellar mass selection

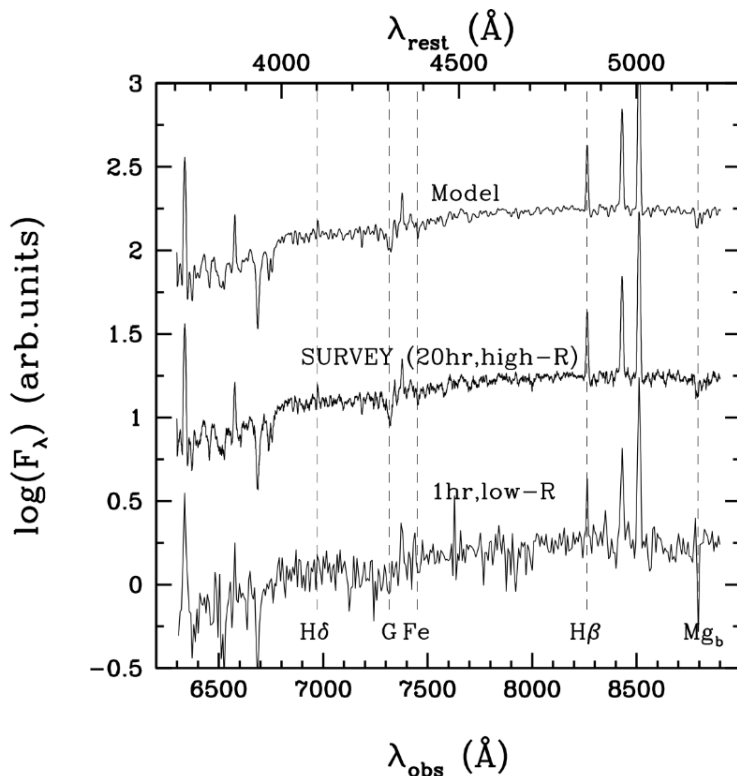


Figure 1.4: Simulated spectrum of a typical galaxy in the LEGA-C sample. The top panel shows a noise-free model spectrum with a 20 hour integration time, the middle spectrum has an added noise model and the bottom panel shows a simulated spectrum with a 1 hour integration time, which is typically used in redshift surveys, for comparison. Prominent diagnostic spectral features are indicated with vertical, dashed lines.

but it is not model dependant. Consequently, the dataset will not be affected by changes in methods used to estimate stellar masses and has a reduced dependence on variations in age, SF activity and extinction. K -band selection also ensures that the targets are spectroscopically bright enough in the desired observed wavelength range ($0.6\mu m - 0.9\mu m$). Each galaxy was observed for ~ 20 h, which results in spectra with signal-to-noise ratio (S/N) $\sim 20\text{\AA}^{-1}$ (with resolution $R \sim 3000$), comparable in quality to those obtained in the local universe after only an hour.

The LEGA-C survey provides us with high- S/N , high-resolution spectra of a representative sample of intermediate redshift galaxies that can be used to measure stellar population parameters like age and metallicity, as well as kinematic parameters like stellar velocity dispersion and dynamical mass. It the largest spectroscopic survey of distant galaxies to date, and will allow us to have a deeper understanding of the galaxy population at half the Universe's present age. Many studies which are analogous to those carried out for local galaxies with SDSS, for example, can now be carried out for galaxies at $z \sim 1$ which have a wider variation in age and SF activity.

Figure 1.4 shows a simulated spectrum of a typical LEGA-C galaxy with a 20 hour integration time, where the top spectrum is noise-free and the middle panel has an added realistic noise model. For comparison, the bottom panel shows the typical quality of spectra, with a 1 hour integration time, that would be obtained from redshift surveys (bottom panel). LEGA-C spectra, in contrast to typical spectra from redshift surveys, have the required quality to accurately measure diagnostic spectral features that can constrain the ages (e.g. Balmer absorption and emission lines) and metallicity (e.g. Mg) of $z \sim 1$ galaxies.

The survey aims to reconstruct the star formation histories of individual galaxies at intermediate redshifts; to investigate the conditions under which star formation quenches; and to determine how and to what extent galaxies grow after quenching. Several studies using the LEGA-C dataset have already been published (e.g. Barišić et al., 2017; Bezanson et al., 2018; Chauke et al., 2018; Spilker et al., 2018; Wu et al., 2018), and many more in the works. This includes work that will be presented in this thesis (see the following section).

1.4 Thesis Outline

In this thesis, I investigate the stellar population properties of $z \sim 1$ galaxies, uniquely enabled by the high- S/N , high-resolution continuum spectra provided by the LEGA-C survey. I demonstrate the advantage of measuring stellar population parameters of more distant galaxies, which have a wider variety in structure and SF activity, by determining their individual evolutionary paths, in order to gain knowledge on the processes that drive their evolution. In addition to making analogous measurements to those made by SDSS studies of nearby galaxies, I also compute individual evolution parameters that are not easily made with local galaxies, but they can be compared with results from simulations.

In Chapter 2, I present an algorithm that reconstructs the SFHs of LEGA-C's primary sample, in order to resolve the main formation phase of $z \sim 1$ galaxies and identify their evolutionary paths. I also investigate the dependence of individual SFHs on stellar mass, stellar velocity dispersion and SF activity. In Chapter 3, I use the reconstructed SFHs to trace the stellar mass evolution of $z \sim 1$ galaxies backwards out to redshift $z = 3$, in order to investigate whether galaxies maintain their mass ranking as they evolve and constrain the connection between progenitors and descendants. In Chapter 4, I determine whether rejuvenation episodes contribute significantly to the SFRD in the Universe as well as investigate rejuvenation properties in $z \sim 1$ quiescent galaxies. Finally, in Chapter 5, I give a summary of the results of these studies as well as future prospects. This thesis is based on my following papers: Chauke et al. (2018), Chauke et al. (2019), and Chauke et al. (2019b, in prep.)

STAR FORMATION HISTORIES OF $Z \sim 1$ GALAXIES IN LEGA-C[†]

In order to analyse the stellar population properties of galaxies in the LEGA-C Survey, we have to resolve their main formation phase and identify their evolutionary paths. In this chapter, I present an algorithm that reconstructs the SFHs of the primary sample, using a custom full-spectrum fitting algorithm that incorporates the *emcee* and *FSPS* packages. I then analyse the correlation between individual SFHs and a number of galaxy parameters.

2.1 Introduction

The ability to reconstruct the star-formation histories of galaxies, by characterising their stellar populations, allows one to trace their individual evolution through time, and thereby directly connect their descendants to their progenitors at higher redshifts. Thus far, high-redshift galaxy surveys have produced snapshots of the galaxy population at different points in cosmic time, which produces tight boundary conditions for galaxy formation models. However, the importance of the many physical processes included in these models are not directly constrained. We still do not know individual star-formation histories (SFHs) and how these are related to global galaxy properties. To constrain galaxy formation theories more directly, ‘archaeological’ reconstruction can be used to trace the evolution of individual galaxies over time, and then the dependence of individual SFHs on stellar mass, stellar velocity dispersion and star-formation (SF) activity can be explored.

[†]The contents of this chapter are adapted from Chauke et al. (2018). The paper is published in the *Astrophysical Journal*. I myself conducted the research, analysed the results and wrote the text for the paper.

Reconstructing SFHs requires high resolution spectra of galaxies. Ideally, individual stars would be resolved, as they are for local dwarf galaxies (e.g., Weisz et al., 2011). However, in most cases we have to rely on integrated stellar light, though if a galaxy’s main star formation (SF) epoch lies at $z > 1$, we cannot temporally resolve its stellar age distribution, even with the highest-quality spectra. While there is a plethora of high resolution spectra of galaxies in the local universe, most of these galaxies are too old ($> 5\text{Gyrs}$, Gallazzi et al., 2005) to resolve their star-formation histories (SFHs) due to the similarity of stellar spectra in the age range $> 5\text{Gyrs}$. The general insight gained from the ‘archaeological’ studies of these galaxies is that low-mass galaxies have more extended SFHs that peak at later cosmic times compared to high-mass galaxies (‘downsizing’, e.g., Gallazzi et al., 2005; Thomas et al., 2005, 2010). Many of these studies involved the use of fossil record methods on SDSS (Sloan Digital Sky Survey, York et al., 2000) spectra of local galaxies (e.g. Juneau et al., 2005; Thomas et al., 2005; Cid Fernandes et al., 2007; Tojeiro et al., 2009; McDermid et al., 2015; Ibarra-Medel et al., 2016). However, downsizing has also been seen in other studies, such as studies by Cimatti et al. (2006), who corrected luminosity function data of early-type galaxies by adopting the empirical luminosity dimming rate derived from the evolution of the Fundamental Plane of field and cluster massive early-type galaxies, as well as Leitner (2012), who derived the average growth of stellar mass in local star-forming galaxies using a Main Sequence Integration approach.

One approach to probe the high-redshift regime, is to obtain an integrated view of galaxy evolution. Thus far, this has been the focus of spectroscopic observations of distant galaxies: the evolution of the star-formation rate density (SFRD) in the universe has been extensively studied (e.g., Karim et al., 2011; Madau and Dickinson, 2014; Khostovan et al., 2015; Abramson et al., 2016). The majority of these studies indicate that the SFRD increased from high redshift to $z \sim 2$, and has since been decreasing steeply. Coupled with this, are number density evolution studies which show an increasingly dominant population of quiescent galaxies (e.g., Pozzetti et al., 2010; Brammer et al., 2011; Moustakas et al., 2013; Muzzin et al., 2013a).

Another approach is to use advanced analysis techniques to trace SFHs from photometric measurements (Pacifci et al., 2016; Iyer and Gawiser, 2017), however, individual galaxy evolution is not easily traced with this method due to high uncertainties. In this case, one can investigate average SFHs of galaxies as Pacifci et al. (2016) have done by applying spectral energy distribution models to compute the median SFHs of 845 quiescent galaxies at $0.2 < z < 2.1$. They found that galaxy stellar mass is a driving factor in determining how evolved galaxies are, with high mass galaxies being the most evolved at any time. The limitation with these approaches is that we cannot connect progenitors to descendants: studies from mass-matched samples have resulted in multiple solutions (e.g., Torrey et al., 2017). To understand the mechanics of how galaxies evolve, it is crucial to expand our view from focusing on the population of galaxies as a whole, to investigating how the star-formation

rate (SFR) of individual galaxies varies with time.

Probing the SFHs of individual galaxies, however, still requires high-resolution, high-quality stellar continuum spectra, which are expensive to obtain. Consequently, high-redshift samples are small and often selected with criteria to optimize data quality and sample size rather than represent the full galaxy population. Jørgensen and Chiboucas (2013) obtained spectra for ~ 80 cluster galaxies at $z = 0.5 - 0.9$ and found ages of 3 – 6 Gyrs, consistent with passive evolution between $z \sim 2$ and the present. Stellar population measurements of ~ 70 $z \sim 0.7$ galaxies with stellar masses $> 10^{10}M_{\odot}$ were performed by Gallazzi et al. (2014); they found that passive galaxies have ages and metallicities consistent with those of present-day galaxies, and that star-forming galaxies require further star-formation and metal enrichment to evolve into present-day descendants. Choi et al. (2014) analysed stacked spectra of thousands of passive galaxies in the redshift range $0.1 < z < 0.7$ and also found age evolution consistent with mostly passive evolution, with little dependence on mass at $z > 0.5$. Belli et al. (2015) measured ages of 1 – 4 Gyrs for several dozen passive galaxies at redshifts $1 < z < 1.6$, indicating that we are approaching the cosmic epoch at which massive, passive galaxies stopped forming stars. Finally, at $z > 1.5$, measurements are limited to stacked spectra (e.g., Whitaker et al., 2013; Onodera et al., 2015) or sample sizes ranging from single objects to a handful (e.g., van Dokkum and Brammer, 2010; Toft et al., 2012; van de Sande et al., 2013; Kriek et al., 2016). The typical age of massive, passive galaxies at those redshifts is found to be 1 Gyr or less, with short formation time scales. From this brief review, it is evident that samples at large lookback time are generally small and/or stacked. Furthermore, ages are usually estimated by assuming a single stellar population, which is arguably justified for very massive galaxies at late cosmic epochs, but not in general.

The LEGA-C (Large Early Galaxy Astrophysics Census, van der Wel et al., 2016) survey is collecting high S/N spectra of ~ 3000 galaxies in the redshift range $0.6 < z < 1$, selected only by their K -band magnitude (a proxy for stellar mass). The data, which are comparable in quality to those obtained in the nearby universe, probe the internal kinematics of stars and gas, and the ages and metallicities of stellar populations. This enables us, for the first time, to reconstruct the SFHs of individual galaxies at large look-back time that are representative of the population. These reconstructed SFHs can provide a direct connection between progenitors and descendants, and allow us to constrain when, and how quickly, galaxies formed their stars.

Over the past decade, there have been several algorithms developed to recover SFHs, viz. *MOPED*, *STARLIGHT*, *STECMAP*, *VESPA*, *ULYSS* and *FIREFLY* (Heavens et al., 2000; Cid Fernandes et al., 2005; Ocvirk et al., 2006; Tojeiro et al., 2007; Koleva et al., 2009; Wilkinson et al., 2015). We develop our own approach in this study to tailor the problem for galaxies at $z \sim 1$. The main differences between our

algorithm and some of those listed above are the use of composite stellar populations (a group of stars which range in age within a given interval) instead of simple stellar populations (stars born from a single burst in star formation); using a defined set of template spectra which allow for direct comparisons of the SFHs; as well as the assumption of constant star formation within a given time interval. The galaxy spectra are also not continuum-normalised in the fitting process, but photometry is used to calibrate the fluxes.

The goal of this paper is to reconstruct the SFHs of galaxies in the LEGA-C sample and investigate the dependence of individual SFHs on stellar mass, stellar velocity dispersion and star-formation (SF) activity. The paper is outlined as follows. In Section 4.2 we give a brief overview of the LEGA-C dataset. In Section 2.3 we introduce the model for reconstructing the SFHs of the galaxies as well as tests of the model. In Section 2.4 we present a sample of the resultant fits and general trends of measured parameters. In Section 2.5 we investigate the SFH as a function of stellar velocity dispersion and stellar mass. We demonstrate that we can verify the relation between the evolution of SFHs and mass, and we investigate the variation in the reconstructed SFHs, at fixed stellar velocity dispersion. Finally, in Section 2.5 we summarise the results. A Λ CDM model is assumed with $H_0 = 67.7 \text{ km s}^{-1} \text{ Mpc}^{-1}$, $\Omega_m = 0.3$ and $\Omega_\Lambda = 0.7$.

2.2 Data

LEGA-C (van der Wel et al., 2016) is an ongoing ESO Public Spectroscopic survey with VLT/VIMOS of ~ 3000 galaxies in the COSMOS field ($R.A. = 10^h 00^m$; $Dec. = +2^\circ 12'$). The galaxies were selected from the Ultra-VISTA catalog (Muzzin et al., 2013b), with redshifts in the range $0.6 < z < 1.0$. The galaxies were K-band selected with a magnitude limit ranging from $K(AB) = 21.08$ at $z = 0.6$ to $K(AB) = 20.7$ at $z = 0.8$ to $K(AB) = 20.36$ at $z = 1.0$ (stellar masses $M_* > 10^{10} M_\odot$). These criteria were chosen to reduce the dependence on variations in age, SF activity and extinction, as well as ensure that the targets were bright enough in the observed wavelength range ($0.6 \mu\text{m} - 0.9 \mu\text{m}$) to obtain high quality, high resolution spectra ($R \sim 3000$). Each galaxy is observed for ~ 20 h, which results in spectra with $S/N \sim 20 \text{ \AA}^{-1}$.

The analyses in this work are based on the first-year data release¹, which contains spectra of 892 galaxies, 678 of which are in the primary sample and have a $S/N > 5 \text{ \AA}^{-1}$ between rest-frame wavelengths 4000 \AA and 4300 \AA (typically, $S/N \sim 20 \text{ \AA}^{-1}$). Emission line subtracted spectra are used in the fitting algorithm; therefore, the emission line spectrum of each galaxy, computed using the Penalized Pixel-

¹<http://www.eso.org/qi/catalogQuery/index/93>

Table 2.1: Properties of the *FSPS* template spectra.

Age Bin ^a	SFR ^b	M _* ^c	L _{bol} ^d
log(yr)	M _⊙ /yr	M _⊙	log(L _⊙)
0.000-8.000	1.000×10 ⁻⁸	0.837	1.964
8.000-8.300	1.005×10 ⁻⁸	0.711	0.885
8.300-8.475	1.010×10 ⁻⁸	0.748	0.650
8.475-8.650	6.750×10 ⁻⁹	0.731	0.497
8.650-8.750	8.646×10 ⁻⁹	0.718	0.382
8.750-8.875	5.332×10 ⁻⁹	0.707	0.285
8.875-9.000	3.998×10 ⁻⁹	0.695	0.187
9.000-9.075	5.305×10 ⁻⁹	0.685	0.127
9.075-9.225	2.040×10 ⁻⁹	0.671	0.099
9.225-9.375	1.444×10 ⁻⁹	0.652	-0.043
9.375-9.525	1.022×10 ⁻⁹	0.639	-0.161
9.525-9.845	2.681×10 ⁻¹⁰	0.618	-0.347

^a Age interval of CSP templates. ^b SFR s.t. 1M_⊙ of stars formed within the interval. ^c Stellar mass (including stellar remnants) with mass loss accounted for. ^d Bolometric luminosity.

Fitting method (pPXF, Cappellari and Emsellem, 2004), is subtracted from the observed spectrum. For details of the emission line fitting procedure, see Bezanson et al. (2018). As part of the analysis of the model, we use the following measured quantities: stellar velocity dispersions (σ_*), 4000Å break (D_n4000) and H δ equivalent width indices [EW(H δ)], U-V colours, stellar masses ($M_{*,FAST}$), UV+IR SFRs, and UV+IR specific SFRs (sSFR_{UV+IR}). Stellar masses are determined using FAST (Kriek et al., 2009) based on photometric measurements, Bruzual and Charlot (2003) stellar population libraries, adopting a Chabrier (2003) Initial Mass Function (IMF), Calzetti et al. (2000) dust extinction, and exponentially declining SFRs. The UV+IR SFRs are estimated from the UV and IR luminosities, following Whitaker et al. (2012). For details of the data reduction procedure, see van der Wel et al. (2016).

2.3 Spectral Fitting Technique

2.3.1 Stellar Population Model

To reconstruct the SFHs of galaxies, one needs to gauge the various ages of stellar populations within these galaxies. This is done using stellar population spectra generated with the Python implementation of the Flexible Stellar Population Synthesis package (*FSPS v3.0*; Conroy and Gunn, 2010; Conroy et al., 2009; Foreman-

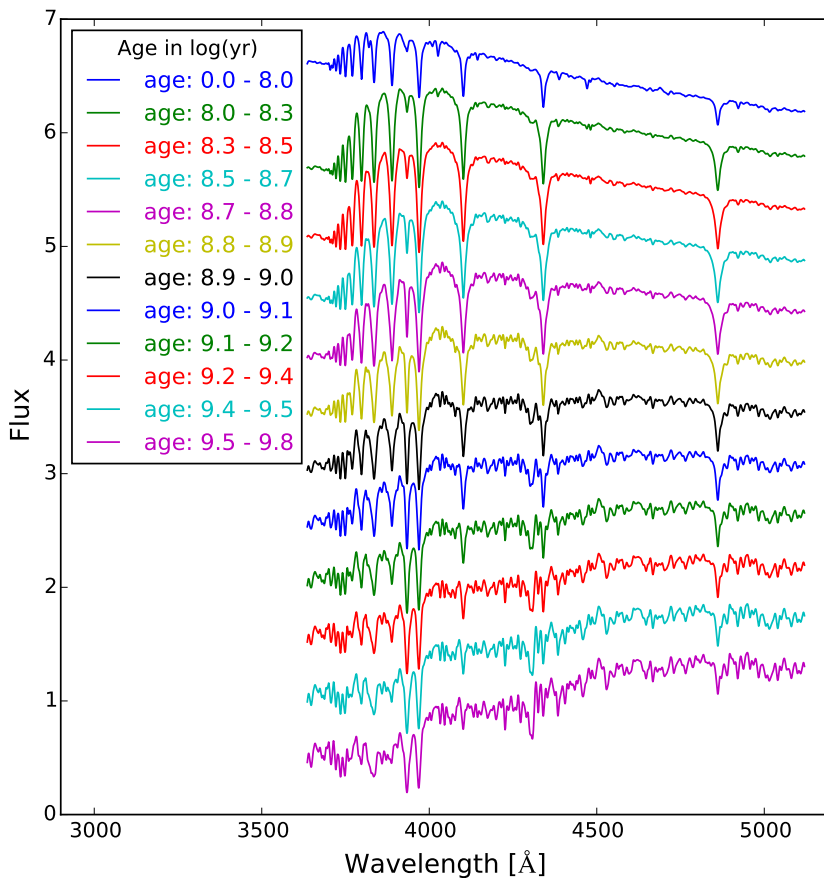


Figure 2.1: Template CSP spectra used to fit LEGA-C galaxies. They were generated from *FSPS*, using the time intervals listed in Table 2.1, with solar metallicity and arbitrary velocity dispersion; and they have been normalised and shifted here for comparison purposes.

Mackey et al., 2014), using the MILES spectral library (Sánchez-Blázquez et al., 2006), Padova isochrones (Girardi et al., 2000; Marigo and Girardi, 2007; Marigo et al., 2008) and a Kroupa initial mass function (Kroupa et al., 2001).

A galaxy spectrum is approximated to be a linear combination of template spectra at varying ages, attenuated by dust:

$$f_{\lambda} = \sum_{i=1}^n m_i T_{\lambda,i} 10^{-0.4k_{\lambda}E(B-V)_i}, \quad (2.1)$$

$$k_{\lambda} = 2.659 \left(-2.156 + \frac{1.509}{\lambda} - \frac{0.198}{\lambda^2} + \frac{0.011}{\lambda^3} \right) + 4.05$$

where n is the number of stellar population spectra to fit to the galaxy, $T_{\lambda,i}$ are the template spectra, m_i are the weights that scale the templates to match the spectra

of the galaxy, k_λ is the reddening curve (Calzetti et al., 2000), and $E(B - V)_i$ are the dust reddening values.

We generate 12 composite stellar population spectra (CSPs), with solar metallicity (see Section 2.3.3), covering ages from 0 to about 7Gyrs, the age of the Universe in LEGA-C’s redshift range. To determine the intervals of the 12 age bins of the CSPs, simple stellar population spectra (SSPs) were generated and the cumulative absolute difference from one spectrum to another was calculated as the age was increased; which was then divided into 12 percentiles with equal width (see Table 2.1 and Figure 2.1 for the properties of the CSPs in each age bin). This method of determining the time intervals generates template spectra that optimise the temporal sampling of an evolving stellar population. In practice, the age bins are ~ 0.15 dex wide over the age range 0 – 7Gyrs.

The template spectra are generated with a constant SFR and are normalised such that $1M_\odot$ of stars are formed within each time bin (stellar masses include stellar remnants). Note that there is mass loss in each bin as massive stars die off (see Table 2.1). We assume a constant SFR within each time bin as it presents a more realistic evolution of a galaxy’s star formation with time, and can take into account rapid changes in the SFH. Choosing SSP templates would not lead to significantly different SFHs, however, it would lead to aliasing effects when reconstructing the SFHs for samples of galaxies. The templates are also broadened to the velocity dispersion of the galaxies (Bezanson et al., 2018). It is assumed that dust reddening is the same for all populations except for the youngest population (age < 100 Myrs). Dust extinction is expected to be different for young stellar populations as they are usually observed to be nested in the dust of their molecular birth clouds (Charlot and Fall, 2000). Therefore, two dust reddening values are fit for: $E(B - V)_1$, for the age range 0 – 100Myrs, and $E(B - V)_2$, for the rest of the age ranges.

2.3.2 Fitting Algorithm

To find the optimal values for the 14 parameters, viz. the 12 weight factors (m_i) for the 12 CSP templates and 2 dust reddening values ($E(B - V)_i$), we used *emcee*, a Python implementation of an affine invariant ensemble sampler for MCMC (Foreman-Mackey et al., 2013) which was proposed by Goodman and Weare (2010). It uses MCMC ‘walkers’ which randomly explore the parameter space, where each proposed step for a given walker depends on the positions of all the other walkers in the ensemble, with the aim of converging to the most likely parameter values.

The priors for the 14 parameters were set such that all parameter values were always greater or equal to 0, and the upper limit for $E(B - V)_i$ was set to 3. The parameter value for the youngest bin was initially set to be equal to the measured SFR from

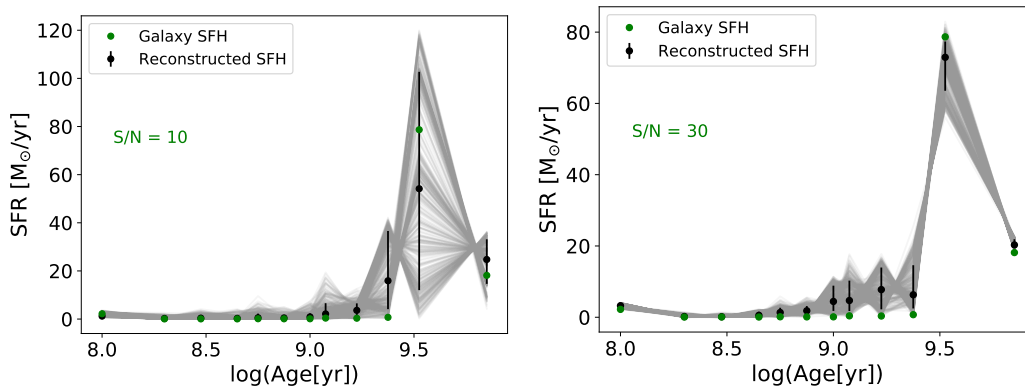


Figure 2.2: Reconstructed SFH (black) of a synthetic galaxy (green) with $S/N = 10 \text{ \AA}^{-1}$ (left) and $S/N = 30 \text{ \AA}^{-1}$ (right). The converged walkers are shown in grey and the upper and lower uncertainties are based on the 16th and 84th percentiles, respectively, as explained in Section 2.3.2. By $S/N = 30 \text{ \AA}^{-1}$, the recovered SFHs predict the stellar mass, age and luminosity with precision $\leq 0.1 \text{ dex}$.

UV+IR measurements, but it was allowed to vary between 1/3 and 3 times that value during the fitting process, allowing for measurement errors. For the other bins, the best fitting single template, computed using least-squares fitting, was assigned all the stellar mass, with all other parameter values set to 10^{-6} . Starting with equal SFRs in all bins also recovers the SFHs, however, the algorithm may take longer to converge to the optimal values.

For each galaxy, 100 MCMC walkers were used, initiated in a small region around the starting values mentioned above. A total of 20000 samples were taken and 1000 steps were kept after burn-in. The mean acceptance fraction was $\gtrsim 0.2$ and the typical autocorrelation time was ~ 95 iterations. The optimal values for the parameters are taken as the 50th percentile of the list of samples of the converged walkers, and the lower and upper uncertainties are the 16th and 84th percentiles, respectively. The fitting algorithm resulted in 607 good fits based on their normalised χ^2 values (< 5 , from visual inspection of the fits), and these were used in the analyses. The spectra that were not well-fit were mainly due to low S/N and AGN.

2.3.3 Robustness of Fitting Results

To assess the robustness of the model, we performed the following tests: generate and fit synthetic spectra; compare model stellar mass measurements of the LEGA-C population with those obtained from broad-band photometry (see Section 4.2); fit a sample of SDSS spectra and compare model stellar masses with literature measurements; and test the assumption of solar metallicity.

Synthetic galaxy spectra were generated with varying SFHs using the CSPs in Section 2.3.1, including simulated noise that mimics LEGA-C variance spectra, to compare how well the algorithm recovered the SFHs. 20 SFHs were generated for each S/N (5, 10, 20, 30, 40, 50 and 60 \AA^{-1}), and the average deviations of the true $a_{\langle MW \rangle}$, stellar mass and luminosity from the best-fitting model parameters were computed. In general, the model sufficiently recovered the SFHs, however, we note that the quality of the results depends on the noise introduced into a spectrum (see Figure 2.2 for two examples). Stellar mass and luminosity are recovered with precision $\leq 0.1\text{dex}$ for $S/N \geq 20$, while $a_{\langle MW \rangle}$ only requires $S/N \geq 10$ to reach the same level of precision. We note that these tests only constrain the purely random uncertainties due to the noise in the spectra while they do not include systematic errors in the data (e.g., sky subtraction, flux calibration) and systematic uncertainties in the FSPS model spectra.

Imposing the MCMC model on the LEGA-C dataset and comparing the stellar masses measured from the model to those measured from FAST (using photometric measurements), resulted in very good agreement between the two methods, with a scatter of $\sim 0.2\text{dex}$ and an offset of $\sim 0.03\text{dex}$. This scatter is larger than the formal uncertainty on our mass measurements ($\sim 0.15\text{dex}$).

We used the fitting algorithm on a sample of 20 SDSS spectra of massive local galaxies ($z \sim 0.1$), selected by stellar mass ($M_* > 10^{10}$), to determine whether the model could recover the stellar masses measured in the literature. We compared the model stellar masses to measurements from the Portsmouth method (Maraston et al., 2009) and found satisfactory agreement, with a $\sim 0.2\text{dex}$ scatter. The maximum age of the templates was increased to $\sim 12\text{Gyrs}$ to account for the low redshift (~ 0.1) of the SDSS galaxies. The 0.2dex random uncertainty is an indication of how results vary as a consequence of using a different SPS model (here, Maraston et al. (2009) vs. *FSPS*) and fitting algorithm.

Solar metallicity was used to generate all the CSPs because according to Gallazzi et al. (2005, 2014), the metallicity-mass relation flattens out to solar metallicity in LEGA-C’s mass range ($\log(M) \gtrsim 10.5$), for $z \sim 0.7$ galaxies. On the other hand, Jørgensen et al. (2017) find evidence for evolution in the metallicity for cluster galaxies, as well as a trend of increasing metallicity with increasing velocity dispersion. We test our approach by repeating our fits with implausibly low metallicity ($0.4 Z_{\odot}$, sub-solar) and high metallicity ($2.5 Z_{\odot}$, super-solar) CSPs. We find no significant differences in the χ^2 values of the fits, but, naturally, the inferred ages depend on the chosen metallicity. If we assign sub-solar metallicity for galaxies in our sample, the derived mass-weighted and light-weighted ages are older by 0.05 and 0.08dex, respectively, with a standard deviation of 0.16 and 0.24dex, respectively. If we assign super-solar metallicity for the sample, the light-weighted ages are younger by 0.03dex, with a standard deviation of 0.20dex. The mass-weighted age changes from solar to high metallicity are not normally distributed: 80% of the galaxies have the

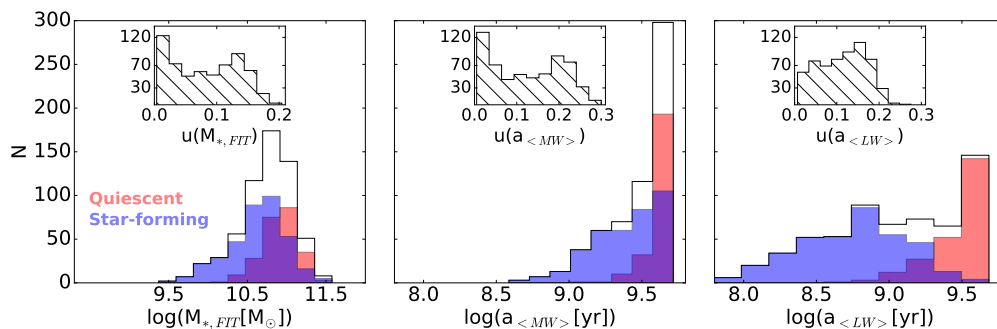


Figure 2.3: Distributions of $M_{*,spec}$ (left), $a_{<MW>}$ (middle) and $a_{<LW>}$ (right) of the LEGA-C sample. The quiescent and star-forming populations (as defined in Section 2.5.1) are shown in red and blue, respectively. The distribution of the uncertainties for each parameter are shown at the top of each figure.

same age to within 0.20dex, while for the remaining 20% the change in age ranges from 0.2 to 0.9dex. However, only 10 of these galaxies’ mass-weighted ages change by ≥ 0.5 dex and they have a mean light-weighted age of ~ 0.4 Gyr. The age changes do not depend on the measured stellar mass or stellar velocity dispersion.

The velocity dispersion-metallicity trend presented by Jørgensen et al. (2017) implies that our assumption of solar metallicity for all galaxies may introduce a correlation between velocity dispersion and age. Our tests show that across the velocity dispersion range $\sigma_* = 100 - 250 \text{ km s}^{-1}$, the magnitude of this effect would be at most 0.15dex and likely less. This potential bias is insufficient to explain the σ_* -age relation we find in Section 2.4.2. Follow-up studies that explore the interdependence of age, metallicity and other galaxy properties will need to take metallicity variations into account.

2.4 Fitting Results

2.4.1 Model Outputs

Figure 2.3 shows the distribution of the model-measured stellar masses ($M_{*,spec}$, left panel), mean mass-weighted ages² ($a_{<MW>}$, middle panel) and mean light-weighted ages² ($a_{<LW>}$, right panel) of the LEGA-C sample, along with the distribution of uncertainties for each parameter. The distributions are separated into the quiescent (red) and star-forming (blue) populations to show the differences in the distributions based on current SF activity (see Section 2.5). The galaxies in the LEGA-C sample span a broad range of ages: $a_{<LW>}$ can be as young as 60Myrs and as old as

²Mean mass-weighted and light-weighted ages are obtained by averaging the midpoint ages of the CSPs weighted by luminosity and mass, respectively.

4.8Gyrs, and has a median value of 1.2Gyrs (see Figure 2.3). $a_{\langle MW \rangle}$ ranges from about 400Myrs to about 5.2Gyrs, with a median value of 3.8Gyrs. However, most of these galaxies are old, with about 60% being older than 3Gyrs. The $M_{*,spec}$ of the galaxies ranges from $\sim 2 \times 10^9 M_{\odot}$ to $\sim 4 \times 10^{11} M_{\odot}$, with a median value of about $6 \times 10^{10} M_{\odot}$. The formal age and mass uncertainties lie in the ranges 1-60% and 1-40%, respectively. As stated in Section 2.3.3, these uncertainties do not include systematic errors.

2.4.2 Sample SFHs

Figure 4.5 shows the spectra of a sample of LEGA-C galaxies (in $a_{\langle MW \rangle}$ order) along with the best-fitting model spectra as described by Equation 2.1 using the optimal parameter values from *emcee*. The weight factors, m_i , represent the star formation histories of these galaxies (shown on the bottom-right of each figure). The resultant normalised χ^2 , dust reddening values ($E(B-V)_i$), stellar masses ($M_{*,spec}$), luminosities (L_{spec}) and mean mass-weighted ages ($a_{\langle MW \rangle}$) from the model are shown in red. The sample was selected to display the wide range of SFHs recovered.

The reconstructed SFHs reveal that although most galaxies at $z \sim 1$ have $a_{\langle MW \rangle} > 3$ Gyrs, the sample spans a wide range of histories. For the older massive galaxies, the oldest template (stars in the age range ~ 3 -7Gyrs) contributes to the majority of their mass. Some of these galaxies only contain the oldest stars and have since been quiescent, i.e. for the past ~ 3 Gyrs (see the SFHs of 108361, 211736 and 130052 in Figure 4.5). However, some galaxies were quiescent for several Gyrs and then had a renewed period of growth, either due to SF rejuvenation, or merging with a younger population. A merger could result in either an integration of the younger population with no further activity, or trigger bursts of star formation. This young population of stars accounts for $\sim 10\%$ of the mass of these galaxies (e.g. 206042, 131869 and 131393 in Figure 4.5). We will explore the frequency of such rejuvenation events in more detail in a follow-up study.

2.4.3 General Trends

Figure 2.5a presents the distribution of $EW(H\delta)$ as a function of the D_n4000 break colour-coded by the time after which the final 10% of stars were formed (a_{10} , left panel), $a_{\langle LW \rangle}$ (middle panel) and $a_{\langle MW \rangle}$ (right panel), estimated from the model. The $EW(H\delta)$ - D_n4000 distribution is analysed in depth in Wu et al. (2018). As expected, for all three age parameters, galaxies generally evolve from the upper-left region (high $EW(H\delta)$ and low D_n4000) to the lower-right region (low $EW(H\delta)$ and high D_n4000) as they age. a_{10} and $a_{\langle LW \rangle}$ are more correlated with each other than $a_{\langle MW \rangle}$ because they track young stars; they also have smoother transitions in

2.4.3. General Trends

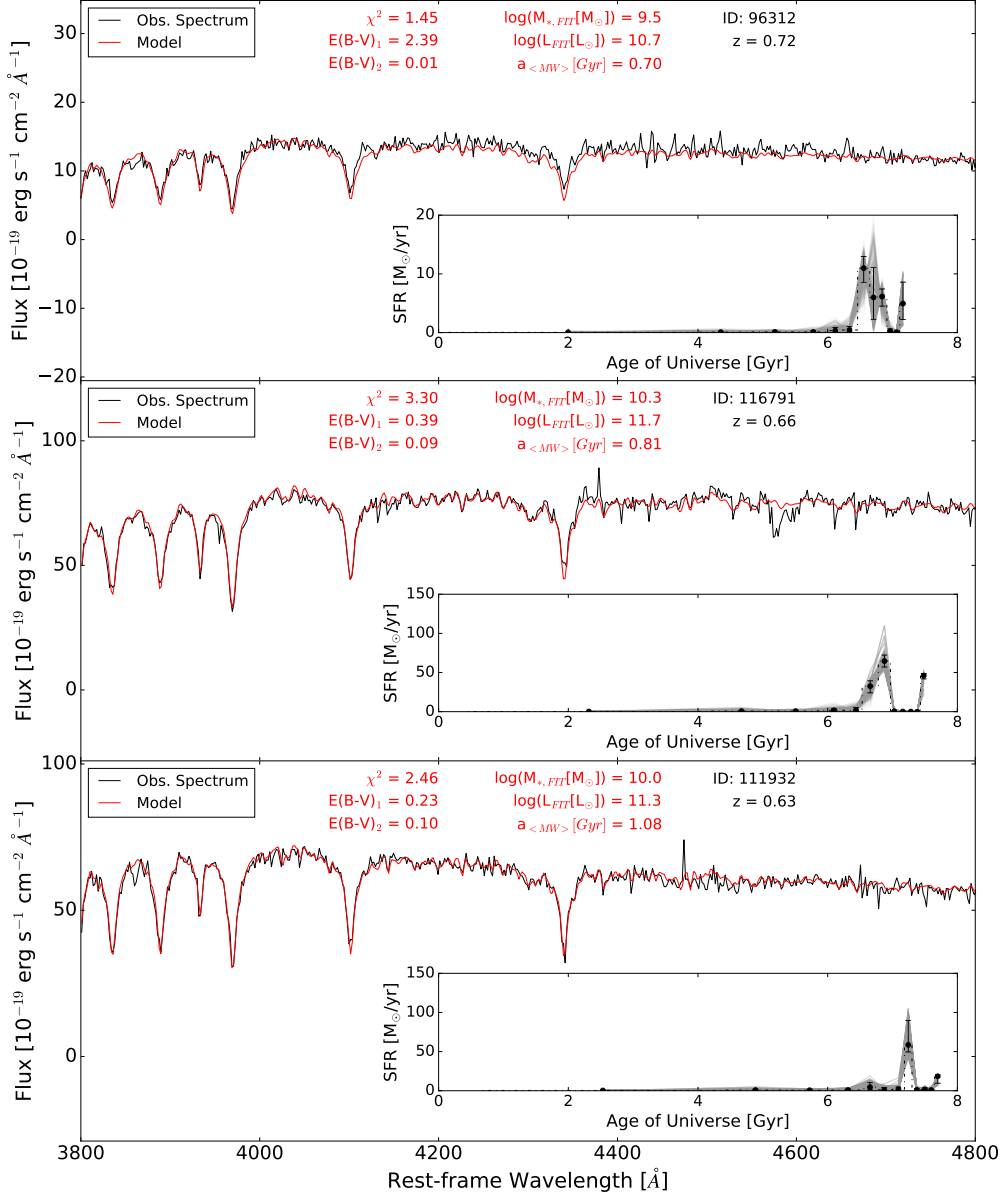


Figure 2.4: Sample of emission line subtracted spectra of 12 LEGA-C galaxies with the best fitting model obtained from combining the 12 template spectra using MCMC. The bottom-right figure, in each plot, is the reconstructed star formation history (the converged walkers are shown in grey). The MCMC resultant mass, luminosity, mass-weighted age and dust reddening values are shown in red. The spectra are ordered by $a_{\langle MW \rangle}$.

the $\text{EW}(\text{H}\delta)\text{-D}_n4000$ plane because those features primarily track recent SF activity ($\lesssim 1\text{Gyr}$). Figure 2.5b shows the rest-frame U-V colour as a function of restframe V-J colour-coded by the same 3 age parameters as above. Once again, expected trends are seen: a_{10} , $a_{\langle LW \rangle}$ and $a_{\langle MW \rangle}$ correlate with the restframe colours as U-V and V-J primarily reflect recent star formation ($\sim 1\text{Gyr}$). There is a notable

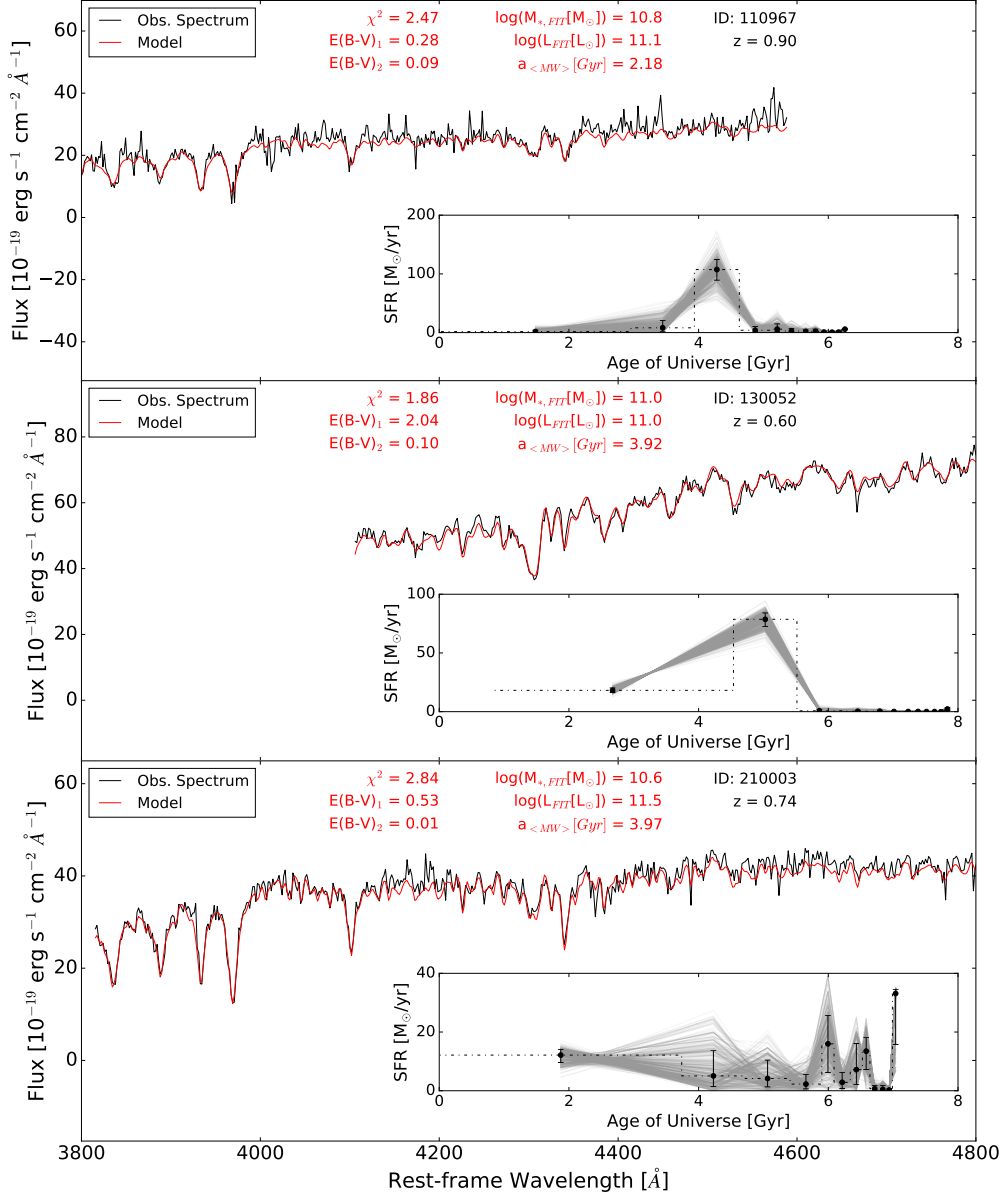


Figure 2.4 (Continued)

population of old galaxies ($a_{\langle MW \rangle} > 3.5 \text{ Gyrs}$) with relatively blue colours, which indicates that these galaxies have extended SFHs.

To demonstrate the validity of the old galaxies ($a_{\langle MW \rangle} > 3.5 \text{ Gyrs}$) in the young region of the $\text{EW}(\text{H}\delta)\text{-}D_n4000$ plane, i.e. galaxies in red in Figure 2.5's right panel, with $D_n4000 < 1.3$ and $\text{EW}(\text{H}\delta) > 2$, we refer to their SFHs. These galaxies formed most of their stars early on, but also have significant recent star formation. While some seem to have been quiescent at some point in their history before they were possibly rejuvenated or merged with another galaxy (e.g. 206042 in Figure 4.5), others formed stars throughout their history (e.g. 210003 in Figure 4.5). Moreover,

2.4.3. General Trends

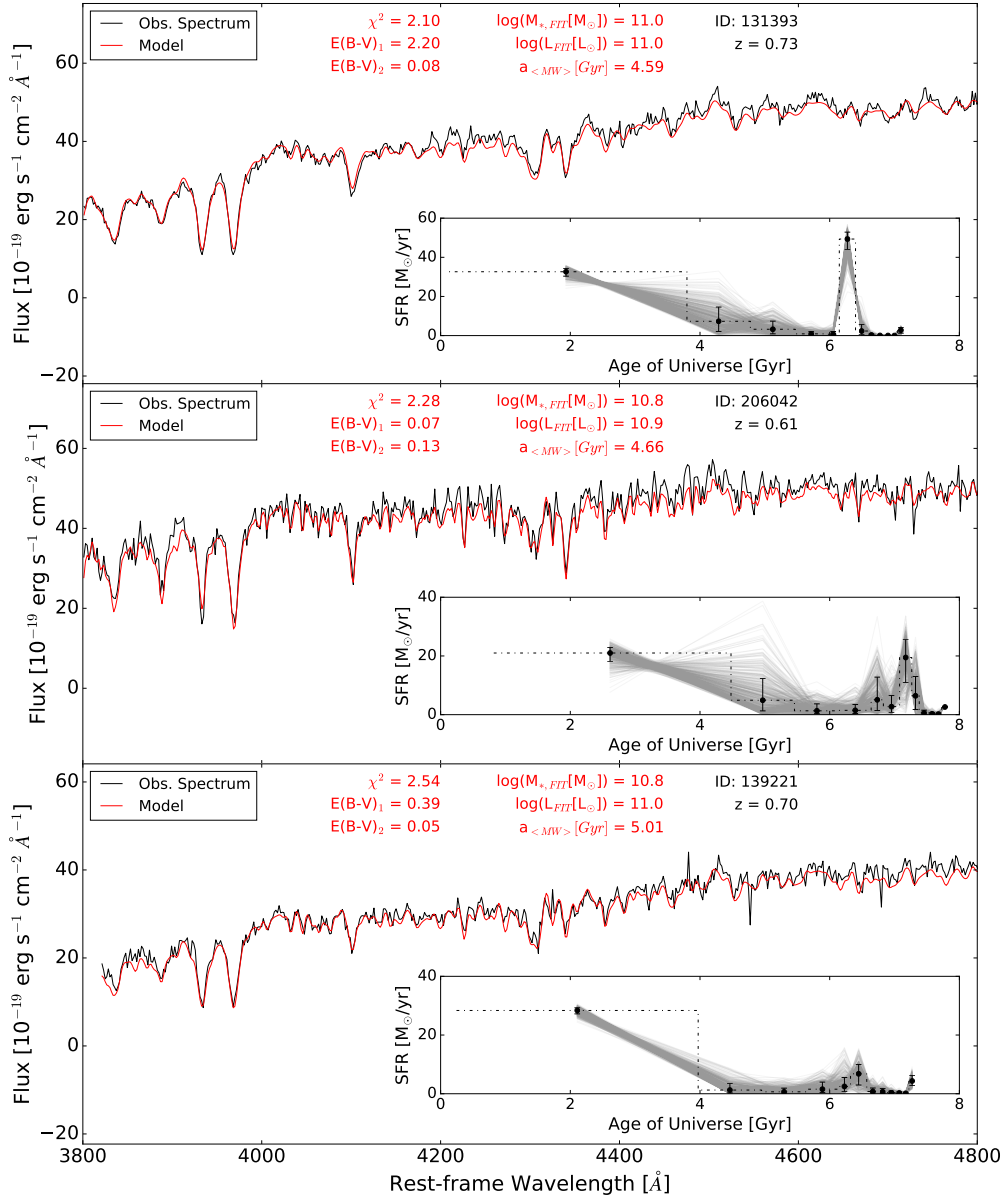


Figure 2.4 (Continued)

the presence of young and old populations can be seen in their spectra: they have clearly visible Balmer lines, characteristic of younger galaxies; but they also have H and K absorption lines of singly ionized Calcium with similar strengths, which is typical of older galaxies, in addition to the presence of the G-band (absorption lines of the CH molecule) around 4300\AA . As a test, we reran the fits of these galaxies excluding the 3 oldest templates and found that the spectra cannot be well fit.

There is also a population of galaxies that seem to contain only young stars (e.g. 111932 and 116791 in Figure 4.5), which would imply that these galaxies formed more than 90% of their mass recently (when the Universe was $> 6\text{Gyr}$). To test if

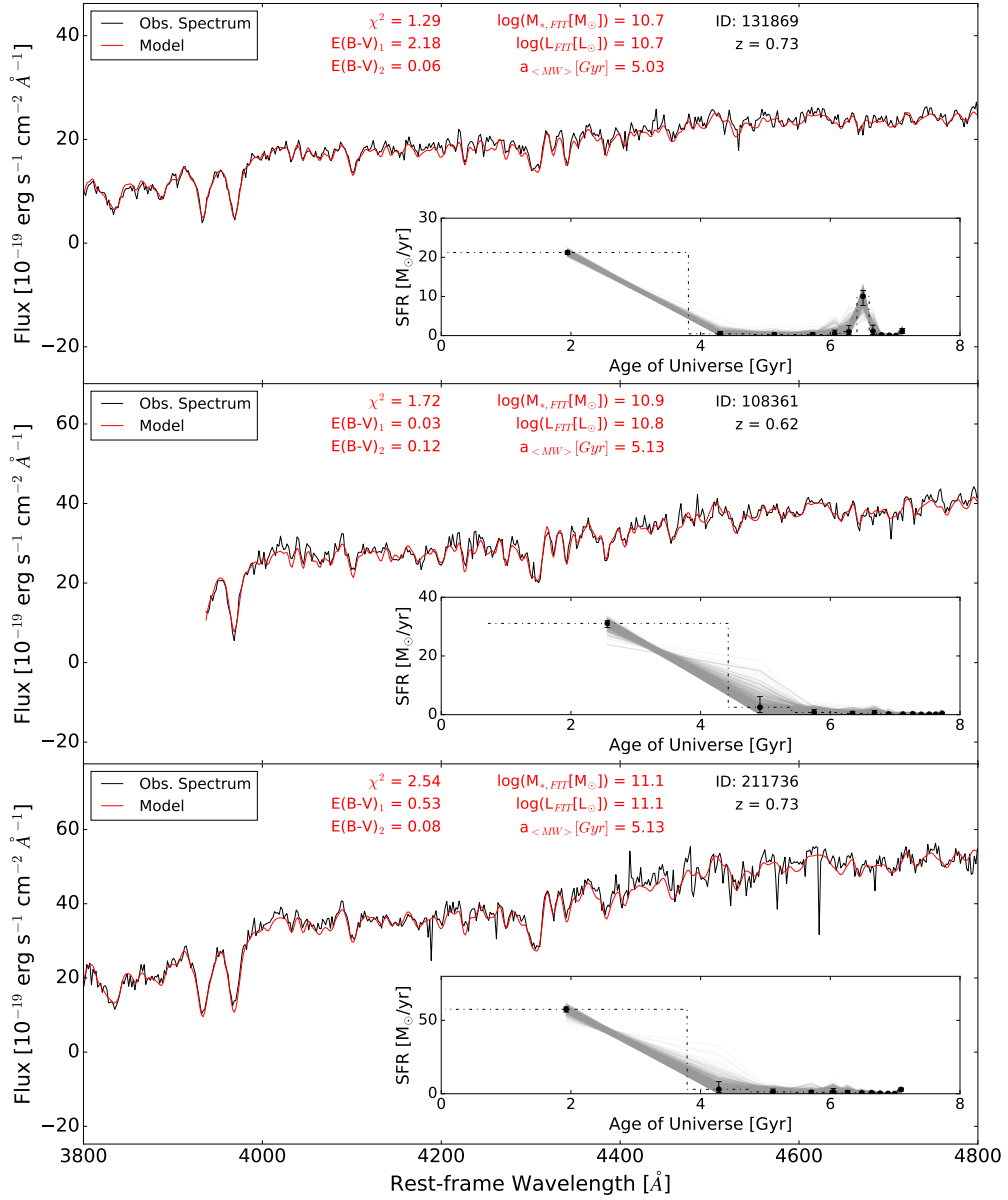


Figure 2.4 (Continued)

young populations are ‘outshining’ the rest of these galaxies, i.e. if there are hidden populations of old stars, we reran the fits of these galaxies allowing only the oldest template parameter to vary. We found that the contribution in mass of the old population can increase by $\sim 5 - 10\%$ before the normalised χ^2 changes by more than 0.08dex. The change in χ^2 is mainly due to the continuum shape of the spectra. Therefore, these galaxies do not harbour significant populations of old stars that are concealed by the light of very young stars.

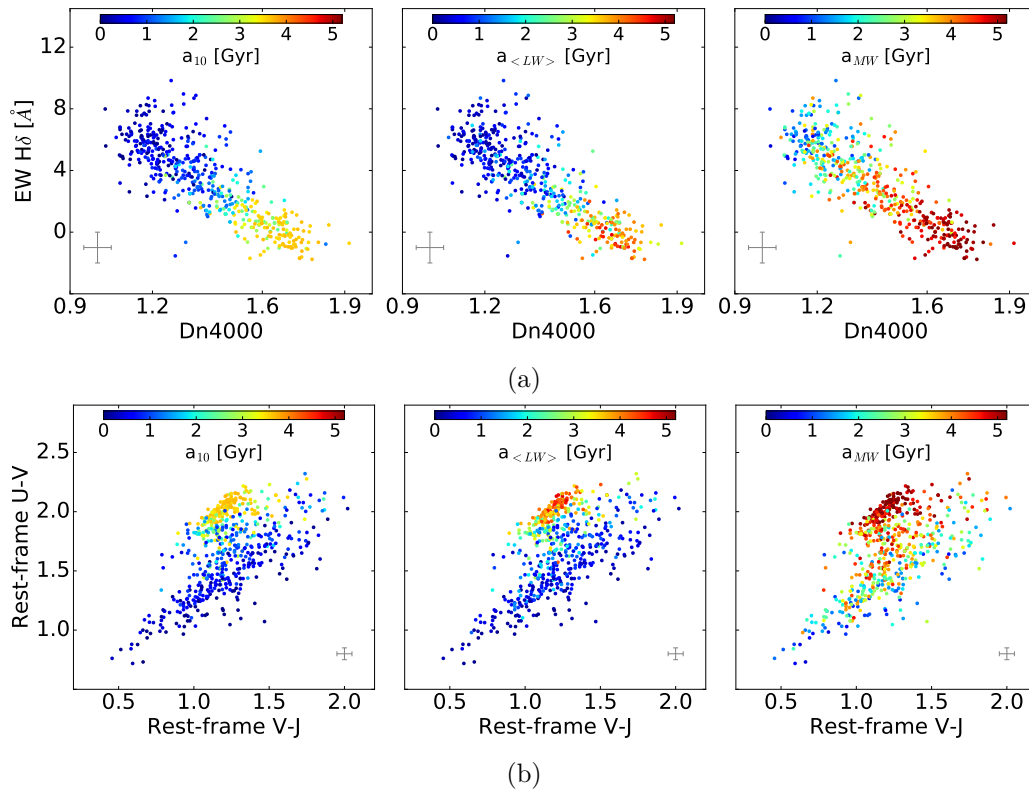


Figure 2.5: $EW(H\delta)$ versus D_n4000 (upper panel) and $U-V$ colour versus $V-J$ colour (lower panel) colour-coded by the time after which the final 10% of stars were formed (left), the mean light-weighted age (middle), and the mean mass-weighted age (right). Typical error bars are indicated in grey.

2.5 SFHs of the Galaxy Population

2.5.1 Correlations between Age, $M_{*,spec}$ and σ_*

Figure 2.6 shows $a_{<MW>}$ as a function of stellar mass ($M_{*,spec}$ left panel) and stellar velocity dispersion (σ_* right panel) colour-coded by current SF activity, i.e. whether the galaxy is quiescent ($\log(\text{sSFR}_{UV+IR}[\text{Gyr}^{-1}]) < -1$) or star-forming. Selecting quiescent galaxies by their $U-V$ and $V-J$ colors would result in similar trends. $a_{<MW>}$ generally correlates more strongly with $M_{*,spec}$ than σ_* . However, there is a σ_* threshold above which galaxies are almost exclusively old and quiescent: galaxies with $\sigma_* > 200 - 250 \text{ km s}^{-1}$ and $a_{<MW>} < 4 \text{ Gyrs}$ are very rare. Such a clear threshold does not exist for $M_{*,spec}$: high-mass galaxies ($M_{*,spec} \gtrsim 10^{11} M_\odot$) show a variety of ages.

To further illustrate these trends, we show σ_* as a function of $M_{*,spec}$ colour-coded by $a_{<MW>}$ (left panel) and divided by current SF activity (middle and right panels)

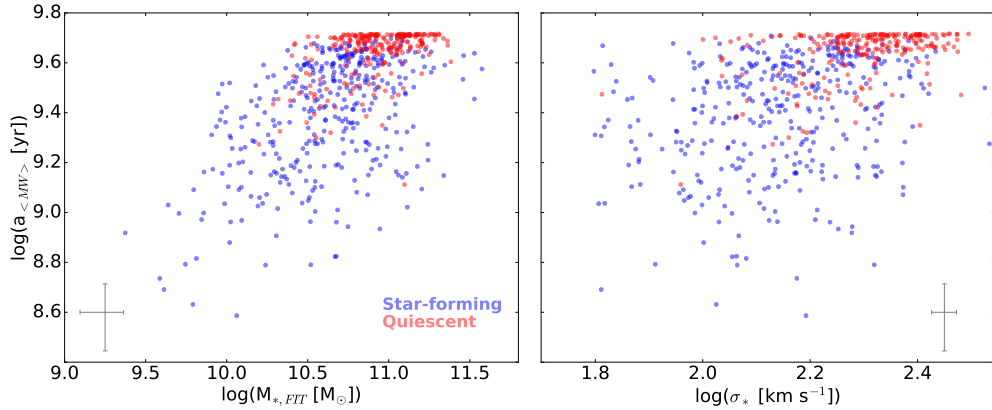


Figure 2.6: $a_{<MW>}$ as a function of $M_{*,spec}$ (left) and σ_* (right). The star-forming and quiescent populations are indicated in blue and red, respectively, and typical error bars are indicated in grey. Galaxies with $\sigma_* \gtrsim 200 \text{ km s}^{-1}$ are almost exclusively old ($> 4 \text{ Gyrs}$) and quiescent, which indicates that σ_* is a stronger predictor of age and SF activity.

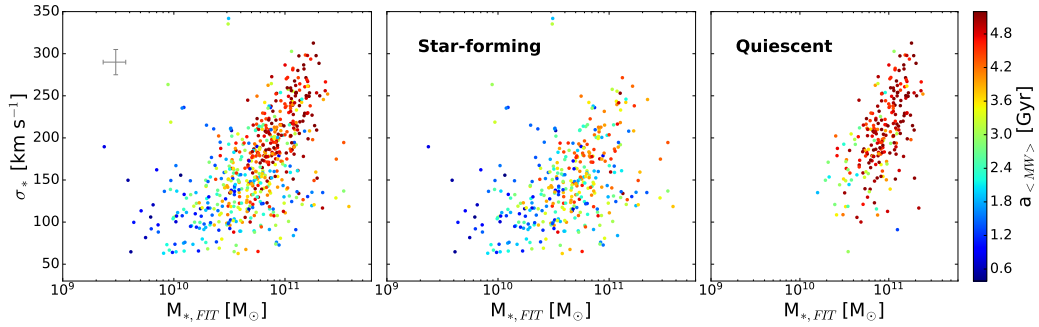


Figure 2.7: σ_* versus $M_{*,spec}$, colour-coded by $a_{<MW>}$. The star-forming and quiescent populations are shown in the middle and right panels, respectively. Typical error bars are indicated in grey. The clear separation between young and old galaxies at $\sigma_* \sim 170 \text{ km s}^{-1}$ shows a stronger correlation between $a_{<MW>}$ and σ_* over $M_{*,spec}$, which also depends on the current SF activity.

in Figure 2.7. There is a discernible separation between old ($> 4 \text{ Gyrs}$) and young ($< 4 \text{ Gyrs}$) galaxies at a velocity dispersion of $\sigma_* \sim 170 \text{ km s}^{-1}$. Taken together with the trends seen in Figure 2.6, we can conclude that $\sigma_* > 250 \text{ km s}^{-1}$ is a sufficient requirement for having an old age and $\sigma_* \sim 170 \text{ km s}^{-1}$ is a necessary requirement for old age. This extends the properties of present-day early-type galaxies, for which a correlation between velocity dispersion (and closely related quantities such as surface mass density and central mass density) and stellar age has been shown to be more fundamental than age trends with stellar mass (Kauffmann et al., 2003; van der Wel et al., 2009a; Graves et al., 2009), to higher redshift. Our results also extend the widely reported correlation between velocity dispersion (as well as surface mass density and central mass density) and SF activity (e.g., Franx et al., 2008; Mosleh et al., 2017; Barro et al., 2017) to an underlying correlation with overall stellar age.

The scaling relation between σ_* and black hole (BH) mass implies that large BH mass is correlated with early SF and the ceasing thereof. Such a scenario is supported by the direct correlation between BH mass and SF activity (e.g., Terrazas et al., 2016) and the large fraction of radio AGN among galaxies with large velocity dispersions both at low and high redshift (e.g., Best et al., 2005; Barišić et al., 2017).

It is interesting to note that the correlation between $a_{\langle MW \rangle}$ and σ_* seen in Figure 2.7 is significantly weakened after dividing the population by current SF activity. Instead, for the star-forming population, galaxy age is better correlated with $M_{*,spec}$ (also seen in Figure 2.6). A straightforward interpretation is that when galaxies are growing rapidly through SF—that is, when they are located on or near the SF ‘Main Sequence’—then M_* mostly traces how long this main SF phase has lasted so far. In other words, M_* simply traces the build-up of the stellar population over time, while σ_* is related to the end of this main SF phase, i.e. to the regulation and cessation of SF, presumably through AGN feedback.

2.5.2 Evolution of the average SFHs

The average SFHs of galaxies, normalised by stellar mass, as a function of σ_* and $M_{*,spec}$ are shown in Figures 2.8a and 2.8b, respectively. The average SFHs were corrected for completeness by weighing each galaxy by a completeness correction factor to create a volume-limited quantity (see Wu et al., 2018). The population is divided by its current star-formation activity in order to disentangle the effects from these two populations as well as compare them. The velocity dispersion and mass ranges and were selected such that there were enough galaxies in each bin (≥ 10), in both quiescent and star-forming galaxies. These relations are used to determine whether $z \sim 1$ galaxies also show a downsizing trend in their SFHs, as many studies have pointed to using local galaxies. However, the SFHs seen at $z \sim 1$ would not be resolved at $z \sim 0.1$, as the stellar populations would be too old.

On average, high- σ_* galaxies ($\sigma_* \geq 170 \text{ km s}^{-1}$) had higher SFRs at earlier epochs which started to decline rapidly, at a rate that increases with σ_* and stellar mass, when the Universe was $\sim 3 \text{ Gyrs}$ old. Most galaxies with lower velocity dispersions ($\sigma_* < 170 \text{ km s}^{-1}$) gradually build their stellar mass as the Universe evolves; however, the SFR of a minority, i.e. the quiescent population, began to decline when the Universe was $\sim 5 \text{ Gyrs}$ old. Higher-mass star-forming galaxies ($M_{*,spec} \geq 10^{10.5} M_\odot$) have SFHs that are consistent with constant star-formation with time, while the lower mass galaxies ($M_{*,spec} < 10^{10.5}$) still have rising SFRs. The star-forming population is still undergoing its main formation phase. The SFH trend is clear with $M_{*,spec}$ and not σ_* for the star-forming population, which extends from $M_{*,spec}$ being better correlated with SFHs for star-forming galaxies as discussed in Section 2.5.1 (see Figure 2.6 and 2.7).

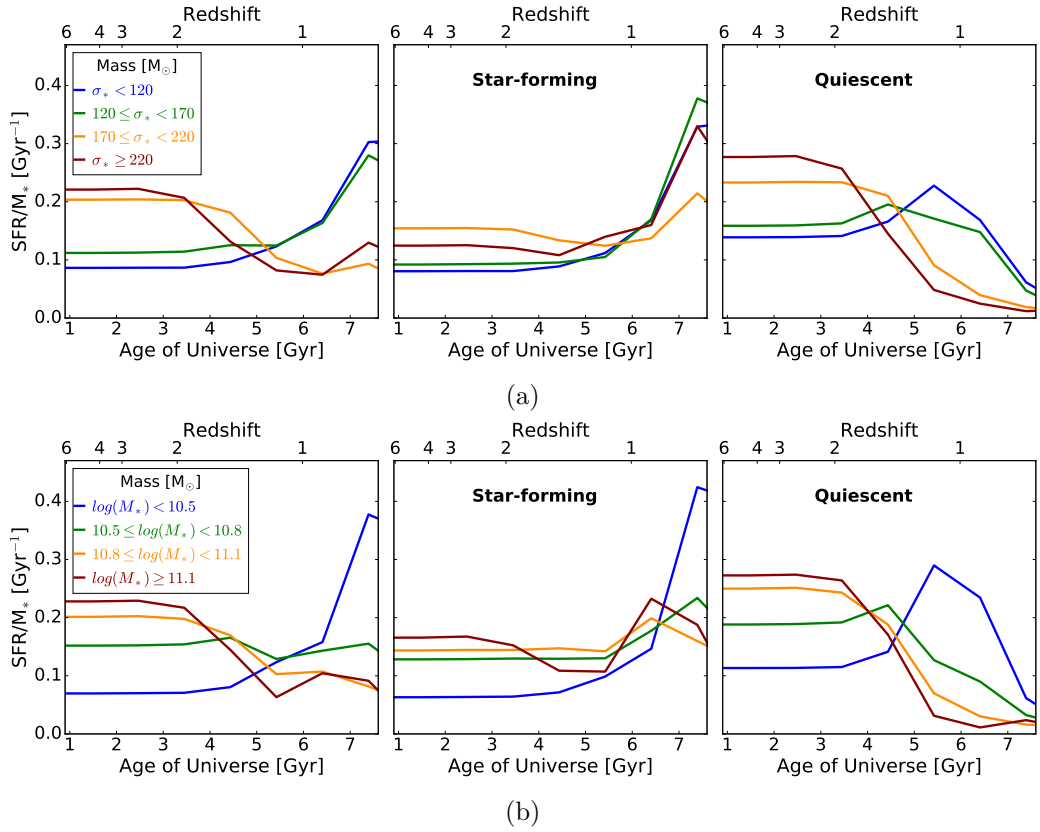


Figure 2.8: Ensemble-averaged SFHs of LEGA-C galaxies, normalised by stellar mass and separated into various σ_* (top) and $M_{*,spec}$ bins (bottom). The histories are divided into the star-forming and quiescent populations in the middle and right panels, respectively. The stellar content in massive galaxies formed earlier and faster, regardless of current SF activity.

Figure 2.8 reveals that, on average, most galaxies in the sample were forming stars quite early on; however, the SFRs were systematically higher and the eventual decline systematically more rapid with increasing σ_* ($M_{*,spec}$ for the star-forming population). This is clear evidence for the top-down scenario; where galaxies downsize in their star formation with time (more massive galaxies have older stars). This is seen in the overall population, and more strongly so in the quiescent population. While this result is in alignment with previous studies for the local universe (e.g. Juneau et al., 2005; Thomas et al., 2005; Tojeiro et al., 2009; McDermid et al., 2015; Ibarra-Medel et al., 2016), our work establishes this trend at $z \sim 1$ (half the current age of the Universe) using full spectrum fitting. Wu et al. (2018)’s study of the D_n4000 and $H\delta$ spectral features also support the downsizing scenario.

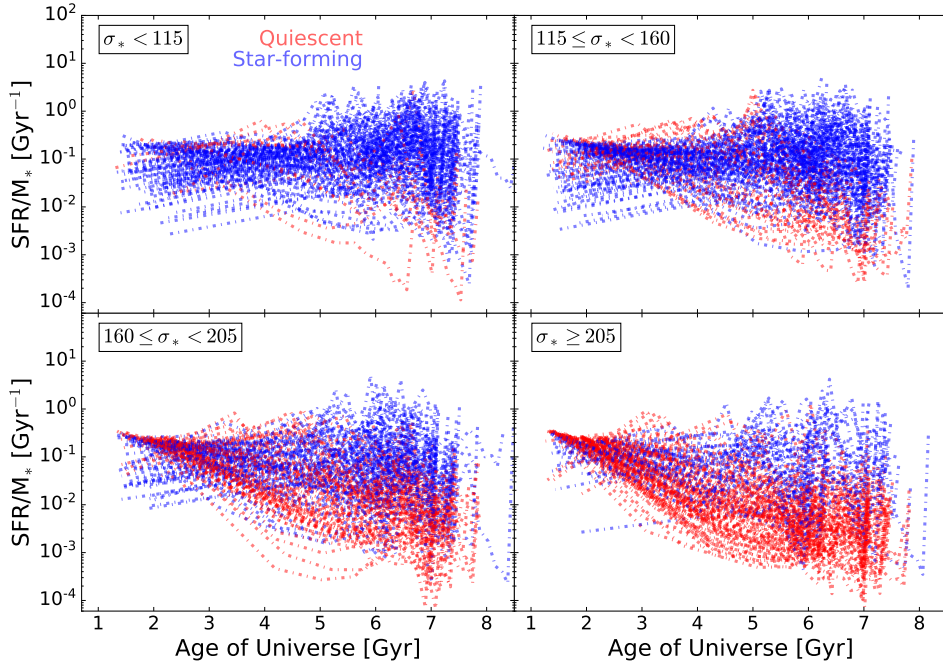


Figure 2.9: SFHs of the LEGA-C sample (normalised by stellar mass) as a function of the age of the Universe separated into four σ_* bins indicated by the labels. The colours differentiate between the star-forming and quiescent populations at the observed redshift.

2.5.3 The variety of SFHs

In Figure 2.9, we show all the stellar mass normalised SFHs in the LEGA-C sample, separated into four velocity dispersion bins and divided into the quiescent and star-forming population (at the observed redshift) as defined in Section 2.5.1. This reveals the large scatter in the SFHs at fixed mass, in addition to discerning the differences in the histories based on the current star-formation activity of the galaxies.

The SFHs of quiescent galaxies peaked early on in the Universe and thereafter, their activity generally decreases with time; while star-forming galaxies gradually grow in SFR, which peaked at later epochs. The quiescent population has consistently higher SFRs at early epochs, whereas its star-forming counterpart has higher SFRs at later epochs. This indicates that star-forming galaxies aggregate their mass slower than the quiescent population. The dominance of the quiescent population increases from low to high-mass galaxies, and vice versa for the star-forming population.

The SFRs of low mass galaxies ($\sigma_* < 115 \text{ km s}^{-1}$) have been gradually increasing, with large scatter at all epochs. These galaxies are currently undergoing the main stages of their star formation. Note that the lowest dispersion bin suffers from incompleteness, due to the survey sample selection approach. K-band quiescent galaxies are fainter than equally massive star-forming galaxies which causes an

under-representation in the LEGA-C sample. However, it is well known that low-mass star-forming galaxies outnumber quiescent galaxies of the same mass; therefore, the SFHs in Figure 2.9 can be considered as illustrative.

The quiescent and star-forming populations are more evenly distributed (in number and variation of SFHs) in the intermediate- σ_* regime (between 160 and 205 km s⁻¹) while the high- σ_* population ($\sigma_* \geq 205$ km s⁻¹) is dominated by quiescent galaxies. The disparity between the SFHs of the quiescent and star-forming populations in the high- σ_* regime indicates that galaxies ‘remember’ their past. There is a strong coherence among the SFHs of quiescent and star-forming galaxies, respectively. This behaviour extends to the peak of cosmic SF activity at $z \sim 2-3$. This implies that SF activity at the moment of observation is strongly correlated with the SF activity ~ 3 Gyrs prior. The results of this work indicate that many evolutionary paths can lead to galaxies at a given velocity dispersion. This illustrates the difficulty of connecting progenitor and descendant populations at different cosmic epochs.

2.5.4 Comparisons to Literature Measurements

As stated in Section 2.5.2, the deconstructed SFHs in this study support the galaxy downsizing scenario which has long been studied (see Section 4.1). Leitner (2012)’s finding that star-forming galaxies formed only $\sim 15\%$ of their mass before $z = 1-2$ (mass dependent), suggesting that present-day star-forming galaxies are not the descendants of massive star-forming galaxies at $z > 2$, is in line with our results since the peak in star formation occurs after $z < 1.5$ for almost all star-forming galaxies in the LEGA-C sample.

Intermediate-redshift stellar population studies are sparse, due to the high S/N required to undertake such studies (see Section 4.1). Pertaining to this work, there are a few studies we can draw comparisons from, viz. Choi et al. (2014) and Gallazzi et al. (2014). Measurements by Choi et al. (2014) and Gallazzi et al. (2014) indicating that passive galaxies have ages consistent with mostly passive evolution are also in alignment with this study as the reconstructed SFHs indicate that galaxies stay quiescent, barring some histories that showed low-level star formation after quiescence. Gallazzi et al. (2014) reported an average lighted-weighted age of ~ 5 Gyrs for a $4 \times 10^{10} M_\odot$ galaxy, consistent with our value of 4.8 Gyrs, for a galaxy of the same mass.

Diemer et al. (2017) tested Gladders et al. (2013)’s hypothesis that the SFHs of individual galaxies are characterised by a log-normal function in time, which implies a slow decline in SFRs rather than rapid quenching. They did this by comparing the log-normal parameter space of total stellar mass, peak time, and full width at half maximum of simulated galaxies from Illustris (Vogelsberger et al., 2014b) and

Gladders et al. (2013), as well as Pacifici et al. (2016)’s derived SFHs of a sample of quiescent galaxies using a large library of computed theoretical SFHs. They found good agreement for all three studies, however, Illustris predicted more extended SFHs on average. LEGA-C galaxies support the slow-quenching picture of galaxy evolution as Gladders et al. (2013) have suggested, with a rate of decline that is mass dependent as we have seen. More comparisons will be performed in later papers.

2.6 Summary

We have reconstructed the SFHs of galaxies in the current LEGA-C sample, which contains 678 primary sample galaxies with $S/N \sim 20 \text{ \AA}^{-1}$ in the redshift range $0.6 < z < 1$. We have done this by implementing an algorithm to fit flexible SFHs to the full spectrum, using *FSPS* and *emcee*. The galaxy spectra were fit to a linear combination of a defined set of 12 CSPs, with solar metallicity and constant star formation within the time interval of the templates. In 90% of the cases the algorithm produced good fits based on the normalised χ^2 values. We found a wide variety of SFHs, although 60% of the galaxies have $a_{<MW>} > 3 \text{ Gyrs}$ by the time we observe them (Figures 2.3 and 4.5). However, we note that age estimates from spectral fits experience increasing degeneracy of spectral features as the stellar populations age. Most of the old galaxies ($a_{<MW>} \gtrsim 3 \text{ Gyrs}$) had very low SFRs early on ($\gtrsim 6 \text{ Gyrs}$ after the Big Bang, Figure 4.5). However, some exhibit subsequent peaks in star formation, which could be an indication of rejuvenated star formation, or a merger with a younger population. However, the mass formed from this more recent star formation activity is only about 10% of the mass formed throughout the galaxies’ histories. The median $a_{<LW>}$, $a_{<MW>}$ and $M_{*,spec}$ were found to be 1.2Gyrs, 3.8Gyrs and $10^{10.8} M_{\odot}$, respectively.

The main objective of this work was to investigate how our reconstructed SFHs behave as a function of stellar mass, stellar velocity dispersion and star-formation (SF) activity, as well as the variation they show at fixed velocity dispersion. We found that galaxies at $z \sim 1$ have similar trends in their SFHs compared to local galaxies, i.e. the stellar content in massive galaxies formed earlier and faster (Figure 2.8). This top-down scenario is a known trend from fossil record inferences using SDSS spectra; however, in this study, it is shown for $z \sim 1$ galaxies for the first time using full spectrum fitting. We found that the scatter between the quiescent and star-forming populations increases towards lower redshift (Figure 2.9), which indicates that current SF activity is strongly correlated with past SF activity. High-dispersion quiescent galaxies had their star formation peak early, $> 9.5 \text{ Gyrs}$ ago, and exhibit decreasing SFRs throughout the rest of their history, for the most part. We found that the lowest dispersion galaxies in our sample are undergoing the main stage of their star formation as we observe them (7Gyrs ago).

The results of the spectral fits were used to measure a number of galaxy properties, viz. ages ($a_{\langle LW \rangle}$, $a_{\langle MW \rangle}$, $a_{\langle MW \rangle}$, etc.) and stellar mass, in order to test the model by investigating how these properties relate to one another as well as other properties measured from the galaxy spectra, e.g. velocity dispersion, $H\delta$, D_n4000 , etc. We showed that galaxies evolve from the top-left to the bottom-right of the $EW(H\delta)$ - D_n4000 plane as they age, as would be expected (Figure 2.5).

Recovering the full SFHs of intermediate-redshift galaxies opens up a multitude of avenues of research. In this work we have shown the clear differences between the SFHs of quiescent and star-forming galaxies and how these SFHs are scattered at fixed velocity dispersion. We have also shown that velocity dispersion is a better indicator of the age and current SF activity of galaxies as a whole than stellar mass, while stellar mass is a better indicator of the age of star-forming galaxies (Figure 2.6 and 2.7). In future studies, we will use the reconstructed SFHs to constrain the quenching speed and rate, as well as investigate the relationship between galactic structure and SFHs. These constraints will become valuable for future surveys like JWST that will be investigating the properties of galaxies beyond $z \sim 2$, and will need $z \sim 1$ measurements as a benchmark to connect those populations to the local Universe.

STELLAR MASS EVOLUTION AND RANKING OF $z \sim 0.8$ GALAXIES IN LEGA-C[†]

Understanding how galaxies evolve requires us to be able to constrain the connection between the descendants of galaxies and their progenitors at higher redshifts. Thus far, we have relied on simulations and analytical models to constrain individual evolution parameters at varying redshift. In this chapter, I use reconstructed star-formation histories to track the total stellar mass evolution of galaxy populations between redshifts $z \sim 0.8$ and $z = 3$, and determine whether galaxies maintain their mass ranking as they evolve.

3.1 Introduction

One of the main challenges in understanding galaxy evolution is connecting the descendants of galaxies to their progenitors at higher redshifts. Thus far, extragalactic observations have provided snapshots of galaxies at different points in cosmic time, which have allowed us to obtain an integrated view of galaxy evolution. They have enabled studies to constrain the number and mass density evolution of star-forming and quiescent galaxies (e.g., Pozzetti et al., 2010; Brammer et al., 2011; Moustakas et al., 2013; Muzzin et al., 2013a), as well as the evolution of the star-formation rate density (SFRD) in the universe (e.g., Karim et al., 2011; Madau and Dickinson, 2014; Khostovan et al., 2015; Abramson et al., 2016). However, a link between

[†]The contents of this chapter are adapted from Chauke(2019b, in prep.). The paper is in preparation and will soon be submitted to the *Astrophysical Journal*. I myself conducted the research, analysed the results and wrote the text for the paper.

descendent galaxies and their progenitors cannot be directly obtained from extragalactic observations. One can compare galaxies at different redshifts to determine this link; however, that would require some assumptions about how galaxies evolve throughout time.

An initial approach for passive galaxies was to compare these galaxies at fixed stellar mass at different redshifts (e.g. van Dokkum and Franx, 1996). This method works well in that passive galaxies' properties do not change much over time; however, it is subject to progenitor bias because some passive galaxies at low redshifts did not have passive progenitors at higher redshifts. For star-forming galaxies, one can connect progenitors to descendants by using the star-forming sequence to imply mass evolution (e.g. Leitner, 2012). However, this method suffers from significant systematic uncertainties in measured star-formation rates (SFRs) and assumes that mergers are negligible. More recent studies (e.g., van Dokkum et al., 2010; Brammer et al., 2011; Muzzin et al., 2013a) remedy some of these issues by assuming that the number density of galaxies does not evolve when galaxies are ordered by some property such as stellar mass. This constant number density technique assumes that stellar mass (or velocity dispersion) rank order is preserved, i.e. the most massive galaxies at higher redshifts evolve to be the most massive galaxies at lower redshifts. It also assumes that mergers are negligible. Therefore, if one has a galaxy stellar mass function, one can use the stellar mass of a galaxy at one redshift to identify its number density at that redshift, and then predict the stellar mass that corresponds to that same number density at any other redshift. This technique has been used to study several galaxy properties: mass evolution (e.g., van Dokkum et al., 2010), star-formation histories (e.g. Papovich et al., 2011), velocity dispersion (e.g., Bezanson et al., 2011), size (e.g., Patel et al., 2013), etc.

However, mergers are thought to explain a variety of observations. For example, the spheroidal shape of massive (stellar masses $> 10^{11}M_{\odot}$) quiescent galaxies at $z < 1$ suggests that they are formed through dry mergers (e.g van der Wel et al., 2009b; Hill et al., 2019); and the size evolution of quiescent galaxies from high to low redshifts suggests that quiescent galaxies grow through the accretion of smaller stellar systems or gas-poor mergers (e.g. van der Wel et al., 2008). The constant number density method, though, does recover the median stellar mass evolution of galaxies to within a factor ~ 2 -3. However, hydrodynamical simulations, abundance matching models and semi-analytical models showed that the scatter in median stellar masses is mainly due to scatter in stellar mass growth rates and mergers (e.g. Leja et al., 2013; Behroozi et al., 2013; Torrey et al., 2015), which means that galaxies' number densities evolve with time. Galaxies that have similar stellar masses at one redshift, have diverse evolutionary paths that lead a wide range of stellar masses (e.g. Torrey et al., 2015; Wellons et al., 2016).

Galaxy formation semi-analytic models and simulations have an advantage over observations in that one can directly observe the evolutionary paths of galaxies

from one redshift to another. These theoretical works, using the hydrodynamical cosmological simulation Illustris (Genel et al., 2014; Vogelsberger et al., 2014b,a), have shown that the number densities of tightly grouped galaxies do not only evolve, but also spread out over time (e.g., Wellons et al., 2016; Wellons and Torrey, 2017; Torrey et al., 2017). Furthermore, Wellons and Torrey (2017) have developed a probabilistic method that describes the evolution and spread of the number density of galaxy populations. This method results in more accurate predictions for the evolution of galaxies’ physical properties than the assumption of a constant number density, and it can be applied to observational data.

An alternate method to connect the progenitors of galaxies to their descendants and measure their stellar mass evolution, is to reconstruct their star-formation histories (SFHs) through full-spectrum fitting. This requires high resolution, high quality spectra, which are scarce at high redshifts but are now available at $z \sim 1$ because of the LEGA-C survey (van der Wel et al., 2016; Straatman et al., 2018). In an earlier paper (Chauke et al., 2018), we reconstructed the SFHs of galaxies at $z \sim 1$ using LEGA-C spectra. We cannot track the main progenitors of galaxies with SFHs because we do not have galaxy merger histories. However, we can trace galaxies’ total SF as a function of time, which enables us to track galaxies’ total stellar mass evolution. In this study, we use the reconstructed SFHs from Chauke et al. (2018) to investigate if galaxies do not move along constant number density tracks, as simulations have suggested. In Section 4.2 we give a brief overview of the sample. In Section 3.3 we trace the stellar mass evolution backward from $z \sim 0.8$ to $z = 3$ and analyse the spread in mass. In Section 3.4, we investigate forward and backward evolutionary tracks between $z = 1$ and $z = 3$ and analyse the spread in mass as a function of time. Finally, in Section 5 we summarise the results. We assume a Λ CDM model with $H_0 = 67.7 \text{ km s}^{-1} \text{ Mpc}^{-1}$, $\Omega_m = 0.3$ and $\Omega_\Lambda = 0.7$.

3.2 Data

This work is based on the first two years of data from the LEGA-C survey¹ (van der Wel et al., 2016). LEGA-C is an ESO Public Spectroscopic survey with VLT/VIMOS of K-band selected galaxies, with a redshift dependent K-band magnitude limit ($K_{ab} = 20.7 - 7.5 \times \log[(1+z)/1.8]$), in the COSMOS field with redshifts in the range of $0.6 < z < 1.0$. Each galaxy is observed for ~ 20 h, which results in spectra with $S/N \sim 20 \text{ \AA}^{-1}$ (resolution $R \sim 3000$). The second data release contains 1550 primary sample galaxies. For details of the data reduction procedure, see van der Wel et al. (2016) and Straatman et al. (2018). We make use of the following measured catalog quantities in the analysis: rest-frame UV+IR SFRs, stellar masses ($M_{*,spec}$), UV+IR specific SFRs ($sSFR_{UV+IR}$, i.e. UV+IR SFRs divided by $M_{*,spec}$),

¹<http://www.eso.org/sci/publications/announcements/sciann17120.html>

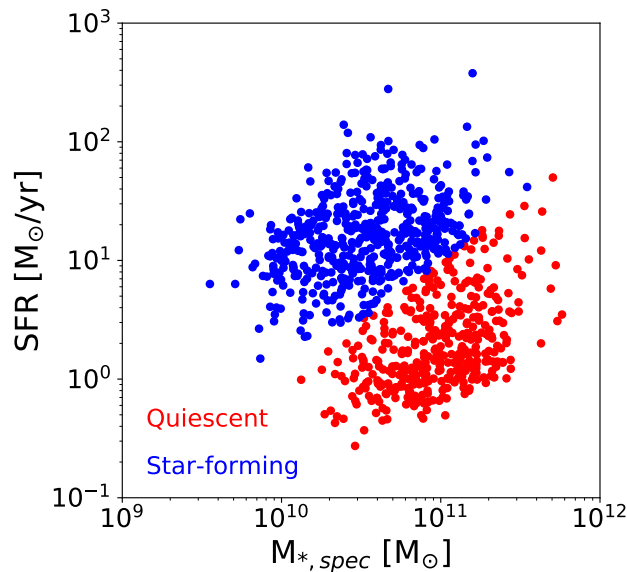


Figure 3.1: SFR as a function of $M_{*,spec}$ of the LEGA-C sample at the observed redshift. Star-forming and quiescent populations are indicated in blue and red, respectively.

velocity dispersions (σ_*) and central mass densities ($1M_{cen,*}$). The UV+IR SFRs are estimated from UV and IR luminosities, following Whitaker et al. (2012), and $M_{*,spec}$ is the stellar mass estimate obtained from full-spectrum fitting (see Section 4.2.1). Figure 3.1 shows SFR as a function of $M_{*,spec}$ of the LEGA-C sample at the redshift of observation. The population is colour-coded by current SF activity, where a galaxy is defined as either quiescent ($\log(\text{sSFR} [\text{Gyr}^{-1}]) < -1$, red) or star-forming (blue) at the observed redshift.

3.2.1 Star Formation Histories

In an earlier paper, Chauke et al. (2018), we reconstructed the SFHs of the LEGA-C sample, using a full-spectrum fitting algorithm. Our algorithm incorporates stellar population spectra generated with *FSPS v3.0*, the Python implementation of the Flexible Stellar Population Synthesis package (Conroy and Gunn, 2010; Conroy et al., 2009; Foreman-Mackey et al., 2014), using the MILES spectral library (Sánchez-Blázquez et al., 2006), Padova isochrones (Girardi et al., 2000; Marigo and Girardi, 2007; Marigo et al., 2008) and a Kroupa initial mass function (Kroupa et al., 2001); and *emcee* (Foreman-Mackey et al., 2013), an affine invariant ensemble sampler for MCMC. *emcee* uses MCMC ‘walkers’ that randomly explore the parameter space, where each proposed step for a given walker depends on the positions of all the other walkers in the ensemble, with the aim of converging to the most likely parameter values.

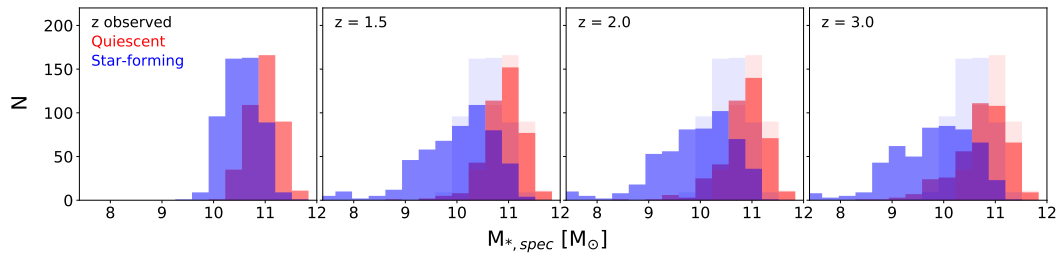


Figure 3.2: Stellar mass evolution of LEGA-C galaxies from their observed redshift back to redshifts 1.5, 2 and 3. Galaxies that are star-forming and quiescent at the observed redshift are indicated in blue and red, respectively.

The galaxy spectra were fit to a linear combination of a set of 12 composite stellar populations (CSPs), with solar metallicity and constant star formation within the time interval of the templates; as well as 2 dust reddening values ($E(B - V)_i$), using Calzetti et al. (2000)’s dust reddening curve, one for the youngest (more dust-obscured) stellar population and the second for the other stellar populations. The algorithm uses emission-line subtracted spectra. Emission line spectra are computed using the Penalized Pixel-Fitting method (pPXF, Cappellari and Emsellem, 2004). For details of the emission line fitting procedure, see Bezanson et al. (2018).

The time intervals of the 12 CSP age bins were chosen to optimise the temporal sampling of evolving stellar populations, which results in wider bins for older CSPs. However, for the purpose of this study, we use a set of 8 CSPs with 1 Gyr time intervals, with the exception of the youngest CSP which has the same age range as Chauke et al. (2018, 0-100Myrs). This is done to probe the first few Gyrs of galaxies’ SFHs in order to more accurately trace the evolutionary paths of these galaxies. The model results in measurements of SFRs, stellar masses ($M_{*,spec}$), luminosities (L_{spec}), mean mass-weighted and light-weighted ages ($a_{<MW>}$ and $a_{<LW>}$, respectively) and the dust reddening values. The stellar masses derived using our method, $M_{*,spec}$, are in good agreement with photometry-based stellar masses derived with FAST (Kriek et al., 2009). See Chauke et al. (2018) for a more detailed description of the fitting algorithm as well as results thereof.

3.3 Evolution of the Galaxy Population from $z \sim 0.8$ backward to $z = 3$

3.3.1 Stellar mass evolution and SF activity

Figure 3.2 shows the evolution of the stellar mass distribution of the LEGA-C sample, from the observed redshift backward to redshifts 1.5, 2 and 3, colour-coded

3.3.2. Evolution as a function of current stellar mass

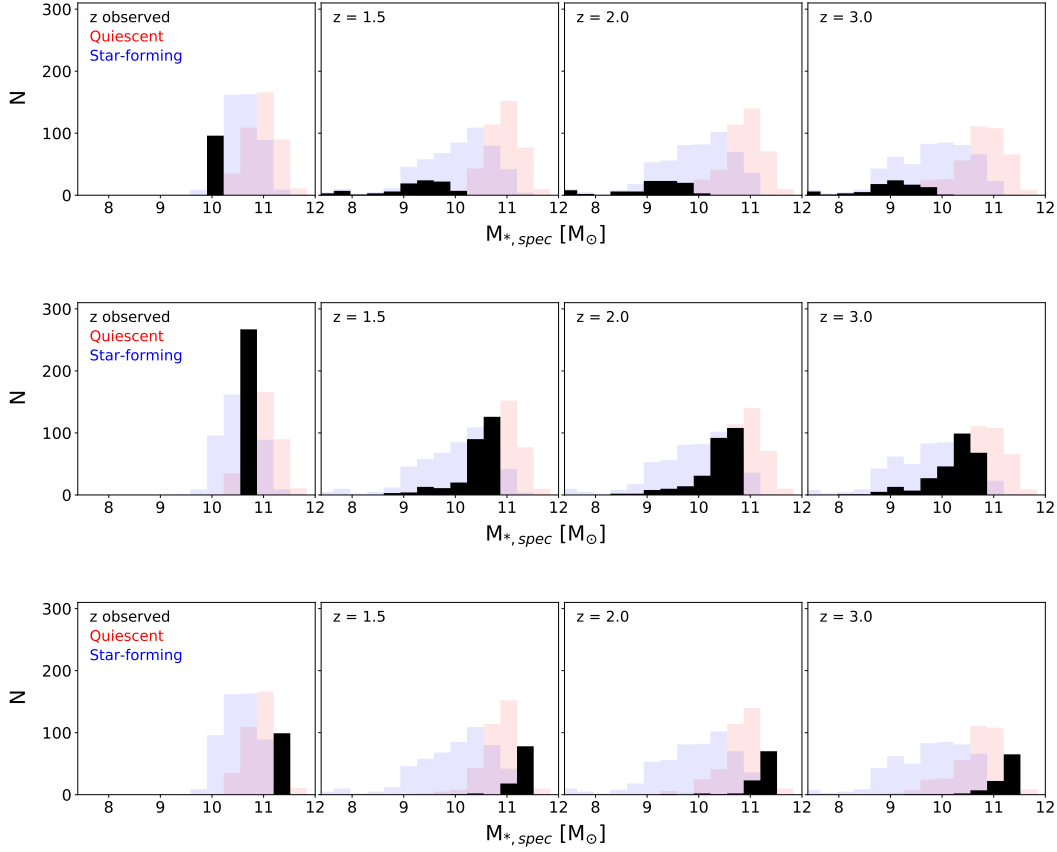


Figure 3.3: Stellar mass evolution of $M_{*,spec}$ selected galaxies (shown in black) from the redshift of observation backward to redshifts 1.5, 2 and 3. The star-forming and quiescent populations from Figure 3.2 are shown in the background for comparison.

by current SF activity. Star-forming and quiescent galaxies are indicated in blue and red, respectively. The spread in the stellar mass of both distributions increases with redshift; however, star-forming galaxies have a wider range of stellar masses by $z = 3$. The difference in the median and spread of the two distributions increases by 0.5dex and 0.2dex, respectively, from $z \sim 0.8$ until $z = 3$. The coherence of current SF activity with stellar mass evolution indicates the underlying correlation between current SF activity and past SF activity which we discussed in Chauke et al. (2018).

3.3.2 Evolution as a function of current stellar mass

In Figure 3.3, we show the evolution, from the observed redshift backward to redshifts 1.5, 2 and 3, of the stellar mass distribution of a set of three LEGA-C populations, distinguished by stellar mass at the observed redshift. The low-mass regime contains galaxies with $9.6 < \log(M_{*,spec}) \leq 9.9$, the intermediate-mass regime contains galaxies with $10.2 < \log(M_{*,spec}) \leq 10.5$, and the high-mass regime contains

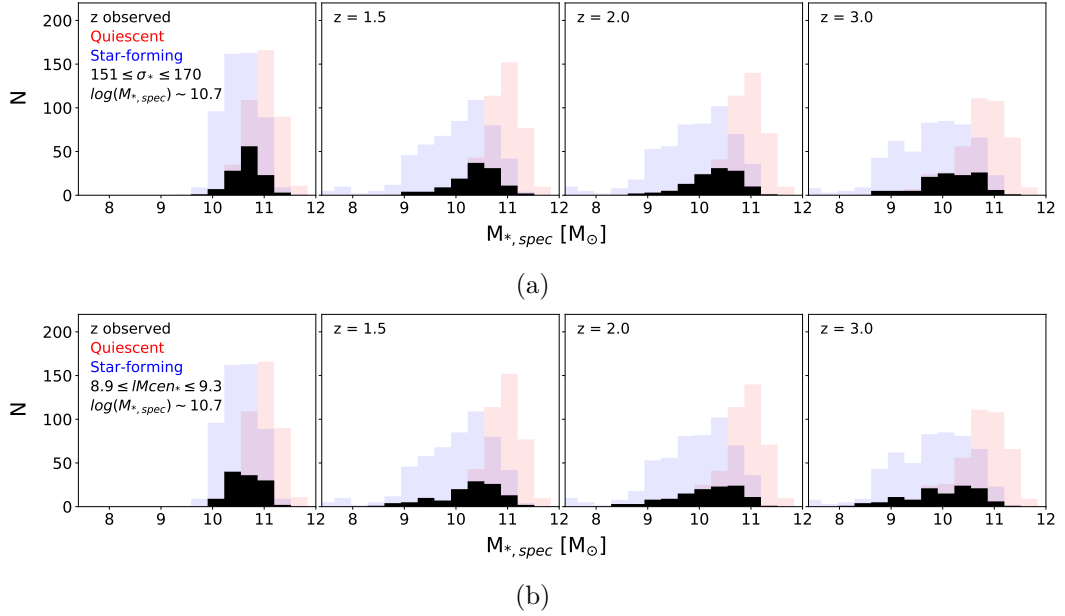


Figure 3.4: Stellar mass evolution of σ_* (a) and IMcen_* (b) selected galaxies (shown in black) that have a median stellar mass $\sim 10^{10.7}M_\odot$ from the redshift of observation backward to redshifts 1.5, 2 and 3. The star-forming and quiescent populations from Figure 3.2 are shown in the background for comparison.

galaxies with $10.9 < \log(M_{*,\text{spec}}) \leq 11.2$.

In all three cases, the galaxies have a $\sim 0.3\text{dex}$ variation in stellar mass at $z \sim 0.8$. They end up with a wide spread in stellar mass by $z = 3$; the spread is over two orders of magnitude for the low and intermediate-mass bins. The spread in stellar mass increases with increasing redshift and decreasing current stellar mass. These trends show that galaxies with similar stellar masses at $z = 0.8$, have varying growths that diverge with time, which points to the diverse evolutionary paths of galaxies. This behaviour is not expected from the constant number density assumption invoked in galaxy population studies. The assumption requires that the most massive galaxies at higher redshifts evolve to be the most massive galaxies at lower redshifts, and that mergers are negligible. Under this assumption, galaxies with similar stellar masses would have similar stellar mass growth rates such that mass rank order is preserved. The trends are an indication of scatter in stellar mass growth rates, which are suggested, in theoretical studies (e.g. Leja et al., 2013; Torrey et al., 2015), to be caused by mergers and stochastic growth rates.

3.3.3 Stellar mass evolution, velocity dispersion and central mass density

Stellar velocity dispersion and central mass density have long been linked to stellar mass evolution and quenching. The central mass density at which galaxies quench increases with stellar mass (e.g. Fang et al., 2013), and the contribution of dense cores to the total stellar mass budget of the Universe decreases with redshift (e.g. van Dokkum et al., 2014). Stellar velocity dispersion is considered to be better correlated with age and colour than stellar mass and surface mass density (e.g. Kauffmann et al., 2003; Wake et al., 2012). Therefore, it is important to investigate how σ_* and IMcen_* are correlated with individual stellar mass evolution. We cannot trace the evolution of σ_* and IMcen_* with our SFHs; instead, we probe the effect of these parameters by tracing the stellar mass evolution from a narrow range in σ_* and IMcen_* .

Figure 3.4 shows the evolution of the stellar mass distribution of a set of two LEGA-C populations, from their observed redshift backward to redshifts 1.5, 2 and 3, distinguished by velocity dispersion and central mass density. The range in velocity dispersion ($151 \leq \sigma_* [\text{km s}^{-1}] \leq 170$) and central mass density ($9.95 \leq \text{IMcen}_* [\log(M_\odot \text{ kpc}^{-2})] \leq 10.05$) is chosen such that the average stellar mass of the population is $\sim 10^{10.7} M_\odot$. Both of these parameters are not exactly correlated with stellar mass; therefore, even a narrow range in σ_* and IMcen_* at $z \sim 0.8$, introduces an initial spread in stellar mass. However, as in Figure 3.3, the spread in stellar mass increases with increasing redshift. This indicates that the σ_* or IMcen_* rank order may not be preserved as galaxies evolve and assemble their stellar mass.

3.4 Stellar mass evolutionary tracks

3.4.1 Individual galaxy evolutionary tracks

Figure 3.5 shows the stellar mass evolution, from $z = 1$ backward to $z = 3$, of thirty selected galaxies in three stellar mass bins, viz. $(M_{*,\text{spec}} - 3 \times 10^{10}) < 3 \times 10^9$, $(M_{*,\text{spec}} - 5 \times 10^{10}) < 5 \times 10^9$ and $(M_{*,\text{spec}} - 10^{11}) < 10^{10}$. Stellar masses of all selected galaxies diverge with time: the difference in stellar masses that were similar at $z = 1$ can increase to over an order of magnitude by $z = 3$. Although a majority of the galaxies have smooth growth rates that preserve their mass rank order, a significant portion of galaxies' stellar masses grow so substantially, that the galaxies change their rank order. At the high-mass end ($M_{*,\text{spec}} \simeq 10^{11} M_\odot$), two galaxies have significantly lower masses ($> 1\text{dex}$) at $z = 3$, lower than most galaxies in the lowest mass bin. By $z \sim 1.5$, their stellar masses are nearly identical to the rest of the galaxies whose stellar masses only increased by $\lesssim 0.3\text{dex}$ over the same period.

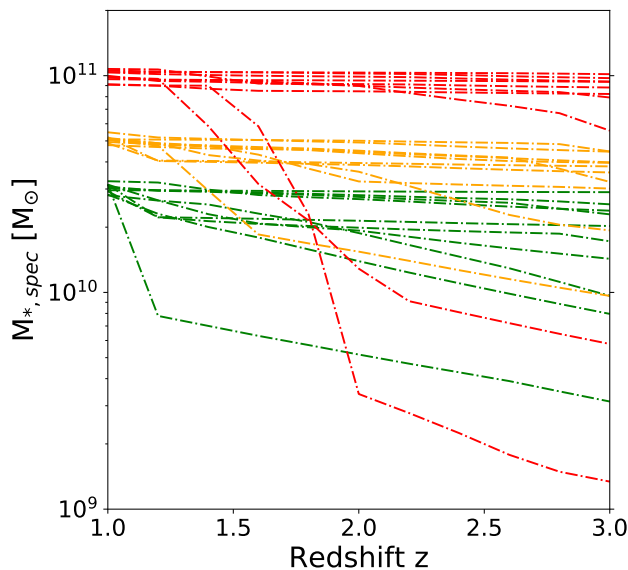


Figure 3.5: Stellar mass evolution of selected galaxies (10 in each of the 3 stellar mass bin) from $z = 1$ backward to $z = 3$. In some cases, the stellar mass growth of less massive galaxies at $z = 3$ surpasses that of more massive galaxies by $z = 1$, in contrast with constant number density assumptions.

Figure 3.5 indicates that galaxies with similar stellar masses at lower redshifts not only had increasingly divergent stellar masses at larger redshifts, but some also had growth rates so significant it resulted in stellar mass rank order not being preserved. Both of these effects are in contrast with stellar mass evolution tracks that would be obtained from constant number density assumptions (e.g. van Dokkum et al., 2013). SFHs do not inform us of galaxies' merger histories; therefore, we can only speculate on the causes for such drastic growth rates. Semi-analytical and abundance matching models as well as Illustris simulations have shown that the scatter in stellar mass evolution is driven by both stochasticity in stellar mass growth rates and mergers (Leja et al., 2013; Behroozi et al., 2013; Torrey et al., 2015), with Torrey et al. (2017) suggesting that mergers dominate the evolution at lower redshifts and stellar masses, while scattered growth rates dominate at higher redshifts and stellar masses. This is in line with this study because we find that most growth rates are smoother for more massive galaxies and at $z \gtrsim 2$. However, the stellar mass growth rates could also be smoother at $z \gtrsim 2$ because we cannot temporally resolve the stellar populations beyond $z = 2$ due to the similarity of stellar spectra in the age range > 5 Gyrs (Gallazzi et al., 2005).

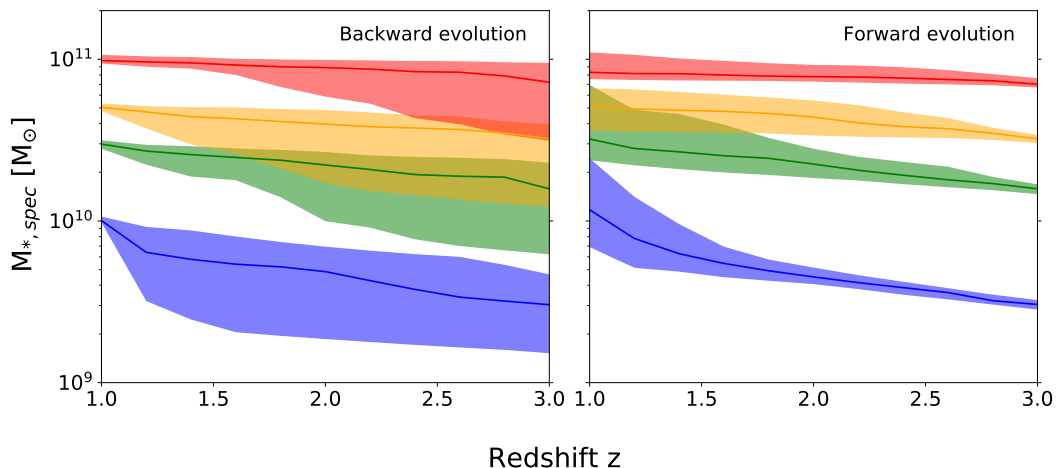


Figure 3.6: Stellar mass evolution of galaxy populations between $z = 1$ and $z = 3$. The left panel shows selected masses at $z = 1$ traced backward in time to $z = 3$ and the right panel shows selected masses at $z = 3$ traced forward in time to $z = 1$. The solid lines indicate the median mass evolution of each population and the shaded regions indicate the 16th and 84th percentiles of the distributions.

3.4.2 Tracing the galaxy population forward and backward in time

Figure 3.6 shows the stellar mass evolution between $z = 1$ and $z = 3$ of four LEGA-C galaxy populations. The left panel shows the backward evolution in four stellar mass bins, viz. $(M_{*,spec} - 10^{10}) < 10^9$, $(M_{*,spec} - 3 \times 10^9) < 3 \times 10^9$, $(M_{*,spec} - 5 \times 10^9) < 5 \times 10^9$ and $(M_{*,spec} - 10^{11}) < 10^{10}$. The right panel shows the forward evolution of four galaxy populations whose initial stellar masses (at $z = 3$) are similar to the median stellar masses of populations on the left panel at $z = 3$. The stellar mass bins are selected such that there are at least 20 galaxies in each bin. The solid lines indicate the median mass evolution of each population and the shaded regions indicate the 16th and 84th percentiles of the distributions.

The mass evolution in Figure 3.6 is consistent with the trends seen in Figure 3.5. Galaxies with a narrow range in stellar mass at $z = 1$ ($z = 3$), have a wide range of stellar masses by $z = 3$ ($z = 1$). Their stellar masses increase and diverge as a function of time, with scattered growth rates that can break the mass rank order of galaxies. This trend is seen irrespective of stellar mass or whether galaxies are tracked backward or forward in time. This indicates that galaxies grow their mass in various ways, which results in a variety of evolutionary paths, and that number density is not a conserved quantity. If the constant number density assumption was accurate, the scatter in stellar mass growth rates would be small, and mass rank order would be preserved.

Additionally, Figure 3.6 exposes a difference between tracing galaxies forward and

backward in time: the increased scatter in stellar mass is larger when galaxies are tracked backward in time. There is a $\sim 30\%$ reduction in scatter when galaxies are traced forward in time. This behaviour is also seen in number density and stellar mass evolution measurements of simulated galaxies from Torrey et al. (2015) and Torrey et al. (2017). They measure a $\sim 20\%$ reduction in scatter and they suggest that the main driver of the difference is the relative overabundance of fast growth tracks owing to the higher abundance of low-mass galaxies. That is, when tracing galaxies backward in time, there is a wider range of stellar masses that they could have evolved from because there are more low-mass galaxies at higher redshifts. On the other hand, low and high mass galaxies at higher redshifts end up in a narrower range of stellar masses as they evolve and assemble their mass. Due to the survey K-band selection approach, LEGA-C is biased against old galaxies, especially for $\log(M_{*,spec}) < 10.5$. Therefore, the scatter when tracing galaxies backward in time, might be larger than our measurement because we are missing a fraction of older galaxies that are fainter than equally massive young galaxies. In addition, when tracing galaxies backward in time, many of the progenitors at $z = 3$ will be missed.

3.5 Summary

In this paper, we have investigated the stellar mass evolution of the LEGA-C sample using Chauke et al. (2018)'s reconstructed SFHs, which were obtained from full spectrum fitting. We have traced the evolutionary paths of galaxies forward and backward in time in order to investigate stellar mass growth and whether galaxies preserve their mass rank order as they evolve.

We have shown that the disparity between the stellar mass distribution of galaxies that are star-forming and those that are quiescent galaxies at $z \sim 0.8$ increases with increasing redshift (Figure 3.2), which indicates that SF activity is correlated with past SF activity, and accordingly with stellar mass evolution. Galaxies that are tightly grouped in stellar mass at $z \sim 0.8$, have a wide range of stellar masses by $z = 3$. The spread in stellar mass increases with redshift and it is larger for lower mass stars (Figure 3.3). Furthermore, galaxies that are grouped in velocity dispersion or central mass density at $z \sim 0.8$, have a range of stellar masses at $z \sim 0.8$, and the range increases with redshift (Figure 3.4). Using these parameters to track galaxy populations still results in a spread in stellar mass with redshift.

Individual stellar mass evolution is smoother for more massive galaxies and at $z \gtrsim 2$ (Figure 3.5). This is in line with previous studies from simulated data that suggest that it is because mergers dominate the evolution at lower redshifts and stellar masses, while stochastic growth rates dominate at higher redshifts and stellar masses. However, it could also be that we cannot temporally resolve stellar populations beyond $z = 2$. Some stellar mass growth rates are so drastic that galaxies break

their mass rank order. This implies that the assumption of a constant number density in galaxy population studies is inaccurate.

Whether galaxies are traced backward or forward in time, if they have similar stellar masses at one redshift, their stellar masses will not only evolve, but they will also diverge with time (Figure 3.6). We conclude that the evolution of the median and scatter in their stellar masses indicates the different processes that grow galaxies' stellar masses. For example, mergers and scatter in stellar mass growth rates are suggested as the causes in studies from simulated data and semi-analytical models. We measured an asymmetry between tracing galaxies backward and forward in time. There is a $\sim 30\%$ reduction in scatter for galaxies that are tracked forward in time compared to those that are traced backward in time. The reduction is likely due to the lack of lower mass galaxies at lower redshifts, which results in a lower variety of evolutionary paths.

Our reconstructed SFHs have allowed us to make conclusions which were previously made from studies using simulations, and semi-analytical and abundance matching models. Although we cannot obtain galaxy merger histories from SFHs, which would allow us to track galaxies' main progenitors, tracing the total mass evolution enables us to conclude that the number density of galaxies evolves, and that stellar mass rank order is not preserved.

REJUVENATION IN $z \sim 0.8$ QUIESCENT GALAXIES IN LEGA-C[†]

Investigating whether galaxies accumulate a significant portion of their mass after their main formation phase is important in constraining galaxy evolution theories/models. Galaxies are known to have secondary SF phases, however, measurements still need to be made on when/how often/the extent to which these episodes cause galaxies to rejuvenate, that is, transition back to the blue cloud from the red sequence. In this chapter, I use reconstructed star-formation histories to investigate rejuvenation properties in quiescent galaxies in order to determine if rejuvenation episodes contribute significantly to the growth of the red sequence, and whether colour space studies are affected by their occurrence.

4.1 Introduction

The colors of galaxies are known to be bimodal, not only in the local universe (e.g., Strateva et al., 2001; Baldry et al., 2004), but also at redshift $z \sim 1$ and beyond (e.g. Bell et al., 2004; Franzetti et al., 2007; Whitaker et al., 2011; Straatman et al., 2016). Galaxies are classified as either part of the ‘blue cloud’ or ‘red sequence’, where the blue cloud contains galaxies that are actively forming new stars, while the red sequence contains quiescent galaxies that have very low ongoing star-formation (SF). Ages and metallicities of massive quiescent galaxies (stellar mass $\gtrsim 10^{10.5} M_{\odot}$)

[†]The contents of this chapter are adapted from Chauke et al. (2019). The paper is published in the *Astrophysical Journal*. I myself conducted the research, analysed the results and wrote the text for the paper.

at $z \sim 1$ are consistent with passive evolution to the present-day (e.g., Gallazzi et al., 2014; Choi et al., 2014), although Gallazzi et al. (2014) require additional quenching of a fraction of massive star-forming galaxies at $z \sim 1$ to account for the scatter in the ages of present-day quiescent galaxies. Schiavon et al. (2006), however, compared stacked spectra of red sequence galaxies at redshifts $0.7 \leq z \leq 1$ to local SDSS galaxies (York et al., 2000) and found that their ages are inconsistent with passive evolution, which suggests that either new galaxies with younger stars continually transition to the red sequence, or individual quiescent galaxies experience ‘frosting’, where continuing low-level star formation adds a minority of young stars to an older base population (Trager et al., 2000). Wu et al. (2018) and Spilker et al. (2018) reached the same conclusion using high-resolution spectra of massive (stellar mass $> 10^{11}M_{\odot}$) $z \sim 0.8$ galaxies from the Large Early Galaxy Astrophysics Census Survey (LEGA-C, van der Wel et al., 2016).

The increasingly dominant population of quiescent galaxies measured in number density evolution studies (e.g., Pozzetti et al., 2010; Brammer et al., 2011; Moustakas et al., 2013; Muzzin et al., 2013a) indicates that star-forming galaxies have their star-formation quenched and transition from the blue cloud to the red sequence. The nature of this quenching process is still not understood, although the ‘maintenance mode’ of AGN feedback is widely believed to suppress star-formation in massive galaxies by providing sufficient energy to keep the halo gas from cooling (e.g., Goto, 2006; Heckman and Best, 2014). Therefore, if AGN feedback fails to keep halo gas hot, the star-formation in a galaxy could be reignited.

Although the aforementioned evolution studies indicate that galaxies evolve from being star-forming to quiescent, secondary SF has been found to be a common phenomenon in local early-type galaxies: the fraction of early-type galaxies showing evidence of recent star formation is thought to be between ~ 10 and 30% (Schawinski et al., 2007; Donas et al., 2007). This fraction is higher in low-density environments (e.g., Schawinski et al., 2007; Thomas et al., 2010), which is consistent with H I being detected more often in field galaxies than in clusters (e.g., Oosterloo et al., 2010). Treu et al. (2005) and Thomas et al. (2010) found that the fraction of stellar mass formed from secondary SF episodes decreases with galactic mass, ranging from $< 1\%$ for stellar masses $> 10^{11.5}M_{\odot}$ to $\sim 10\% - 40\%$ for stellar masses $< 10^{11}M_{\odot}$. This is in line with Kaviraj et al. (2007) who found that star-formation is more efficiently quenched in high-mass galaxies (for stellar masses $> 10^{10}M_{\odot}$).

Secondary SF episodes have been linked to either H I gas accretion or mergers which bring in gas, often resulting in only a small population of relatively young stars (e.g. Yi et al., 2005; Kaviraj et al., 2009; Marino et al., 2009). There is no general trend between stellar population and H I properties, however, galaxies with a significant young sub-population have inner gas discs (Oosterloo et al., 2010). Post-starburst (PSB) or ‘E+A’ galaxies, i.e. young quiescent galaxies with strong Balmer absorption lines and weak to no SF-related emission lines (Dressler and Gunn, 1983;

Dressler et al., 1999; Tran et al., 2004), have also been linked to secondary SF episodes in order to reconcile the number density of PSBs with the slow growth of the quiescent population at the high-mass end ($> 10^{11}M_{\odot}$) at $z < 1$ (e.g., Rowlands et al., 2018), as well as using starburst timescales ($\sim 500\text{Myr}$) to show that PSBs are likely not a major component in the growth of the passive galaxy population (e.g., Dressler et al., 2013). E+A galaxies are also likely caused by interactions or mergers (Goto, 2005; Yamauchi et al., 2008).

There are multiple measurements of the fraction of galaxies that undergo secondary SF, however, previous studies were mostly limited to low redshifts because of the abundance of high-resolution spectra in the local Universe. Furthermore, many of these studies do not determine whether the galaxies ‘rejuvenate’, i.e. transition back to the blue cloud from the red sequence. Recently, Pandya et al. (2017) analysed a semi-analytical model of galaxy formation as well as GAMA and CANDELS observations out to $z = 3$ to constrain the frequency of rejuvenation episodes. They measured the transition of massive galaxies ($> 10^{10}M_{\odot}$) from the star-forming ‘main sequence’ (SFMS) to both the ‘transition region’ between the blue cloud and red sequence, and the quiescent sequence. Using their semi-analytical model, they found that the average $z = 0$ quiescent galaxy first joined the quiescent population at $z \sim 0.4$ and that 31% of quiescent galaxies have experienced at least one rejuvenation event since $z = 3$. However, these rejuvenation timescales are short as the average time a galaxy spends in quiescence between $z = 3$ and $z = 0$ is comparable for rejuvenated and non-rejuvenated galaxies in their model. Behroozi et al. (2019) applied empirical models of galaxy formation to dark halo merger trees to determine individual galaxies’ SFRs that are consistent with observations (e.g. stellar mass functions, specific and cosmic SFRs, quenched fractions, etc.). They found that, at $z = 1$, rejuvenation fractions range from $\sim 10\%$ to $\sim 20\%$ for stellar masses in the range $10^{10} - 10^{11}M_{\odot}$, with the rejuvenation fraction peaking around $4 \times 10^{10}M_{\odot}$. Their rejuvenation fractions at $z = 0$ are significantly higher ($\sim 30 - 60\%$ in the same stellar mass range), presumably because galaxies at lower redshifts have had more time to quench and then rejuvenate at a later stage.

The magnitude of the effect of rejuvenation processes still needs to be addressed. Specifically, we do not know if the stellar mass formed from such events is a significant portion of the cosmic star-formation rate density (SFRD) of the Universe and on what timescale these events occur, or how often secondary SF episodes cause galaxies to transition back to the blue cloud during the event (i.e. rejuvenation). In an earlier paper (Chauke et al., 2018), we reconstructed the star-formation histories (SFHs) of galaxies at $z \sim 1$ using the high-resolution spectra from LEGA-C. These SFHs revealed secondary star-formation episodes in a minority of the quiescent population. This allows us to be able to investigate rejuvenation timescales as well as the frequency and magnitude of such events. In this study, we use the reconstructed SFHs from Chauke et al. (2018) to investigate quiescent galaxies with

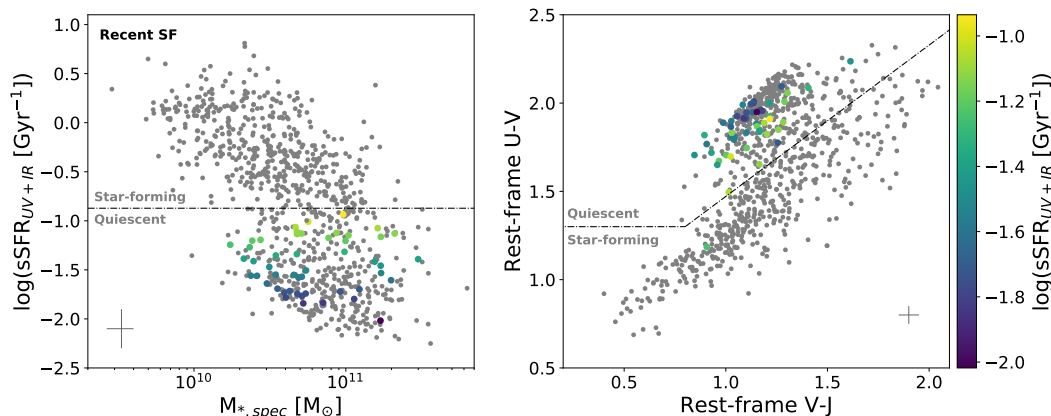


Figure 4.1: sSFR_{UV+IR} as a function of $M_{*,spec}$ (left) and the rest-frame UVJ diagram (right) of the LEGA-C population. The dashed line distinguishes the star-forming and quiescent populations. The rejuvenated quiescent population is color-coded by sSFR_{UV+IR} for comparison. Typical error bars are indicated in dark grey.

rejuvenation episodes. In Section 4.2 we give a brief overview of the sample. In Section 4.3 we investigate the properties of rejuvenated galaxies, viz. the timescales of rejuvenation episodes, the local environmental density and mass dependence of these episodes, as well as whether the mass formed from such events is significant. Finally, in Section 5 we summarise the results. We assume a Λ CDM model with $H_0 = 67.7 \text{ km s}^{-1} \text{ Mpc}^{-1}$, $\Omega_m = 0.3$ and $\Omega_\Lambda = 0.7$.

4.2 Data

LEGA-C (van der Wel et al., 2016) is an ESO Public Spectroscopic survey with VLT/VIMOS of ~ 3000 galaxies in the COSMOS field with redshifts in the range $0.6 < z < 1.0$. The galaxies were selected from the Ultra-VISTA catalog (Muzzin et al., 2013b), with a redshift dependent K-band limit ($K_{ab} = 20.7 - 7.5 \times \log[(1+z)/1.8]$). Each galaxy is observed for ~ 20 h, which results in spectra with $S/N \sim 20 \text{ \AA}^{-1}$ (with resolution $R \sim 3000$) in the wavelength range $\sim 0.6 \mu\text{m} - 0.9 \mu\text{m}$. For details of the data reduction procedure, see van der Wel et al. (2016) and Straatman et al. (2018). This work is based on the second data release¹, which contains 1550 primary sample galaxies. We make use of the following measured quantities in the analysis: rest-frame U-V and V-J colors, UV+IR star formation rates (SFRs), stellar masses ($M_{*,spec}$), UV+IR specific SFRs (sSFR_{UV+IR} , i.e. UV+IR SFRs divided by $M_{*,spec}$), and scale-independent local overdensities, $\log(1 + \delta)$, i.e. the local surface density divided by the mean local surface density. The UV+IR SFRs are estimated from UV and IR luminosities, following Whitaker et al. (2012). $M_{*,spec}$ is the stellar mass estimate obtained from full-spectrum fitting (see Section 4.2.1). The $\log(1 +$

¹<http://www.eso.org/sci/publications/announcements/sciann17120.html>

δ) values are estimated from redshift slices using the Voronoi tessellation method (Darvish et al., 2016). Figure 4.1 shows $sSFR_{UV+IR}$ as a function of $M_{*,spec}$ (left panel), and the rest-frame UVJ diagram (right panel) of the LEGA-C population at the observed redshift. Star-forming and quiescent populations are distinguished by the dashed lines and quiescent galaxies whose SF was rejuvenated, are color-coded by $sSFR_{UV+IR}$ for comparison. See Section 4.2.2 for definitions of quiescence and rejuvenation.

4.2.1 Star Formation Histories

Chauke et al. (2018) used a custom full-spectrum fitting algorithm to reconstruct the SFHs of the LEGA-C sample. The algorithm incorporates *emcee* (an affine invariant ensemble sampler for MCMC, Foreman-Mackey et al., 2013) and *FSPS v3.0* (the Python implementation of the Flexible Stellar Population Synthesis package, Conroy and Gunn, 2010; Conroy et al., 2009; Foreman-Mackey et al., 2014). *emcee* makes use of MCMC ‘walkers’ which randomly explore the parameter space and converge to the most likely parameters values. The galaxy spectra were fit to a linear combination of a set of 12 composite stellar populations (CSPs), with solar metallicity and constant star formation within the time interval of the templates. The algorithm uses Calzetti et al. (2000)’s dust reddening curve to fit for 2 dust reddening values, $E(B - V)_i$, one for the youngest (more dust-obscured) stellar population (0 – 100Myr) and the second for the other stellar populations. The algorithm uses emission-line subtracted spectra. Emission line spectra are computed using the Penalized Pixel-Fitting method (pPXF, Cappellari and Emsellem, 2004). For details of the emission line fitting procedure, see Bezanson et al. (2018). The model results in measurements of stellar masses ($M_{*,spec}$), luminosities (L_{spec}), mean mass-weighted and light-weighted ages ($a_{<MW>}$ and $a_{<LW>}$, respectively) and the dust reddening values. The stellar masses derived using our method, $M_{*,spec}$, are in good agreement with photometry-based stellar masses derived with FAST (Kriek et al., 2009). See Chauke et al. (2018) for further details and results of the fitting algorithm.

4.2.2 Identifying Rejuvenated Galaxies

In this section we identify a sample of galaxies that, according to our spectral fits, have a large probability of having experienced a rejuvenation event after an initial period of quiescence. One of the main goals of this study is to measure the contribution of rejuvenation to the total stellar mass of quiescent galaxies, therefore, we select quiescent galaxies by their specific star-formation rate (sSFR). This approach results in an identical sample of rejuvenated galaxies, with the exception of one galaxy, compared to selecting quiescent galaxies by their U-V and V-J colors, see

Figure 4.1 for a comparison at the observed redshift. In this study, sSFR is used as a quiescent selection criterion because we can directly compute the sSFR from our reconstructed SFHs.

We use the reconstructed SFHs to compute the sSFR of a galaxy at time t_i , where i is the time bin number and sSFR is the SFR at t_i divided by the total stellar mass at that time, i.e. $sSFR_{t_i} = SFR_{t_i}/M_{*,t_i}$. A galaxy is defined as quiescent if the $\log(\text{sSFR} [\text{Gyr}^{-1}]) < -1$ at redshift $z = 0.8$. To track the quiescence of galaxies along their SFHs, we use the Speagle et al. (2014) redshift dependent sSFR to adjust our definition for quiescence to larger redshifts. For example, the limit increases to -0.40 and -0.03 at redshifts $z = 2$ and $z = 3$, respectively (see Speagle et al., 2014, for full details). The instant a galaxy’s sSFR falls below the redshift adjusted limit at some point in its history, it is considered to be quiescent at that point (and the accumulated stellar mass is recorded), until such a time that it rises above the limit. The stellar mass accumulated during this period is considered to be mass formed from secondary SF.

To minimise the error of adding false positives, we compute the probability of a rejuvenation event having occurred using the MCMC walkers (see Section 4.2.1 and Figure 4.4). The probability that a galaxy has a rejuvenation episode (p_{REJ}) is equal to the probability that the galaxy is quiescent at t_i (p_{Q_i}) multiplied by the probability that it is star-forming at a later time t_j (p_{SF_j}). We find the time interval where the galaxy is quiescent (i.e. $p_{Q_i} > 0.5$) and the interval where it is star-forming, and then compute the maxima of the product of the probabilities over these time intervals. p_{Q_i} (p_{SF_j}) is the fraction of walkers that lie below (above) the sSFR limit at t_i (t_j). If $p_{REJ} > 0.5$, then the galaxy is considered to have had a rejuvenation episode. For example, 91529 (see Figure 4.4) is star-forming in bin 2 then has a quiescent period in bin 3 and 4, which is followed by a period of rejuvenation from bin 5 to 8 before the galaxy is quiescent again from bin 9 to 12. In this case, $p_{REJ} = p_{Q_3} \times p_{SF_5} = 1$, and the galaxy is classified as a rejuvenated galaxy. If a galaxy alternates between quiescent and star-forming multiple times during its SFH, then p_{REJ} is calculated as above for each episode. If the p_{REJ} requirement is satisfied, then the episode is counted as a rejuvenation episode. We also compute how long the galaxy was quiescent for before the first rejuvenation episode, i.e. the time range where $p_Q > 0.5$ after the initial SF episode and before rejuvenation (bin 3 to bin 4 for 91529), as well as measure how long the rejuvenation episode lasts, i.e. the time range where $p_{SF} > 0.5$ during the rejuvenation episode (bin 5 to 8 for 91529).

All galaxies in our sample, with the exception of 3 (viz. 206858, 228340 and 92132), contain at most 1 rejuvenation episode before becoming quiescent again at the observed redshift. The quiescent sample contains 412 galaxies, 52 (13%) of which have had a rejuvenation episode. These galaxies are shown in Figure 4.1, they are color-coded by sSFR_{UV+IR} for comparison with the rest-frame UVJ diagram on the right

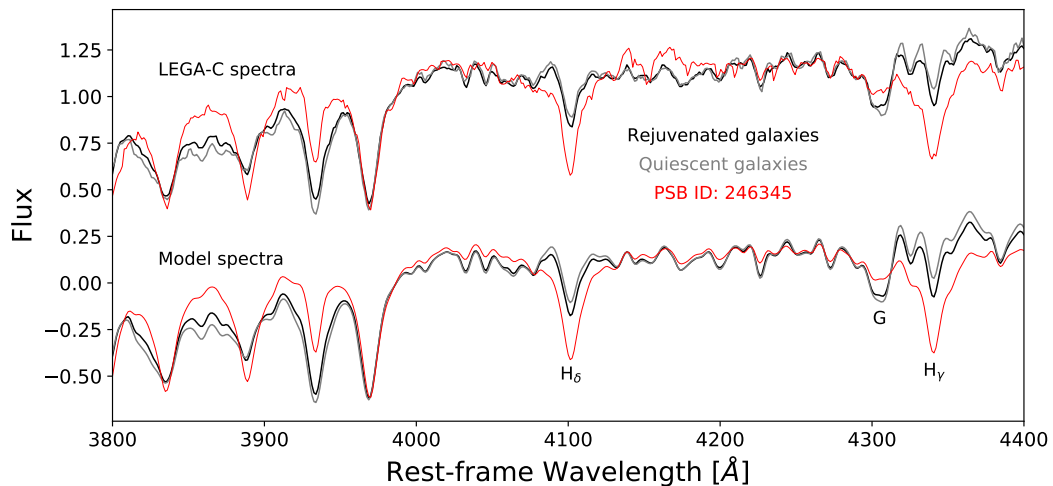


Figure 4.2: Average spectrum (LEGA-C as well as best-fit model) of rejuvenated galaxies (black) compared to the average spectrum of stellar mass and H_{δ} matched quiescent galaxies that do not show evidence of rejuvenation (gray). The PSB spectrum is shown for comparison. The spectra have been normalised and shifted for comparison purposes.

panel. If the sSFR limit were decreased (increased) to -1.3 (-0.7), the fraction of rejuvenated galaxies in our sample would be 19% (9%). Furthermore, using a combination of sub-solar ($0.4 Z_{\odot}$) and solar metallicity CSPs as well as super-solar ($2.5 Z_{\odot}$) and solar metallicity CSPs in our fitting algorithm, instead of solar metallicity CSPs alone, results in 76 and 74% of the sample, respectively, remaining the same. Therefore, mixing metallicities does not significantly change the resulting sample; however, it is unclear how exactly metallicity errors affect the rejuvenation fraction because of the age-metallicity degeneracy in stellar populations. Both the rejuvenated and non-rejuvenated quiescent populations have $S/N \sim 20$, characteristic of LEGA-C galaxies. We have shown in Chauke et al. (2018), using noisy synthetic spectra, that our fitting algorithm converges for this S/N .

In Figure 4.2, we compare the average normalised spectrum (LEGA-C as well as best-fit model) of quiescent galaxies that are identified as rejuvenated to stellar mass and H_{δ} matched quiescent galaxies (i.e. within 0.01dex for stellar mass and 0.5\AA for H_{δ}) that are not identified as such. A PSB spectrum is also shown for comparison. The average rejuvenated galaxy has stronger H_{δ} and H_{γ} lines, which are characteristic of young stellar populations; however, its G-band (absorption lines of the CH molecule around 4300\AA), which is characteristic of older stellar populations, is not as strong as that of quiescent galaxies without rejuvenation episodes. See Figure 4.5 in the appendix for individual best-fit spectra of rejuvenated galaxies in our sample obtained from MCMC full-spectrum fitting (Chauke et al., 2018). Compared to PSB or E+A galaxies, our sample of rejuvenated galaxies have weaker Balmer lines and redder V-J colors. Their V-J colors (see Figure 4.1) are higher than

the typical cut for PSBs ($V-J \lesssim 1$, e.g. Whitaker et al., 2012), and most have H δ equivalent widths ($\text{EW}[\text{H}\delta]$, see Figure 4.2) that are lower than required for PSBs ($\text{EW}[\text{H}\delta] \sim 3 - 5$, Wu et al., 2018). Therefore, our sample of rejuvenated galaxies suggests that most PSB and E+A galaxies are not recently rejuvenated galaxies as suggested in previous studies (e.g., Dressler et al., 2013; Rowlands et al., 2018); instead, they might be galaxies that recently quenched for the first time.

4.2.3 Determining the Rejuvenation Fraction

In this section we consider, for each individual galaxy, the probability that a rejuvenation event occurred and use the sum of those probabilities to assess the importance of rejuvenation events in the context of the cosmological SFH. Some rejuvenation events will be missed by the selection criteria described in Section 4.2.2 above, which motivates us to consider the probability that a rejuvenation event occurred in each quiescent galaxy. For this purpose, we use the MCMC walkers to compute the probability that a galaxy is quiescent (p_{Q_i}) or star-forming (p_{SF_i}) for each of the 12 time bins i . We find the time interval where the galaxy is quiescent (i.e. $p_{Q_i} > 0.5$) after an initial period of SF, and compute the maximum in this range ($p_{Q_{qmax}}$), i.e. when the galaxy has the highest chance of being quiescent. $p_{Q_{qmax}}$ is multiplied to p_{SF_i} , where i ranges from $qmax + 1$ to 12 (the youngest bin), and then the maximum of $p_{Q_{qmax}} \cdot p_{SF_i}$ is determined. Finally, we compute the sum of these maxima for all galaxies in the quiescent sample to determine the fraction of galaxies with rejuvenation episodes. We also measure the mass formed between the first time a galaxy reached quiescence ($i = q1$) and $i = 12$.

We find that $16 \pm 3\%$ of the quiescent population has returned to the star-forming sequence during the epoch $z \sim 0.7 - 1.5$ after reaching quiescence at some earlier time. This is consistent with the fraction of galaxies that have been identified as rejuvenated (Section 4.2.2). However, these rejuvenation events account for only $2 \pm 1\%$ of the stellar mass in quiescent galaxies at $z \sim 0.8$. We have applied a completeness correction to these measurements on a galaxy-by-galaxy basis as described by Wu et al. (2018) to create a volume-limited quantity. The uncertainties are estimated by bootstrapping the sample. These numbers are based on the requirement that a galaxy moves back to the SF sequence, as described in Sec 4.2.2. If we repeat our calculation with a less strict requirement, namely that SF exceeds a fixed value of $\log(\text{sSFR} [\text{Gyr}^{-1}]) < -1$ at any redshift after initial quiescence, instead of an evolving limit, the fraction of galaxies with rejuvenation events increases to $24 \pm 2\%$, with a total mass contribution of $4 \pm 1\%$.

Our rejuvenation fraction lies between Donas et al. (2007) and Schawinski et al. (2007)'s measured values of 10% and 30%, respectively, for $z \sim 0.1$ galaxies, though we note that our value is a lower limit as we only trace rejuvenation episodes in

the redshift range $0.7 < z < 1.5$ due to limitations in the reconstructed SFHs (see Section 4.3.2). Furthermore, Donas et al. (2007) and Schawinski et al. (2007) use UV-color relations to trace recent SF, therefore, their methods trace secondary SF that does not necessarily lead galaxies back to the the star-forming sequence.

Pandya et al. (2017) also measure a higher rejuvenation fraction (31%) in their SAM (see Section 4.1). They define the quiescent region to be 1.4dex below the SFMS, considerably more strict than our definition, and they additionally define a transition region (0.6 – 1.4dex below SFMS) between the star-forming and quiescent sequence. Defining our quiescent region in the same manner results in our rejuvenation fraction decreasing to 5%. However, if we instead define the quiescent region to be 0.6dex below the SFMS, i.e. combine Pandya et al. (2017)’s transition and quiescent population, our rejuvenation fraction increases to 18%, still lower than their value of 31%. The discrepancy between these results may suggest that our sample contains galaxies with hidden rejuvenation at larger lookback times ($\gtrsim 10$ Gyrs), or that the fraction of rejuvenated galaxies is higher at $z = 0$. However, we note that Pandya et al. (2017)’s SAM underproduces quiescent galaxies at $z > 0.5$, and they suggest that one of the reasons could be that quiescent galaxies are rejuvenating too much in their SAM.

Our rejuvenation fraction is in agreement with Behroozi et al. (2019)’s measurements ($\sim 10 - 20\%$). Their SFR distribution is assumed to be the sum of two log-normal distributions corresponding to a quenched population and a star-forming population, at fixed redshift and peak circular velocity at the redshift of peak halo mass, and rejuvenation is defined as at least 300 Myr of quiescence followed by at least 300 Myr of star formation.

4.3 Properties of Rejuvenated population

4.3.1 The Green Valley

Figure 4.3 shows the rest-frame U-V color as a function of $M_{*,spec}$ of rejuvenated galaxies compared to the LEGA-C sample as a whole. The majority of galaxies with rejuvenation episodes have intermediate U-V colors and stellar masses (as well as sSFRs, see Figure 4.1), i.e. they are in the so-called ‘green-valley’, where galaxies are thought to be in the transition phase from the blue cloud to the red sequence. This is to be expected since recent SF should boost the U-V color and rejuvenation episodes decrease with stellar mass (Treu et al., 2005). However, this indicates that a fraction of quiescent green valley galaxies (20%) have made this transition more than once, i.e. they have quiescent progenitors at higher redshifts, which transitioned back to the blue cloud or green-valley, and they are now on their way back to the red

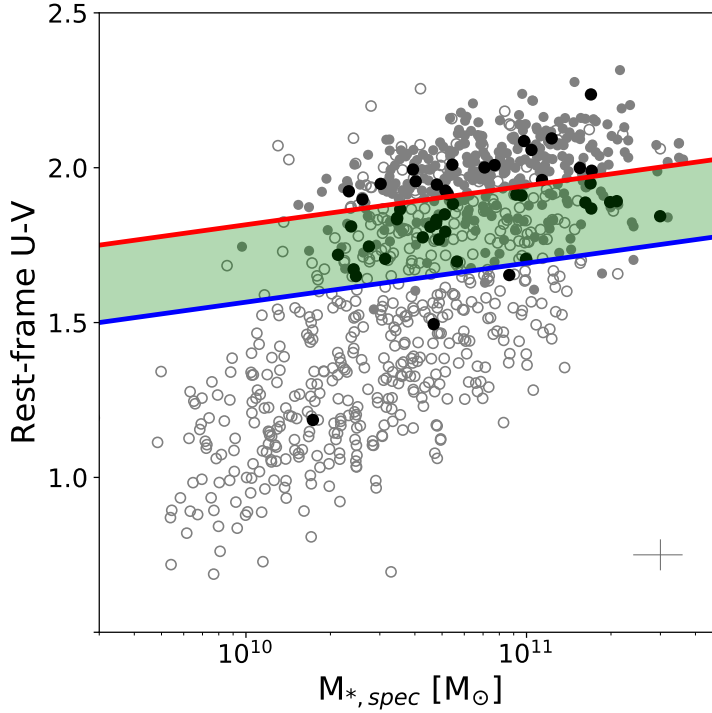


Figure 4.3: Rest-frame U-V color versus $M_{*,spec}$ of the quiescent (filled gray circles) and star-forming (open gray circles) populations in the LEGA-C sample. The black points represent rejuvenated quiescent galaxies, while the green band and the blue and red lines indicate the green valley, star-forming and quiescent regions, respectively. Typical error bars are indicated in dark gray.

sequence.

4.3.2 SFHs and rejuvenation timescales

Figure 4.4 shows rejuvenated galaxies' reconstructed SFHs, the gray lines represent the MCMC walkers (see Section 4.2.1), the black points and the lower and upper error bars represent the 50th, 16th and 84th percentiles of the walkers, and the horizontal dashed lines show the sizes of the (constant star-formation) CSP age bins. The fraction of $M_{*,spec}$ formed from rejuvenation as well as the redshift of the peak SFR of the episode are shown in black. In Figure 4.5, we show the spectra of these rejuvenated galaxies, along with the resulting best-fit spectra. Their IDs and redshifts are shown in black and the resultant normalised χ^2 values and stellar masses are shown in gray. The presence of young and old populations seen in the SFHs is driven by the presence, in the galaxy spectra (Figure 4.5), of both features characteristic of young and older stellar populations, such as Balmer absorption lines and the G-band.

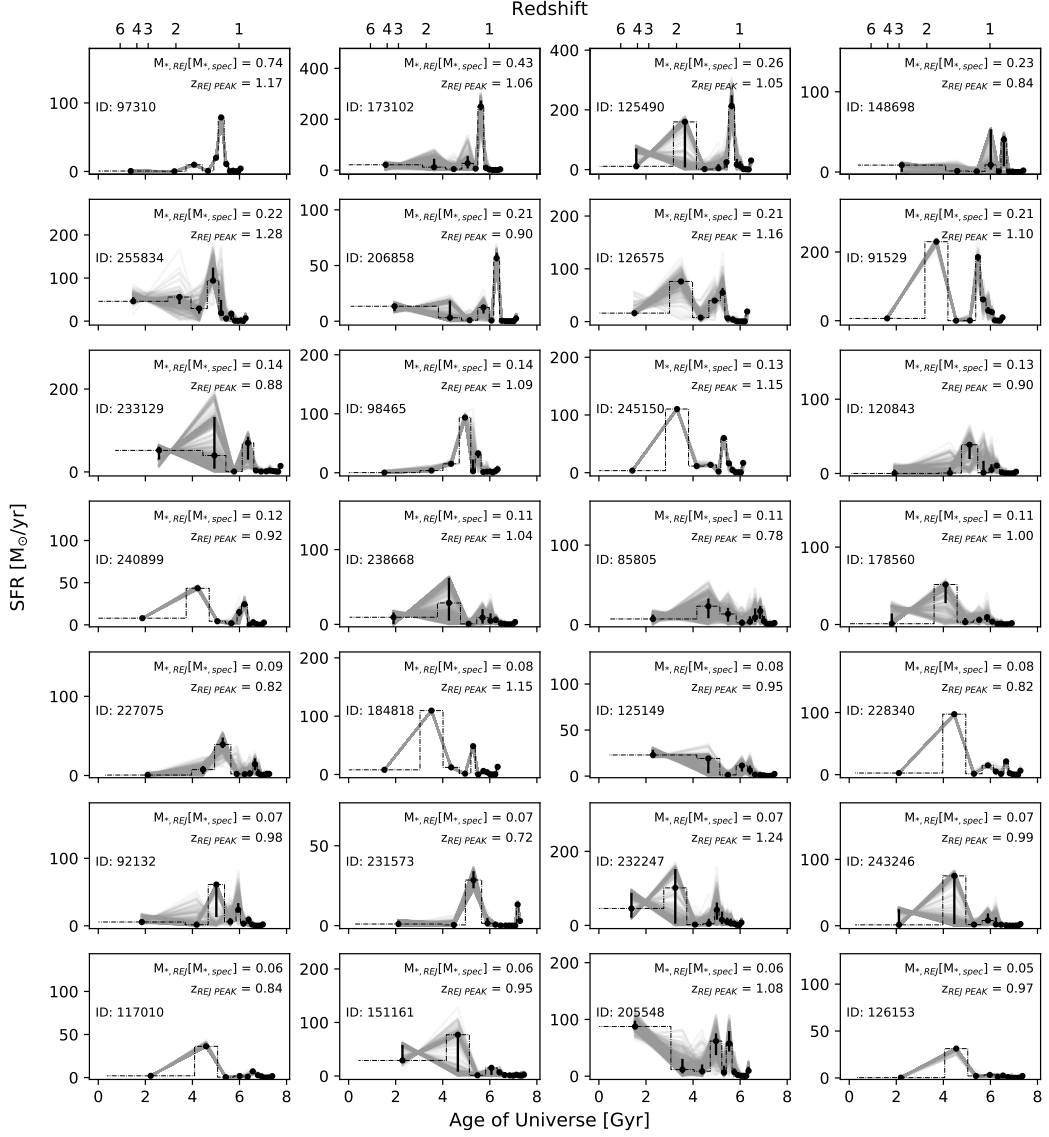


Figure 4.4: The reconstructed star formation histories of rejuvenated galaxies obtained from MCMC full-spectrum fitting (the walkers are shown in gray, Chauke et al., 2018). The fraction of stellar mass formed from the rejuvenation episode and the redshift of the peak SFR of the event are shown in black.

We find that galaxies in the LEGA-C sample have rejuvenation episodes during the redshift range $0.7 < z < 1.5$. This is because our method can only trace rejuvenation events at lookback times $\lesssim 10$ Gyr because our oldest CSP bin is wide (~ 3.5 Gyr), therefore, the algorithm cannot trace rejuvenation for redshifts $z \gtrsim 2$. However, it is not clear whether full spectrum fitting can trace rejuvenation with older stellar populations (> 5 Gyr). On average, we find that galaxies that rejuvenate first become quiescent at $z = 1.2$ for about ~ 1 Gyr before their secondary SF episode, which lasts ~ 0.7 Gyr. Non-rejuvenated galaxies in our sample first

4.3.3. SFR-Mass relation during rejuvenation

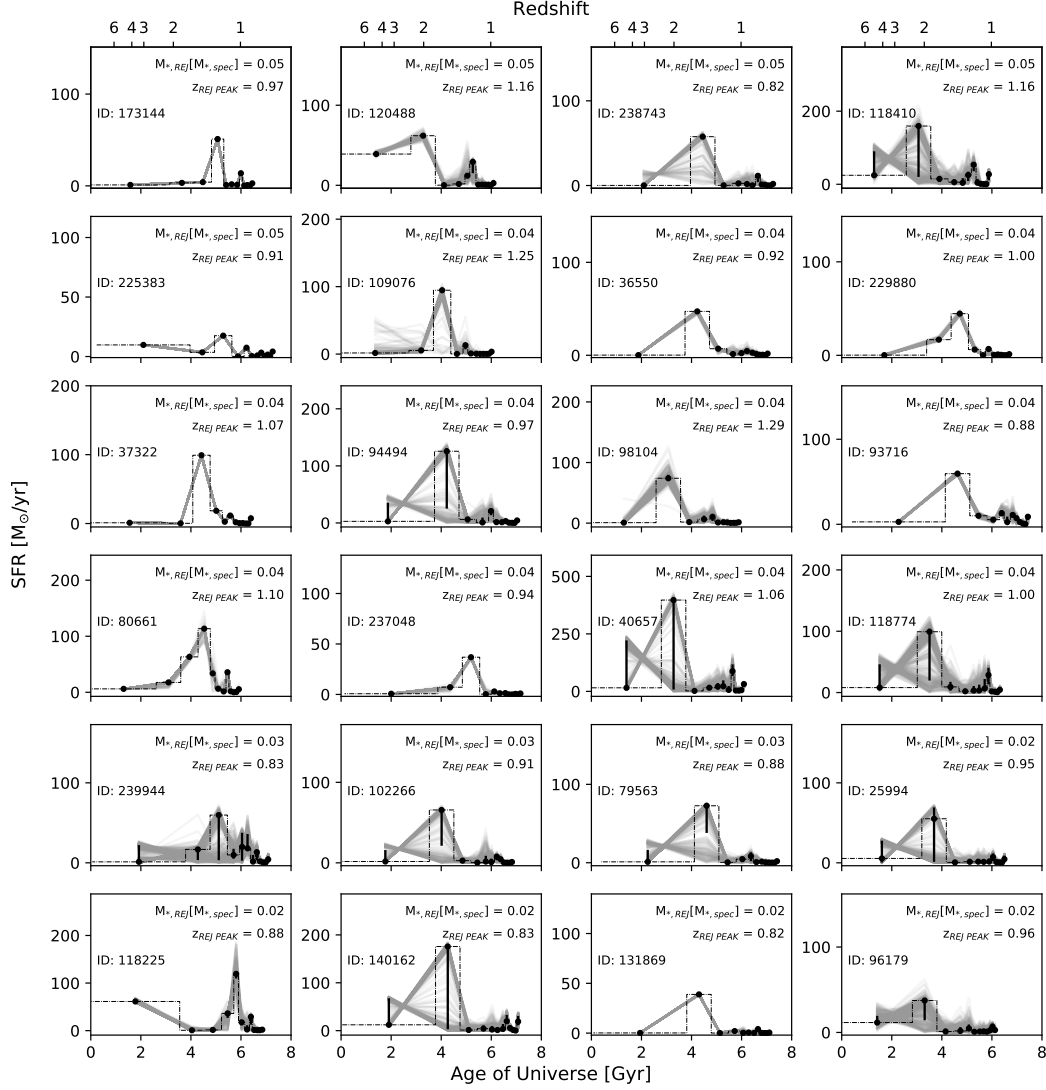


Figure 4.4 (Continued)

become quiescent, on average, at $z = 1.3$. We note that the rejuvenation events we identify are distinct from stochastic variations in the SFR of galaxies on the star-forming sequence. The latter likely occur on shorter time scales ($\sim 100\text{Myr}$) and are consequently averaged out in our SFH reconstruction.

4.3.3 SFR-Mass relation during rejuvenation

In Figure 4.6, we show the SFR- M_* relation of the rejuvenated sample at the peak of their SF episode (black) compared to the relation at their observed redshift (red) when they have transitioned back to quiescence. The gray connecting lines track the evolution of each galaxy in SFR and stellar mass, the blue dashed lines represent

4.3.3. SFR-Mass relation during rejuvenation

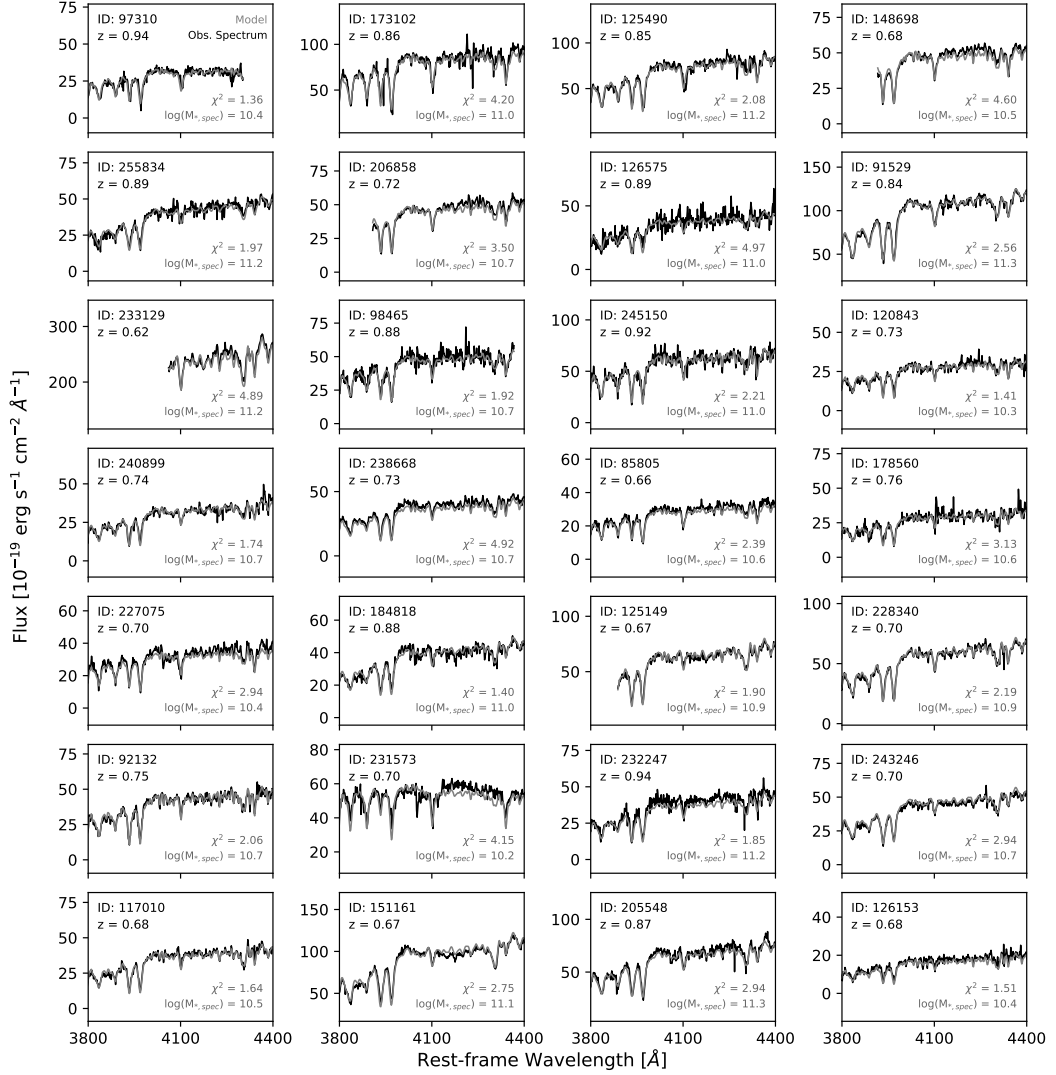


Figure 4.5: Spectra of rejuvenated galaxies along with the resulting spectra obtained from MCMC full-spectrum fitting. Their IDs and redshifts are shown in black and the resultant normalized χ^2 values and stellar masses are shown in gray.

the SFMS at redshift $z = 1$ (Speagle et al., 2014) with a 0.3dex scatter, and the black dashed line distinguishes star-forming and quiescent populations at redshift $z = 1$. This shows that rejuvenation episodes can lead to SFRs which are high enough to cause galaxies to transition back and forth between the SFMS (as well as the starburst region) and the red sequence. These galaxies cover a wide range of SFRs during their rejuvenation episodes, $\sim 50\%$ are within 0.3dex of the SFMS and 3 reach starburst status (0.3dex above the SFMS) during their rejuvenation episode. However, Figure 4.6 also shows that the stellar mass does not increase much after the rejuvenation episode (see Section 4.3.4).

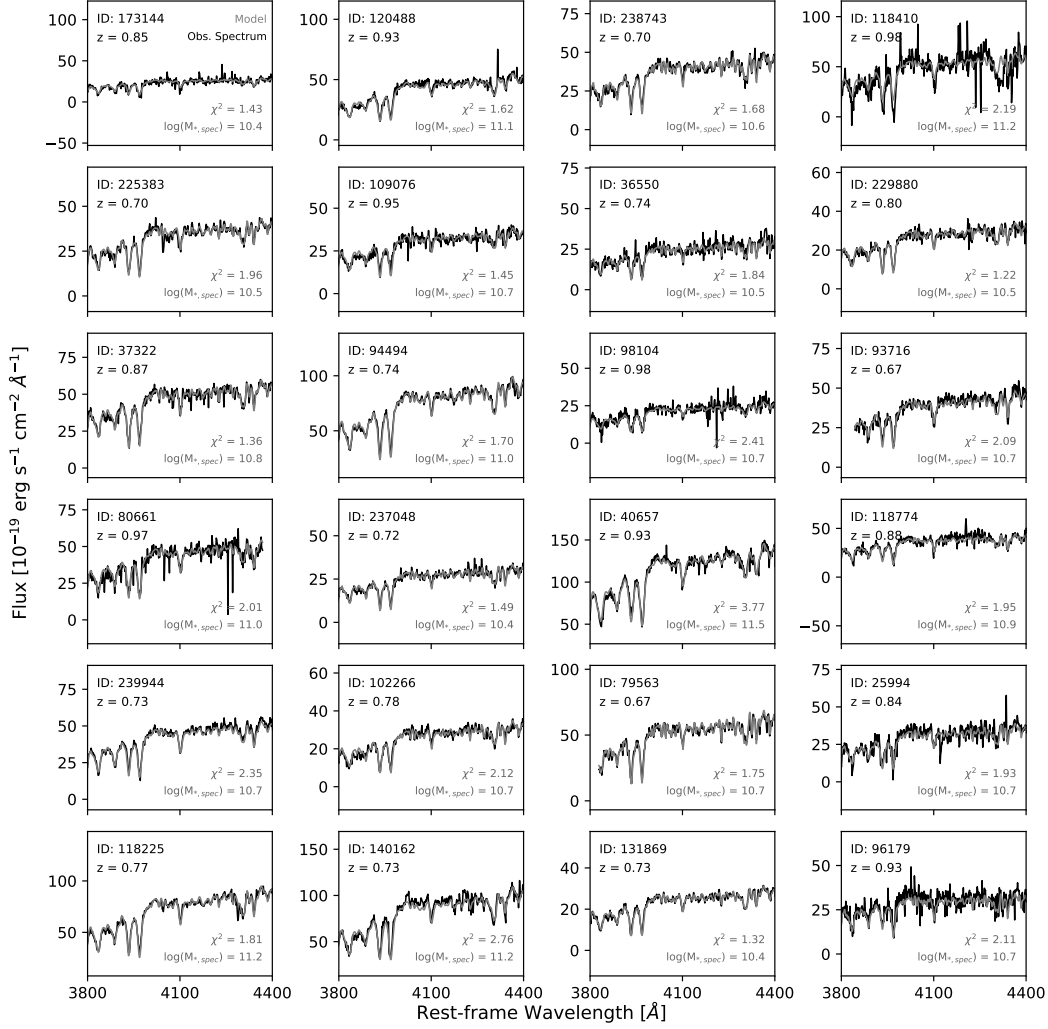


Figure 4.5 (Continued)

4.3.4 Stellar mass and local environmental density dependence

Figure 4.7 shows the fraction of stellar mass attributed to rejuvenation as a function of $M_{*,spec}$. The median trend is indicated in red (computed using ~ 10 galaxies per stellar mass bin) and the upper and lower uncertainties are based on the 16th and 84th percentiles of the walkers of the MCMC algorithm (see Section 4.2.1). On average, rejuvenation events result in the formation of a small fraction of stellar mass: they account for 10% of the stellar mass of these galaxies, with 67% of galaxies having rejuvenated masses $\leq 0.1 \times M_{*,spec}$. The median trend is consistent with a constant rejuvenation mass fraction with stellar mass.

In Figure 4.8, we show the scale-independent local environmental density as a function of galaxy stellar mass. The gray points represent the quiescent sample and the

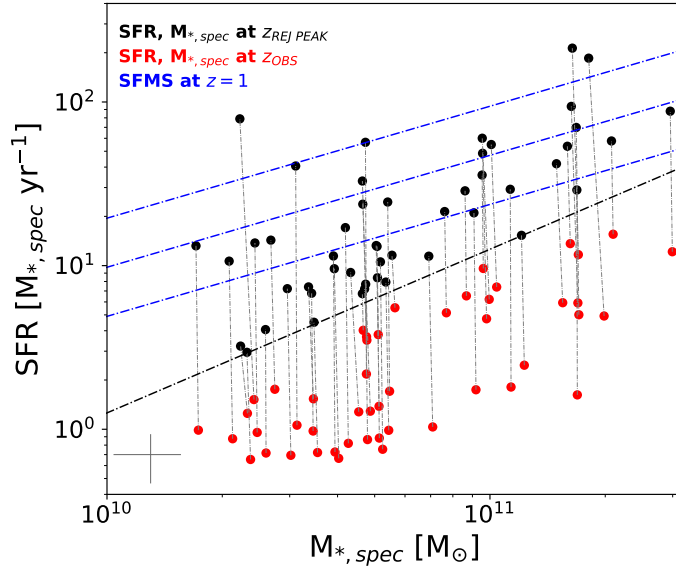


Figure 4.6: The peak SFR versus the stellar mass during the rejuvenation event (black) compared to the SFR- M_* relation of the same sample at the redshift of observation (red). The gray connecting lines track the evolution of each galaxy in SFR and stellar mass. The blue dashed lines represent the Speagle et al. (2014) SFMS at $z = 1$ with a 0.3dex scatter and the black dashed line distinguishes the star-forming sequence from the quiescent sequence. Typical error bars are indicated in dark gray.

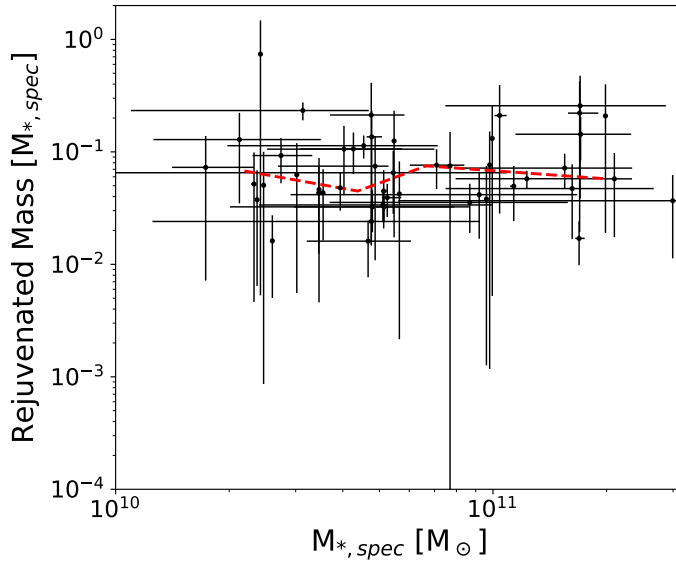


Figure 4.7: Stellar mass of rejuvenated galaxies versus the fraction of stellar mass from the rejuvenation event. The upper and lower uncertainties are based on the 16th and 84th percentiles of the walkers (see Section 4.2.1). The median trend is indicated in red.

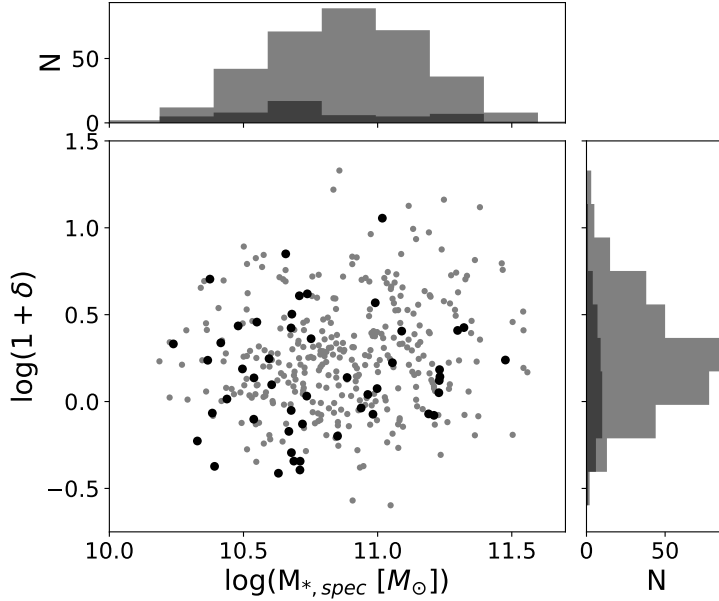


Figure 4.8: Local overdensity versus the stellar mass of quiescent LEGA-C galaxies. The large black points represent galaxies that were rejuvenated. Distributions of the stellar mass and local overdensity are shown on the top and right, respectively.

black points represent rejuvenated galaxies. The rejuvenated and non-rejuvenated populations span the same range in redshift and K-band magnitude and have similar distributions. To test if rejuvenation is density dependent, we use a Kolmogorov-Smirnov test to compare the local overdensity distribution of the rejuvenated sample to the overall quiescent sample. We find that the occurrence of rejuvenated galaxies increases with decreasing local environmental density (D statistic = 0.23, $p < 0.01$), which is in agreement with Schawinski et al. (2007) (see Section 4.1). Rejuvenated galaxies have smaller stellar masses compared to the quiescent sample (D statistic = 0.36, $p < 0.01$). Most galaxies that show evidence of rejuvenation have stellar masses $M_{*,spec} < 10^{11} M_{\odot}$ (see Figure 4.8). These trends are consistent with gas-rich mergers triggering rejuvenation events. Lower-mass galaxies in lower-density environments are more likely to merge with smaller gas-rich galaxies. On the other hand, in more dense environments, the gas in lower-mass galaxies is stripped by high-mass galaxies resulting in dry mergers.

4.3.5 Contribution to the Cosmic Star-formation Rate Density

To determine if rejuvenation episodes contribute significantly to the stellar mass and SF budget in the universe, we compute the fraction of stellar mass formed during rejuvenation events in quiescent galaxies in Section 4.2.3. Rejuvenation events accounting for only $2 \pm 1\%$ of the stellar mass in quiescent galaxies at $z \sim 0.8$, together

with the rejuvenation fraction, means that the average SFRD in the redshift range $0.7 < z < 1.5$ made up by rejuvenation events is $3 \times 10^{-4} \text{M}_{\odot} \text{yr}^{-1} \text{Mpc}^{-3}$, a mere 0.3% of the total Madau and Dickinson (2014) SFRD. This indicates that only a negligible fraction of all SF at this epoch is due to revived quiescent galaxies.

4.4 Summary

We have investigated rejuvenation in quiescent galaxies in the LEGA-C sample using Chauke et al. (2018)'s reconstructed SFHs, which were obtained from full spectrum fitting. We have shown that most galaxies which have had a rejuvenation episode lie in the green valley, i.e. they have intermediate U-V colors and stellar masses (Figure 4.3). We presented the fraction of LEGA-C's quiescent population that have experienced rejuvenation events in their recent past, i.e. galaxies which had at one point transitioned from the star-forming to the quiescent sequence, transitioned back to the star-forming sequence before becoming quiescent again (Figure 4.4).

Limitations from the full spectrum fitting algorithm (see Section 4.3) means that we can only measure rejuvenation from redshift $z \lesssim 2$ (lookback $\lesssim 10 \text{Gyr}$ w.r.t. to the present day). We measure these events in the redshift range $0.7 < z < 1.5$ and they have an average time span of $\sim 0.7 \text{Gyr}$ (Figure 4.4). The occurrence of rejuvenated galaxies is higher in low-density environments, which is in agreement with previous studies (Figure 4.8). We found that rejuvenated galaxies generally have lower stellar masses ($< 10^{11} \text{M}_{\odot}$) compared to the overall quiescent population, however, we do not measure a dependence on other galaxy parameters such as size.

On average, rejuvenation episodes generate 10% of the galaxies' total stellar mass (Figure 4.7). At the peak SFR of the rejuvenation episode, many galaxies transition back to the SFMS (Figure 4.6). $16 \pm 3\%$ of the quiescent population has likely experienced a rejuvenation episode, this is only $2 \pm 1\%$ of the stellar mass in the quiescent sample, which means that rejuvenation episodes in the redshift range $z \sim 0.7 - 1.5$ account for only 0.3% of the SFRD. This shows that although a significant portion of galaxies experience rejuvenation episodes, the mass formed from such events does not significantly contribute to the SFRD in the Universe. Therefore, rejuvenation is not an important factor in the growth of the red sequence, however, it can be a significant factor in detailed color studies.

Summary and Outlook

5.1 Summary

Insights from photometric and spectroscopic surveys over the last two decades have been plentiful. We have discovered that galaxies are bimodal in many of their properties, such as colour, where they are either part of the blue (star-forming) cloud or the red (quiescent) sequence; that more massive galaxies have older stars, i.e. ‘downsizing’; that the SFRD peaked at $z \sim 2$, and has been decreasing steeply since then; and many other revelations that have guided our next steps. However, crucial knowledge of individual galaxy evolution at early cosmic time has been lacking. SDSS spectra have revolutionised our understanding of local galaxies; however, it is difficult to reconstruct their SFHs because most present-day galaxies are old (> 5 Gyrs). With the LEGA-C survey, the largest spectroscopic survey of distant ($z \sim 1$) galaxies to date, we have begun to investigate the stellar population properties of $z \sim 1$ galaxies, gaining knowledge about their individual evolutionary paths, and the processes that drive them. The quality of LEGA-C spectra is equivalent to SDSS spectra, and knowing that 50% of the stars in the Universe formed since $z = 1$, means that we can make analogous measurements with a population of galaxies that is younger, and has a wide variety in structure and SF activity.

In this thesis, I investigated the stellar population properties of $z \sim 1$ galaxies using their SFHs, which were reconstructed from high- S/N , high-resolution continuum spectra provided by the LEGA-C survey.

In Chapter 2, I presented a non-parametric full-spectrum fitting algorithm to reconstruct the SFHs of LEGA-C galaxies, and investigated the dependence of individual SFHs on stellar mass, stellar velocity dispersion and SF activity. $z \sim 1$ galaxies

have a wide variety of SFHs, but they also have similar trends compared to local galaxies. Their mass-weighted age correlates strongly with stellar velocity dispersion and ongoing SF activity; and the stellar content in higher velocity dispersion (mass) galaxies formed earlier and faster. A correlation between velocity dispersion and SF activity has been reported for distant galaxies, but these results extend this to an underlying correlation with overall stellar age. Individual SFHs reveal that the scatter in the SFHs of massive galaxies increases towards lower redshifts, and the quiescent and star-forming populations are increasingly disparate. This indicates that current SF activity is strongly correlated with past ($\sim 3\text{Gyr}$ prior) SF activity. This study shows that galaxies with a given velocity dispersion can have many evolutionary paths. This behaviour has been reported in simulations, but has been confirmed here using reconstructed individual SFHs.

In Chapter 3, I traced the stellar mass evolution of $z \sim 1$ galaxies between $z \sim 1$ and $z = 3$, and investigated whether stellar mass ranking is conserved as galaxies evolve. Galaxies that are similar in stellar mass at redshift $z \sim 1$, have diverse evolutionary paths that lead to a wide range of stellar masses by redshift $z = 3$, and vice versa, and the range increases with redshift. The most massive galaxies at $z \sim 1$ have the smallest difference in stellar mass at $z = 3$. Constant number density assumptions, i.e. galaxy mergers are negligible and mass ranking is conserved as galaxies evolve, have guided many works, which has led to measurements of several galaxy properties, e.g. SFHs, velocity dispersion, size, etc. However, these assumptions have been shown not to hold in simulations and semi-analytical models. This work confirms that mass ranking is not conserved as galaxies evolve, in agreement with theoretical studies.

In Chapter 4, I used the reconstructed SFHs of $z \sim 1$ quiescent galaxies to investigate rejuvenation, i.e. galaxies' transition back to the blue cloud from the red sequence. $16 \pm 3\%$ of $z \sim 1$ quiescent galaxies experienced rejuvenation episodes, and a majority of them lie in the green valley, i.e. they have intermediate U-V colors and stellar masses. The green valley is thought to be where galaxies are in the transition phase from the blue cloud to the red sequence. However, this study reveals that 20% of galaxies that are in the green valley at $z \sim 1$, have quiescent progenitors at higher redshifts, which complicates interpretations in colour space studies. Rejuvenation events are measured in the redshift range $0.7 < z < 1.5$, they have an average time span of $\sim 0.7\text{Gyr}$, and they occur more frequently in low-density environments. Finally, rejuvenation episodes are only $2 \pm 1\%$ of the stellar mass budget in quiescent galaxies, which means that they do not contribute significantly to the growth of the red sequence.

5.2 Outlook

Recovering the SFHs of galaxies at redshift $z \sim 1$ offers a wide range of possibilities. 8 Gyrs ago, galaxies had very different stellar populations. Therefore, there is a wealth of knowledge in LEGA-C galaxies that cannot be gained with local spectra. Furthermore, stellar population measurements from LEGA-C will act as benchmark to connect populations at higher redshifts to the local Universe. This will be important for future surveys with the James Webb Space Telescope that will be investigating the properties of galaxies beyond $z \sim 2$. Below, I list three studies that will be undertaken in the future.

5.2.1 Quenching

Galaxies are known to be bimodal in colour, at both low and high redshifts (e.g. Strateva et al., 2001; Bell et al., 2004). Since quiescent galaxies have been increasingly dominant since $z = 1$, it is believed that significant numbers of galaxies evolve from the blue (star-forming) cloud to the red (quiescent) sequence and remain quiescent thereafter. Understanding the physics of SF quenching, and as a result, the origin of bimodality in some galaxy parameters, is crucial to our understanding of galaxy evolution. However, as stated in Chapter 1, it is not clear what processes cause galaxies to quench, and how quickly it happens. A number of internal and external mechanisms have been proposed, each mechanism either heats gas to the extent that it cannot collapse to form stars or expels gas that would otherwise form stars. The mechanisms have been a matter of debate in the study of galaxy evolution for decades.

Measuring quenching timescales, that is, the number of quenched galaxies as a function of time and the speed at which galaxies quench, allows us to probe quenching mechanisms. Galaxies that quenched slowly are different to those that quenched abruptly in terms of the relative strengths of their Balmer and metal line absorption features. Using the individual SFHs obtained in this study from full-spectrum fitting, we can measure the quenching speed and rate because the SFHs provide us with galaxies' SF activity as a function of time. This will enable us to shed light on the underlying processes that cause galaxies to quench.

5.2.2 SFH and Galaxy Structure

Parameters that correlate with quiescence point to dense central regions, bulge prominence, and therefore, large black hole masses. Quiescence is correlated with galactic structure in that quiescent populations have concentrated light profiles, as

described by their Sérsic indices (e.g. Bell et al., 2012). Additionally, the central mass density at which galaxies quench increases with stellar mass (e.g. Fang et al., 2013). The early formation of dense cores, though, means that their contribution to the total stellar mass budget of the Universe decreases with redshift (e.g. van Dokkum et al., 2014). Although most quiescent galaxies have prominent bulges, many have significant discs, and a number of galaxies with significant star formation also have prominent bulges. This suggests that a dense bulge is necessary but not sufficient to quench a galaxy fully (e.g. Bell et al., 2012; Fang et al., 2013).

The correlation between colour and galaxy structure or morphology (Lee et al., 2013; Correa et al., 2017) suggests a transformation of disc-dominated galaxies into those that are bulge-dominated, either through disc disruption or bulge growth. Age is also correlated with galaxy structure in that lower mass galaxies have young stellar populations, low surface mass densities and low concentrations typical of discs (e.g. Kauffmann et al., 2003). However, we do not as of yet understand how structural changes affect the manner in which SFHs evolve. Measuring stellar population ages and investigating the relationship between SFHs and galaxy structure will help in probing the mechanism that controls galaxy SFRs and how it impacts galaxy structure and morphology. This will lead to establishing how bulges and disks are formed in galaxies.

5.2.3 Comparing Reconstructed SFHs to Simulations

Computational simulations have been useful in the quest to understand how galaxies form and evolve over cosmological timescales that are not easily revealed through observations. They attempt to replicate how galaxies grow and evolve using the evolution theories that have been developed. When compared to observations, they can point to unconsidered processes that play an important role in the formation and evolution of galaxies. By comparing parameters measured from SFH reconstruction to those from simulations like Illustris, we can constrain the processes that drive stellar mass evolution, quenching and rejuvenation after galaxies have quenched. We can determine whether these processes are external, dependent upon the surrounding environment, or internal, dependent upon the galaxy itself.

5.3 Concluding Remarks

The results presented in this thesis have shown the power and advantage of stellar population studies of more distant ($z \sim 1$) galaxies. This study has confirmed some similarities between present-day galaxies and more distant galaxies; and it has also confirmed some results from simulations, which are in contrast with accepted modes

of thought. The knowledge obtained from this work (and LEGA-C studies in general), some of which could not have been gained with local spectra, will be essential for studies at even higher redshifts.

If you are reading this, well done. You have reached the point where the story is complete.

First Author Publications of P. Chauke

P. Chauke, A. van der Wel, C. Pacifici, R. Bezanson, P.-F. Wu, A. Gallazzi, K. Noeske, C. Straatman, J.-C. Muños-Mateos, M. Franx, I. Barišic, E. F. Bell, G. B. Brammer, J. Calhau, J. van Houdt, I. Labbé, M. V. Maseda, A. Muzzin, H.-W. Rix, and D. Sobral. Star Formation Histories of $z\sim 1$ Galaxies in LEGA-C. *ApJ*, 861:13, July 2018. doi: 10.3847/1538-4357/aac324.

This work was used in this thesis.

P. Chauke, A. van der Wel, C. Pacifici, R. Bezanson, P.-F. Wu, A. Gallazzi, C. Straatman, M. Franx, I. Barišic, E. F. Bell, J. van Houdt, M. V. Maseda, A. Muzzin, D. Sobral, and J. Spilker. Rejuvenation in $z\sim 0.8$ Quiescent Galaxies in LEGA-C. *ApJ*, 877(1):48, May 2019. doi: 10.3847/1538-4357/ab164d.

This work was used in this thesis.

P. Chauke, A. van der Wel, et al. Stellar Mass Evolution and Ranking of $z\sim 0.8$ Galaxies in LEGA-C. in prep.

This work was used in this thesis.

Bibliography

- L. E. Abramson, M. D. Gladders, A. Dressler, A. Oemler, Jr., B. Poggianti, and B. Vulcani. Return to [Log-]Normalcy: Rethinking Quenching, The Star Formation Main Sequence, and Perhaps Much More. *ApJ*, 832:7, Nov. 2016. doi: 10.3847/0004-637X/832/1/7.
- Y. M. Bahé and I. G. McCarthy. Star formation quenching in simulated group and cluster galaxies: when, how, and why? *MNRAS*, 447:969–992, Feb. 2015. doi: 10.1093/mnras/stu2293.
- I. K. Baldry, K. Glazebrook, J. Brinkmann, Ž. Ivezić, R. H. Lupton, R. C. Nichol, and A. S. Szalay. Quantifying the Bimodal Color-Magnitude Distribution of Galaxies. *ApJ*, 600:681–694, Jan. 2004. doi: 10.1086/380092.
- I. Barišić, A. van der Wel, R. Bezanson, C. Pacifici, K. Noeske, J. C. Muñoz-Mateos, M. Franx, V. Smolčić, E. F. Bell, G. Brammer, J. Calhau, P. Chauké, P. G. van Dokkum, J. van Houdt, A. Gallazzi, I. Labbé, M. V. Maseda, A. Muzzin, D. Sobral, C. Straatman, and P.-F. Wu. Stellar Dynamics and Star Formation Histories of $z \sim 1$ Radio-loud Galaxies. *ApJ*, 847:72, Sept. 2017. doi: 10.3847/1538-4357/aa8768.
- G. Barro, S. M. Faber, D. C. Koo, A. Dekel, J. J. Fang, J. R. Trump, P. G. Pérez-González, C. Pacifici, J. R. Primack, R. S. Somerville, H. Yan, Y. Guo, F. Liu, D. Ceverino, D. D. Kocevski, and E. McGrath. Structural and Star-forming Relations since $z \sim 3$: Connecting Compact Star-forming and Quiescent Galaxies. *ApJ*, 840:47, May 2017. doi: 10.3847/1538-4357/aa6b05.
- P. Behroozi, R. H. Wechsler, A. P. Hearin, and C. Conroy. UniverseMachine: The Correlation between Galaxy Growth and Dark Matter Halo Assembly from $z = 0 - 10$. *MNRAS*, May 2019. doi: 10.1093/mnras/stz1182.
- P. S. Behroozi, D. Marchesini, R. H. Wechsler, A. Muzzin, C. Papovich, and M. Stefanon. Using Cumulative Number Densities to Compare Galaxies across Cosmic Time. *ApJL*, 777:L10, Nov. 2013. doi: 10.1088/2041-8205/777/1/L10.

- E. F. Bell, C. Wolf, K. Meisenheimer, H.-W. Rix, A. Borch, S. Dye, M. Kleinheinrich, L. Wisotzki, and D. H. McIntosh. Nearly 5000 Distant Early-Type Galaxies in COMBO-17: A Red Sequence and Its Evolution since $z \sim 1$. *ApJ*, 608:752–767, June 2004. doi: 10.1086/420778.
- E. F. Bell, A. van der Wel, C. Papovich, D. Kocevski, J. Lotz, D. H. McIntosh, J. Kartaltepe, S. M. Faber, H. Ferguson, A. Koekemoer, N. Grogin, S. Wuyts, E. Cheung, C. J. Conselice, A. Dekel, J. S. Dunlop, M. Giavalisco, J. Herrington, D. C. Koo, E. J. McGrath, D. de Mello, H.-W. Rix, A. R. Robaina, and C. C. Williams. What Turns Galaxies Off? The Different Morphologies of Star-forming and Quiescent Galaxies since $z \sim 2$ from CANDELS. *ApJ*, 753:167, July 2012. doi: 10.1088/0004-637X/753/2/167.
- S. Belli, A. B. Newman, and R. S. Ellis. Stellar Populations from Spectroscopy of a Large Sample of Quiescent Galaxies at $Z \geq 1$: Measuring the Contribution of Progenitor Bias to Early Size Growth. *ApJ*, 799:206, Feb. 2015. doi: 10.1088/0004-637X/799/2/206.
- P. N. Best, G. Kauffmann, T. M. Heckman, and Ž. Ivezić. A sample of radio-loud active galactic nuclei in the Sloan Digital Sky Survey. *MNRAS*, 362:9–24, Sept. 2005. doi: 10.1111/j.1365-2966.2005.09283.x.
- R. Bezanson, P. G. van Dokkum, M. Franx, G. B. Brammer, J. Brinchmann, M. Kriek, I. Labbé, R. F. Quadri, H.-W. Rix, J. van de Sande, K. E. Whitaker, and R. J. Williams. Redshift Evolution of the Galaxy Velocity Dispersion Function. *ApJL*, 737:L31, Aug. 2011. doi: 10.1088/2041-8205/737/2/L31.
- R. Bezanson, A. van der Wel, C. Pacifici, K. Noeske, I. Barišić, E. F. Bell, G. B. Brammer, J. Calhau, P. Chauke, P. van Dokkum, M. Franx, A. Gallazzi, J. van Houdt, I. Labbé, M. V. Maseda, J. C. Muñoz-Mateos, A. Muzzin, J. van de Sande, D. Sobral, C. Straatman, and P.-F. Wu. Spatially Resolved Stellar Kinematics from LEGA-C: Increased Rotational Support in $z \sim 0.8$ Quiescent Galaxies. *ApJ*, 858:60, May 2018. doi: 10.3847/1538-4357/aabc55.
- G. B. Brammer, K. E. Whitaker, P. G. van Dokkum, D. Marchesini, M. Franx, M. Kriek, I. Labbé, K.-S. Lee, A. Muzzin, R. F. Quadri, G. Rudnick, and R. Williams. The Number Density and Mass Density of Star-forming and Quiescent Galaxies at $0.4 \leq z \leq 2.2$. *ApJ*, 739:24, Sept. 2011. doi: 10.1088/0004-637X/739/1/24.
- G. Bruzual and S. Charlot. Stellar population synthesis at the resolution of 2003. *MNRAS*, 344:1000–1028, Oct. 2003. doi: 10.1046/j.1365-8711.2003.06897.x.
- K. Bundy, M. A. Bershady, D. R. Law, R. Yan, N. Drory, N. MacDonald, D. A. Wake, B. Cherinka, J. R. Sánchez-Gallego, A.-M. Weijmans, D. Thomas, C. Tremonti, K. Masters, L. Coccatto, A. M. Diamond-Stanic, A. Aragón-Salamanca, V. Avila-Reese, C. Badenes, J. Falcón-Barroso, F. Belfiore, D. Bizyaev,

- G. A. Blanc, J. Bland-Hawthorn, M. R. Blanton, J. R. Brownstein, N. Byler, M. Cappellari, C. Conroy, A. A. Dutton, E. Emsellem, J. Etherington, P. M. Frinchaboy, H. Fu, J. E. Gunn, P. Harding, E. J. Johnston, G. Kauffmann, K. Kinemuchi, M. A. Klaene, J. H. Knapen, A. Leauthaud, C. Li, L. Lin, R. Maiolino, V. Malanushenko, E. Malanushenko, S. Mao, C. Maraston, R. M. McDermid, M. R. Merrifield, R. C. Nichol, D. Oravetz, K. Pan, J. K. Parejko, S. F. Sanchez, D. Schlegel, A. Simmons, O. Steele, M. Steinmetz, K. Thanjavur, B. A. Thompson, J. L. Tinker, R. C. E. van den Bosch, K. B. Westfall, D. Wilkinson, S. Wright, T. Xiao, and K. Zhang. Overview of the SDSS-IV MaNGA Survey: Mapping nearby Galaxies at Apache Point Observatory. *ApJ*, 798:7, Jan. 2015. doi: 10.1088/0004-637X/798/1/7.
- D. Calzetti, L. Armus, R. C. Bohlin, A. L. Kinney, J. Koornneef, and T. Storchi-Bergmann. The Dust Content and Opacity of Actively Star-forming Galaxies. *ApJ*, 533:682–695, Apr. 2000. doi: 10.1086/308692.
- M. Cappellari and E. Emsellem. Parametric Recovery of Line-of-Sight Velocity Distributions from Absorption-Line Spectra of Galaxies via Penalized Likelihood. *PASP*, 116:138–147, Feb. 2004. doi: 10.1086/381875.
- S. Carniani, A. Marconi, R. Maiolino, B. Balmaverde, M. Brusa, M. Cano-Díaz, C. Cicone, A. Comastri, G. Cresci, F. Fiore, C. Feruglio, F. La Franca, V. Mainieri, F. Mannucci, T. Nagao, H. Netzer, E. Piconcelli, G. Risaliti, R. Schneider, and O. Shemmer. Fast outflows and star formation quenching in quasar host galaxies. *A&A*, 591:A28, June 2016. doi: 10.1051/0004-6361/201528037.
- G. Chabrier. Galactic Stellar and Substellar Initial Mass Function. *PASP*, 115: 763–795, July 2003. doi: 10.1086/376392.
- S. Charlot and S. M. Fall. A Simple Model for the Absorption of Starlight by Dust in Galaxies. *ApJ*, 539:718–731, Aug. 2000. doi: 10.1086/309250.
- P. Chauke, A. van der Wel, C. Pacifici, R. Bezanson, P.-F. Wu, A. Gallazzi, K. Noeske, C. Straatman, J.-C. Muñoz-Mateos, M. Franx, I. Barišić, E. F. Bell, G. B. Brammer, J. Calhau, J. van Houdt, I. Labbé, M. V. Maseda, A. Muzzin, H.-W. Rix, and D. Sobral. Star Formation Histories of $z \sim 1$ Galaxies in LEGA-C. *ApJ*, 861:13, July 2018. doi: 10.3847/1538-4357/aac324.
- P. Chauke, A. van der Wel, C. Pacifici, R. Bezanson, P.-F. Wu, A. Gallazzi, C. Straatman, M. Franx, I. Barišić, E. F. Bell, J. van Houdt, M. V. Maseda, A. Muzzin, D. Sobral, and J. Spilker. Rejuvenation in $z \sim 0.8$ Quiescent Galaxies in LEGA-C. *ApJ*, 877(1):48, May 2019. doi: 10.3847/1538-4357/ab164d.
- J. Choi, C. Conroy, J. Moustakas, G. J. Graves, B. P. Holden, M. Brodwin, M. J. I. Brown, and P. G. van Dokkum. The Assembly Histories of Quiescent Galaxies since $z = 0.7$ from Absorption Line Spectroscopy. *ApJ*, 792:95, Sept. 2014. doi: 10.1088/0004-637X/792/2/95.

- R. Cid Fernandes, A. Mateus, L. Sodré, G. Stasińska, and J. M. Gomes. Semi-empirical analysis of Sloan Digital Sky Survey galaxies - I. Spectral synthesis method. *MNRAS*, 358:363–378, Apr. 2005. doi: 10.1111/j.1365-2966.2005.08752.x.
- R. Cid Fernandes, N. V. Asari, L. Sodré, G. Stasińska, A. Mateus, J. P. Torres-Papaqui, and W. Schoenell. Uncovering the chemical enrichment and mass-assembly histories of star-forming galaxies. *MNRAS*, 375:L16–L20, Feb. 2007. doi: 10.1111/j.1745-3933.2006.00265.x.
- L. Ciesla, D. Elbaz, and J. Fensch. The SFR- M_* main sequence archetypal star-formation history and analytical models. *A&A*, 608:A41, Dec. 2017. doi: 10.1051/0004-6361/201731036.
- A. Cimatti, E. Daddi, and A. Renzini. Mass downsizing and “top-down” assembly of early-type galaxies. *A&A*, 453:L29–L33, July 2006. doi: 10.1051/0004-6361:20065155.
- C. Conroy. Modeling the Panchromatic Spectral Energy Distributions of Galaxies. *ARA&A*, 51:393–455, Aug. 2013. doi: 10.1146/annurev-astro-082812-141017.
- C. Conroy and J. E. Gunn. The Propagation of Uncertainties in Stellar Population Synthesis Modeling. III. Model Calibration, Comparison, and Evaluation. *ApJ*, 712:833–857, Apr. 2010. doi: 10.1088/0004-637X/712/2/833.
- C. Conroy and P. G. van Dokkum. The Stellar Initial Mass Function in Early-type Galaxies From Absorption Line Spectroscopy. II. Results. *ApJ*, 760:71, Nov. 2012. doi: 10.1088/0004-637X/760/1/71.
- C. Conroy, J. E. Gunn, and M. White. The Propagation of Uncertainties in Stellar Population Synthesis Modeling. I. The Relevance of Uncertain Aspects of Stellar Evolution and the Initial Mass Function to the Derived Physical Properties of Galaxies. *ApJ*, 699:486–506, July 2009. doi: 10.1088/0004-637X/699/1/486.
- C. A. Correa, J. Schaye, B. Clauwens, R. G. Bower, R. A. Crain, M. Schaller, T. Theuns, and A. C. R. Thob. The relation between galaxy morphology and colour in the EAGLE simulation. *MNRAS*, 472:L45–L49, Nov. 2017. doi: 10.1093/mnrasl/slx133.
- B. Darvish, B. Mobasher, D. Sobral, A. Rettura, N. Scoville, A. Faisst, and P. Capak. The Effects of the Local Environment and Stellar Mass on Galaxy Quenching to $z \sim 3$. *ApJ*, 825:113, July 2016. doi: 10.3847/0004-637X/825/2/113.
- A. Dekel and A. Burkert. Wet disc contraction to galactic blue nuggets and quenching to red nuggets. *MNRAS*, 438:1870–1879, Feb. 2014. doi: 10.1093/mnras/stt2331.

- B. Diemer, M. Sparre, L. E. Abramson, and P. Torrey. Log-normal Star Formation Histories in Simulated and Observed Galaxies. *ApJ*, 839:26, Apr. 2017. doi: 10.3847/1538-4357/aa68e5.
- J. Donas, J.-M. Deharveng, R. M. Rich, S. K. Yi, Y.-W. Lee, A. Boselli, A. Gil de Paz, S. Boissier, S. Charlot, S. Salim, L. Bianchi, T. A. Barlow, K. Forster, P. G. Friedman, T. M. Heckman, B. F. Madore, D. C. Martin, B. Milliard, P. Morrissey, S. G. Neff, D. Schiminovich, M. Seibert, T. Small, A. S. Szalay, B. Y. Welsh, and T. K. Wyder. GALEX UV Color Relations for Nearby Early-Type Galaxies. *ApJS*, 173:597–606, Dec. 2007. doi: 10.1086/516643.
- A. Dressler and J. E. Gunn. Spectroscopy of galaxies in distant clusters. II - The population of the 3C 295 cluster. *ApJ*, 270:7–19, July 1983. doi: 10.1086/161093.
- A. Dressler, I. Smail, B. M. Poggianti, H. Butcher, W. J. Couch, R. S. Ellis, and A. Oemler, Jr. A Spectroscopic Catalog of 10 Distant Rich Clusters of Galaxies. *ApJS*, 122:51–80, May 1999. doi: 10.1086/313213.
- A. Dressler, A. Oemler, Jr., B. M. Poggianti, M. D. Gladders, L. Abramson, and B. Vulcani. The IMACS Cluster Building Survey. II. Spectral Evolution of Galaxies in the Epoch of Cluster Assembly. *ApJ*, 770:62, June 2013. doi: 10.1088/0004-637X/770/1/62.
- J. J. Fang, S. M. Faber, D. C. Koo, and A. Dekel. A Link between Star Formation Quenching and Inner Stellar Mass Density in Sloan Digital Sky Survey Central Galaxies. *ApJ*, 776:63, Oct. 2013. doi: 10.1088/0004-637X/776/1/63.
- K. Finlator, R. Davé, and B. D. Oppenheimer. Constraints on physical properties of $z \sim 6$ galaxies using cosmological hydrodynamic simulations. *MNRAS*, 376: 1861–1878, Apr. 2007. doi: 10.1111/j.1365-2966.2007.11578.x.
- D. Foreman-Mackey, D. W. Hogg, D. Lang, and J. Goodman. emcee: The MCMC Hammer. *PASP*, 125:306, Mar. 2013. doi: 10.1086/670067.
- D. Foreman-Mackey, J. Sick, and B. Johnson. python-fsps: Python bindings to fsps (v0.1.1). Oct. 2014. doi: 10.5281/zenodo.12157. URL <https://doi.org/10.5281/zenodo.12157>.
- M. Franx, P. G. van Dokkum, N. M. Förster Schreiber, S. Wuyts, I. Labbé, and S. Toft. Structure and Star Formation in Galaxies out to $z = 3$: Evidence for Surface Density Dependent Evolution and Upsizing. *ApJ*, 688:770-788, Dec. 2008. doi: 10.1086/592431.
- P. Franzetti, M. Scodreggio, B. Garilli, D. Vergani, D. Maccagni, L. Guzzo, L. Tresse, O. Ilbert, F. Lamareille, T. Contini, O. Le Fèvre, G. Zamorani, J. Brinchmann, S. Charlot, D. Bottini, V. Le Brun, J. P. Picat, R. Scaramella, G. Vettolani, A. Zanichelli, C. Adami, S. Arnouts, S. Bardelli, M. Bolzonella, A. Cappi,

- P. Ciliegi, S. Foucaud, I. Gavignaud, A. Iovino, H. J. McCracken, B. Marano, C. Marinoni, A. Mazure, B. Meneux, R. Merighi, S. Paltani, R. Pellò, A. Pollo, L. Pozzetti, M. Radovich, E. Zucca, O. Cucciati, and C. J. Walcher. The VIMOS-VLT deep survey. Color bimodality and the mix of galaxy populations up to $z \sim 2$. *A&A*, 465:711–723, Apr. 2007. doi: 10.1051/0004-6361:20065942.
- J. M. Gabor, R. Davé, K. Finlator, and B. D. Oppenheimer. How is star formation quenched in massive galaxies? *MNRAS*, 407:749–771, Sept. 2010. doi: 10.1111/j.1365-2966.2010.16961.x.
- A. Gallazzi, S. Charlot, J. Brinchmann, S. D. M. White, and C. A. Tremonti. The ages and metallicities of galaxies in the local universe. *MNRAS*, 362:41–58, Sept. 2005. doi: 10.1111/j.1365-2966.2005.09321.x.
- A. Gallazzi, E. F. Bell, S. Zibetti, J. Brinchmann, and D. D. Kelson. Charting the Evolution of the Ages and Metallicities of Massive Galaxies since $z = 0.7$. *ApJ*, 788:72, June 2014. doi: 10.1088/0004-637X/788/1/72.
- M. Geha, T. M. Brown, J. Tumlinson, J. S. Kalirai, J. D. Simon, E. N. Kirby, D. A. Vandenberg, R. R. Muñoz, R. J. Avila, P. Guhathakurta, and H. C. Ferguson. The Stellar Initial Mass Function of Ultra-faint Dwarf Galaxies: Evidence for IMF Variations with Galactic Environment. *ApJ*, 771:29, July 2013. doi: 10.1088/0004-637X/771/1/29.
- S. Genel, M. Vogelsberger, V. Springel, D. Sijacki, D. Nelson, G. Snyder, V. Rodriguez-Gomez, P. Torrey, and L. Hernquist. Introducing the Illustris project: the evolution of galaxy populations across cosmic time. *MNRAS*, 445:175–200, Nov. 2014. doi: 10.1093/mnras/stu1654.
- L. Girardi, A. Bressan, G. Bertelli, and C. Chiosi. Evolutionary tracks and isochrones for low- and intermediate-mass stars: From 0.15 to 7 M_{sun} , and from $Z=0.0004$ to 0.03. *A&AS*, 141:371–383, Feb. 2000. doi: 10.1051/aas:2000126.
- M. D. Gladders, A. Oemler, A. Dressler, B. Poggianti, B. Vulcani, and L. Abramson. The IMACS Cluster Building Survey. IV. The Log-normal Star Formation History of Galaxies. *ApJ*, 770:64, June 2013. doi: 10.1088/0004-637X/770/1/64.
- J. Goodman and J. Weare. Ensemble samplers with affine invariance. *Communications in Applied Mathematics and Computational Science*, Vol. 5, No. 1, p. 65-80, 2010, 5:65–80, 2010. doi: 10.2140/camcos.2010.5.65.
- T. Goto. 266 E+A galaxies selected from the Sloan Digital Sky Survey Data Release 2: the origin of E+A galaxies. *MNRAS*, 357:937–944, Mar. 2005. doi: 10.1111/j.1365-2966.2005.08701.x.
- T. Goto. Post-starburst-active galactic nucleus connection: spatially resolved spectroscopy of H δ -strong active galactic nuclei. *MNRAS*, 369:1765–1772, July 2006. doi: 10.1111/j.1365-2966.2006.10413.x.

- G. J. Graves, S. M. Faber, and R. P. Schiavon. Dissecting the Red Sequence. II. Star Formation Histories of Early-Type Galaxies Throughout the Fundamental Plane. *ApJ*, 698:1590–1608, June 2009. doi: 10.1088/0004-637X/698/2/1590.
- L. Guzzo, M. Scodreggio, B. Garilli, B. R. Granett, A. Fritz, U. Abbas, C. Adami, S. Arnouts, J. Bel, M. Bolzonella, D. Bottini, E. Branchini, A. Cappi, J. Coupon, O. Cucciati, I. Davidzon, G. De Lucia, S. de la Torre, P. Franzetti, M. Fumana, P. Hudelot, O. Ilbert, A. Iovino, J. Krywult, V. Le Brun, O. Le Fèvre, D. Maccagni, K. Małek, F. Marulli, H. J. McCracken, L. Paioro, J. A. Peacock, M. Polletta, A. Pollo, H. Schlegelhauser, L. A. M. Tasca, R. Tojeiro, D. Vergani, G. Zamorani, A. Zanichelli, A. Burden, C. Di Porto, A. Marchetti, C. Marinoni, Y. Mellier, L. Moscardini, R. C. Nichol, W. J. Percival, S. Phleps, and M. Wolk. The VIMOS Public Extragalactic Redshift Survey (VIPERS). An unprecedented view of galaxies and large-scale structure at $0.5 < z < 1.2$. *A&A*, 566:A108, June 2014. doi: 10.1051/0004-6361/201321489.
- A. F. Heavens, R. Jimenez, and O. Lahav. Massive lossless data compression and multiple parameter estimation from galaxy spectra. *MNRAS*, 317:965–972, Oct. 2000. doi: 10.1046/j.1365-8711.2000.03692.x.
- T. M. Heckman and P. N. Best. The Coevolution of Galaxies and Supermassive Black Holes: Insights from Surveys of the Contemporary Universe. *ARA&A*, 52: 589–660, Aug. 2014. doi: 10.1146/annurev-astro-081913-035722.
- A. R. Hill, A. van der Wel, M. Franx, A. Muzzin, R. E. Skelton, I. Momcheva, P. van Dokkum, and K. E. Whitaker. High-redshift Massive Quiescent Galaxies Are as Flat as Star-forming Galaxies: The Flattening of Galaxies and the Correlation with Structural Properties in CANDELS/3D-HST. *ApJ*, 871:76, Jan. 2019. doi: 10.3847/1538-4357/aaf50a.
- J. Huchra, M. Davis, D. Latham, and J. Tonry. A survey of galaxy redshifts. IV - The data. *ApJS*, 52:89–119, June 1983. doi: 10.1086/190860.
- H. J. Ibarra-Medel, S. F. Sánchez, V. Avila-Reese, H. M. Hernández-Toledo, J. J. González, N. Drory, K. Bundy, D. Bizyaev, M. Cano-Díaz, E. Malanushenko, K. Pan, A. Roman-Lopes, and D. Thomas. SDSS IV MaNGA: the global and local stellar mass assembly histories of galaxies. *MNRAS*, 463:2799–2818, Dec. 2016. doi: 10.1093/mnras/stw2126.
- K. Iyer and E. Gawiser. Reconstruction of Galaxy Star Formation Histories through SED Fitting: The Dense Basis Approach. *ApJ*, 838:127, Apr. 2017. doi: 10.3847/1538-4357/aa63f0.
- I. Jørgensen and K. Chiboucas. Stellar Populations and Evolution of Early-type Cluster Galaxies: Constraints from Optical Imaging and Spectroscopy of $z = 0.5$ - 0.9 Galaxy Clusters. *AJ*, 145:77, Mar. 2013. doi: 10.1088/0004-6256/145/3/77.

- I. Jørgensen, K. Chiboucas, E. Berkson, O. Smith, M. Takamiya, and A. Villaume. Galaxy Populations in Massive $z = 0.2 - 0.9$ Clusters. I. Analysis of Spectroscopy. *AJ*, 154:251, Dec. 2017. doi: 10.3847/1538-3881/aa96a3.
- S. Juneau, K. Glazebrook, D. Crampton, P. J. McCarthy, S. Savaglio, R. Abraham, R. G. Carlberg, H.-W. Chen, D. Le Borgne, R. O. Marzke, K. Roth, I. Jørgensen, I. Hook, and R. Murowinski. Cosmic Star Formation History and Its Dependence on Galaxy Stellar Mass. *ApJL*, 619:L135–L138, Feb. 2005. doi: 10.1086/427937.
- A. Karim, E. Schinnerer, A. Martínez-Sansigre, M. T. Sargent, A. van der Wel, H.-W. Rix, O. Ilbert, V. Smolčić, C. Carilli, M. Pannella, A. M. Koekemoer, E. F. Bell, and M. Salvato. The Star Formation History of Mass-selected Galaxies in the COSMOS Field. *ApJ*, 730:61, Apr. 2011. doi: 10.1088/0004-637X/730/2/61.
- G. Kauffmann, T. M. Heckman, S. D. M. White, S. Charlot, C. Tremonti, E. W. Peng, M. Seibert, J. Brinkmann, R. C. Nichol, M. SubbaRao, and D. York. The dependence of star formation history and internal structure on stellar mass for 10^5 low-redshift galaxies. *MNRAS*, 341:54–69, May 2003. doi: 10.1046/j.1365-8711.2003.06292.x.
- S. Kaviraj, L. A. Kirkby, J. Silk, and M. Sarzi. The UV properties of E+A galaxies: constraints on feedback-driven quenching of star formation. *MNRAS*, 382:960–970, Dec. 2007. doi: 10.1111/j.1365-2966.2007.12475.x.
- S. Kaviraj, S. Peirani, S. Khochfar, J. Silk, and S. Kay. The role of minor mergers in the recent star formation history of early-type galaxies. *MNRAS*, 394:1713–1720, Apr. 2009. doi: 10.1111/j.1365-2966.2009.14403.x.
- A. A. Khostovan, D. Sobral, B. Mobasher, P. N. Best, I. Smail, J. P. Stott, S. Hemmati, and H. Nayyeri. Evolution of the $H\beta + [O\ III]$ and $[O\ II]$ luminosity functions and the $[O\ II]$ star formation history of the Universe up to $z \sim 5$ from HiZELS. *MNRAS*, 452:3948–3968, Oct. 2015. doi: 10.1093/mnras/stv1474.
- M. Koleva, P. Prugniel, A. Bouchard, and Y. Wu. ULySS: a full spectrum fitting package. *A&A*, 501:1269–1279, July 2009. doi: 10.1051/0004-6361/200811467.
- J. Kormendy and L. C. Ho. Coevolution (Or Not) of Supermassive Black Holes and Host Galaxies. *ARA&A*, 51:511–653, Aug. 2013. doi: 10.1146/annurev-astro-082708-101811.
- M. Kriek, P. G. van Dokkum, I. Labbé, M. Franx, G. D. Illingworth, D. Marchesini, and R. F. Quadri. An Ultra-Deep Near-Infrared Spectrum of a Compact Quiescent Galaxy at $z = 2.2$. *ApJ*, 700:221–231, July 2009. doi: 10.1088/0004-637X/700/1/221.
- M. Kriek, A. E. Shapley, N. A. Reddy, B. Siana, A. L. Coil, B. Mobasher, W. R. Freeman, L. de Groot, S. H. Price, R. Sanders, I. Shivaeei, G. B. Brammer, I. G.

- Momcheva, R. E. Skelton, P. G. van Dokkum, K. E. Whitaker, J. Aird, M. Azadi, M. Kassis, J. S. Bullock, C. Conroy, R. Davé, D. Kereš, and M. Krumholz. The MOSFIRE Deep Evolution Field (MOSDEF) Survey: Rest-frame Optical Spectroscopy for ~ 1500 H-selected Galaxies at $1.37 < z < 3.8$. *ApJS*, 218:15, June 2015. doi: 10.1088/0067-0049/218/2/15.
- M. Kriek, C. Conroy, P. G. van Dokkum, A. E. Shapley, J. Choi, N. A. Reddy, B. Siana, F. van de Voort, A. L. Coil, and B. Mobasher. A massive, quiescent, population II galaxy at a redshift of 2.1. *Nature*, 540:248–251, Dec. 2016. doi: 10.1038/nature20570.
- P. Kroupa, S. Aarseth, and J. Hurley. The formation of a bound star cluster: from the Orion nebula cluster to the Pleiades. *MNRAS*, 321:699–712, Mar. 2001. doi: 10.1046/j.1365-8711.2001.04050.x.
- O. Le Fèvre, P. Cassata, O. Cucciati, B. Garilli, O. Ilbert, V. Le Brun, D. Maccagni, C. Moreau, M. Scodeggio, L. Tresse, G. Zamorani, C. Adami, S. Arnouts, S. Bardelli, M. Bolzonella, M. Bondi, A. Bongiorno, D. Bottini, A. Cappi, S. Charlot, P. Ciliegi, T. Contini, S. de la Torre, S. Foucaud, P. Franzetti, I. Gavignaud, L. Guzzo, A. Iovino, B. Lemaux, C. López-Sanjuan, H. J. McCracken, B. Marano, C. Marinoni, A. Mazure, Y. Mellier, R. Merighi, P. Merluzzi, S. Paltani, R. Pellò, A. Pollo, L. Pozzetti, R. Scaramella, L. Tasca, D. Vergani, G. Vettolani, A. Zanichelli, and E. Zucca. The VIMOS VLT Deep Survey final data release: a spectroscopic sample of 35 016 galaxies and AGN out to $z \sim 6.7$ selected with $17.5 \leq i_{AB} \leq 24.75$. *A&A*, 559:A14, Nov. 2013. doi: 10.1051/0004-6361/201322179.
- B. Lee, M. Giavalisco, C. C. Williams, Y. Guo, J. Lotz, A. Van der Wel, H. C. Ferguson, S. M. Faber, A. Koekemoer, N. Grogin, D. Kocevski, C. J. Conselice, S. Wuyts, A. Dekel, J. Kartaltepe, and E. F. Bell. CANDELS: The Correlation between Galaxy Morphology and Star Formation Activity at $z \sim 2$. *ApJ*, 774:47, Sept. 2013. doi: 10.1088/0004-637X/774/1/47.
- S. N. Leitner. On the Last 10 Billion Years of Stellar Mass Growth in Star-forming Galaxies. *ApJ*, 745:149, Feb. 2012. doi: 10.1088/0004-637X/745/2/149.
- J. Leja, P. van Dokkum, and M. Franx. Tracing Galaxies through Cosmic Time with Number Density Selection. *ApJ*, 766:33, Mar. 2013. doi: 10.1088/0004-637X/766/1/33.
- T. Lejeune, F. Cuisinier, and R. Buser. Standard stellar library for evolutionary synthesis. I. Calibration of theoretical spectra. *A&AS*, 125:229–246, Oct. 1997. doi: 10.1051/aas:1997373.
- T. Lejeune, F. Cuisinier, and R. Buser. A standard stellar library for evolutionary synthesis. II. The M dwarf extension. *A&AS*, 130:65–75, May 1998. doi: 10.1051/aas:1998405.

- S. J. Lilly, O. Le Fevre, F. Hammer, and D. Crampton. The Canada-France Redshift Survey: The Luminosity Density and Star Formation History of the Universe to Z approximately 1. *ApJL*, 460:L1, Mar. 1996. doi: 10.1086/309975.
- S. J. Lilly, O. Le Fèvre, A. Renzini, G. Zamorani, M. Scodreggio, T. Contini, C. M. Carollo, G. Hasinger, J.-P. Kneib, A. Iovino, V. Le Brun, C. Maier, V. Mainieri, M. Mignoli, J. Silverman, L. A. M. Tasca, M. Bolzonella, A. Bongiorno, D. Bottini, P. Capak, K. Caputi, A. Cimatti, O. Cucciati, E. Daddi, R. Feldmann, P. Franzetti, B. Garilli, L. Guzzo, O. Ilbert, P. Kampeczyk, K. Kovac, F. Lamareille, A. Leauthaud, J.-F. Le Borgne, H. J. McCracken, C. Marinoni, R. Pello, E. Ricciardelli, C. Scarlata, D. Vergani, D. B. Sanders, E. Schinnerer, N. Scoville, Y. Taniguchi, S. Arnouts, H. Aussel, S. Bardelli, M. Brusa, A. Cappi, P. Ciliegi, A. Finoguenov, S. Foucaud, A. Franceschini, C. Halliday, C. Impey, C. Knobel, A. Koekemoer, J. Kurk, D. Maccagni, S. Maddox, B. Marano, G. Marconi, B. Meneux, B. Mobasher, C. Moreau, J. A. Peacock, C. Porciani, L. Pozzetti, R. Scaramella, D. Schiminovich, P. Shopbell, I. Smail, D. Thompson, L. Tresse, G. Vettolani, A. Zanichelli, and E. Zucca. zCOSMOS: A Large VLT/VIMOS Redshift Survey Covering $0 < z < 3$ in the COSMOS Field. *ApJS*, 172:70–85, Sept. 2007. doi: 10.1086/516589.
- P. Madau and M. Dickinson. Cosmic Star-Formation History. *ARA&A*, 52:415–486, Aug. 2014. doi: 10.1146/annurev-astro-081811-125615.
- C. Maraston, G. Strömbäck, D. Thomas, D. A. Wake, and R. C. Nichol. Modelling the colour evolution of luminous red galaxies - improvements with empirical stellar spectra. *MNRAS*, 394:L107–L111, Mar. 2009. doi: 10.1111/j.1745-3933.2009.00621.x.
- P. Marigo and L. Girardi. Evolution of asymptotic giant branch stars. I. Updated synthetic TP-AGB models and their basic calibration. *A&A*, 469:239–263, July 2007. doi: 10.1051/0004-6361:20066772.
- P. Marigo, L. Girardi, A. Bressan, M. A. T. Groenewegen, L. Silva, and G. L. Granato. Evolution of asymptotic giant branch stars. II. Optical to far-infrared isochrones with improved TP-AGB models. *A&A*, 482:883–905, May 2008. doi: 10.1051/0004-6361:20078467.
- A. Marino, E. Iodice, R. Tantalo, L. Piovan, D. Bettoni, L. M. Buson, C. Chiosi, G. Galletta, R. Rampazzo, and R. M. Rich. GALEX UV properties of the polar ring galaxy MCG-05-07-001 and the shell galaxies NGC 1210 and NGC 5329. *A&A*, 508:1235–1252, Dec. 2009. doi: 10.1051/0004-6361/200911819.
- M. Martig, F. Bournaud, R. Teyssier, and A. Dekel. Morphological Quenching of Star Formation: Making Early-Type Galaxies Red. *ApJ*, 707:250–267, Dec. 2009. doi: 10.1088/0004-637X/707/1/250.

- I. G. McCarthy, C. S. Frenk, A. S. Font, C. G. Lacey, R. G. Bower, N. L. Mitchell, M. L. Balogh, and T. Theuns. Ram pressure stripping the hot gaseous haloes of galaxies in groups and clusters. *MNRAS*, 383:593–605, Jan. 2008. doi: 10.1111/j.1365-2966.2007.12577.x.
- R. M. McDermid, K. Alatalo, L. Blitz, F. Bournaud, M. Bureau, M. Cappellari, A. F. Crocker, R. L. Davies, T. A. Davis, P. T. de Zeeuw, P.-A. Duc, E. Emsellem, S. Khochfar, D. Krajnović, H. Kuntschner, R. Morganti, T. Naab, T. Oosterloo, M. Sarzi, N. Scott, P. Serra, A.-M. Weijmans, and L. M. Young. The ATLAS^{3D} Project - XXX. Star formation histories and stellar population scaling relations of early-type galaxies. *MNRAS*, 448:3484–3513, Apr. 2015. doi: 10.1093/mnras/stv105.
- M. Mosleh, S. Tacchella, A. Renzini, C. M. Carollo, A. Molaeinezhad, M. Onodera, H. G. Khosroshahi, and S. Lilly. Connection between Stellar Mass Distributions within Galaxies and Quenching Since $z = 2$. *ApJ*, 837:2, Mar. 2017. doi: 10.3847/1538-4357/aa5f14.
- J. Moustakas, A. L. Coil, J. Aird, M. R. Blanton, R. J. Cool, D. J. Eisenstein, A. J. Mendez, K. C. Wong, G. Zhu, and S. Arnouts. PRIMUS: Constraints on Star Formation Quenching and Galaxy Merging, and the Evolution of the Stellar Mass Function from $z = 0$ -1. *ApJ*, 767:50, Apr. 2013. doi: 10.1088/0004-637X/767/1/50.
- A. Muzzin, D. Marchesini, M. Stefanon, M. Franx, H. J. McCracken, B. Milvang-Jensen, J. S. Dunlop, J. P. U. Fynbo, G. Brammer, I. Labbé, and P. G. van Dokkum. The Evolution of the Stellar Mass Functions of Star-forming and Quiescent Galaxies to $z = 4$ from the COSMOS/UltraVISTA Survey. *ApJ*, 777:18, Nov. 2013a. doi: 10.1088/0004-637X/777/1/18.
- A. Muzzin, D. Marchesini, M. Stefanon, M. Franx, B. Milvang-Jensen, J. S. Dunlop, J. P. U. Fynbo, G. Brammer, I. Labbé, and P. van Dokkum. A Public K_s - selected Catalog in the COSMOS/ULTRAVISTA Field: Photometry, Photometric Redshifts, and Stellar Population Parameters. *ApJS*, 206:8, May 2013b. doi: 10.1088/0067-0049/206/1/8.
- J. A. Newman, M. C. Cooper, M. Davis, S. M. Faber, A. L. Coil, P. Guhathakurta, D. C. Koo, A. C. Phillips, C. Conroy, A. A. Dutton, D. P. Finkbeiner, B. F. Gerke, D. J. Rosario, B. J. Weiner, C. N. A. Willmer, R. Yan, J. J. Harker, S. A. Kassin, N. P. Konidaris, K. Lai, D. S. Madgwick, K. G. Noeske, G. D. Wirth, A. J. Connolly, N. Kaiser, E. N. Kirby, B. C. Lemaux, L. Lin, J. M. Lotz, G. A. Luppino, C. Marinoni, D. J. Matthews, A. Metevier, and R. P. Schiavon. The DEEP2 Galaxy Redshift Survey: Design, Observations, Data Reduction, and Redshifts. *ApJS*, 208:5, Sept. 2013. doi: 10.1088/0067-0049/208/1/5.
- P. Ocvirk, C. Pichon, A. Lançon, and E. Thiébaud. STECMAP: STELLAR Content from high-resolution galactic spectra via Maximum A Posteriori. *MNRAS*, 365: 46–73, Jan. 2006. doi: 10.1111/j.1365-2966.2005.09182.x.

- P. A. Oesch, G. Brammer, P. G. van Dokkum, G. D. Illingworth, R. J. Bouwens, I. Labbé, M. Franx, I. Momcheva, M. L. N. Ashby, G. G. Fazio, V. Gonzalez, B. Holden, D. Magee, R. E. Skelton, R. Smit, L. R. Spitler, M. Trenti, and S. P. Willner. A Remarkably Luminous Galaxy at $z=11.1$ Measured with Hubble Space Telescope Grism Spectroscopy. *ApJ*, 819:129, Mar. 2016. doi: 10.3847/0004-637X/819/2/129.
- M. Onodera, C. M. Carollo, A. Renzini, M. Cappellari, C. Mancini, N. Arimoto, E. Daddi, R. Gobat, V. Strazzullo, S. Tacchella, and Y. Yamada. The Ages, Metallicities, and Element Abundance Ratios of Massive Quenched Galaxies at $z > 1.6$. *ApJ*, 808:161, Aug. 2015. doi: 10.1088/0004-637X/808/2/161.
- T. Oosterloo, R. Morganti, A. Crocker, E. Jütte, M. Cappellari, T. de Zeeuw, D. Krajnović, R. McDermid, H. Kuntschner, M. Sarzi, and A.-M. Weijmans. Early-type galaxies in different environments: an HI view. *MNRAS*, 409:500–514, Dec. 2010. doi: 10.1111/j.1365-2966.2010.17351.x.
- C. Pacifici, S. A. Kassin, B. J. Weiner, B. Holden, J. P. Gardner, S. M. Faber, H. C. Ferguson, D. C. Koo, J. R. Primack, E. F. Bell, A. Dekel, E. Gawiser, M. Giavalisco, M. Rafelski, R. C. Simons, G. Barro, D. J. Croton, R. Davé, A. Fontana, N. A. Grogin, A. M. Koekemoer, S.-K. Lee, B. Salmon, R. Somerville, and P. Behroozi. The Evolution of Star Formation Histories of Quiescent Galaxies. *ApJ*, 832:79, Nov. 2016. doi: 10.3847/0004-637X/832/1/79.
- V. Pandya, R. Brennan, R. S. Somerville, E. Choi, G. Barro, S. Wuyts, E. N. Taylor, P. Behroozi, A. Kirkpatrick, S. M. Faber, J. Primack, D. C. Koo, D. H. McIntosh, D. Kocevski, E. F. Bell, A. Dekel, J. J. Fang, H. C. Ferguson, N. Grogin, A. M. Koekemoer, Y. Lu, K. Mantha, B. Mobasher, J. Newman, C. Pacifici, C. Papovich, A. van der Wel, and H. M. Yesuf. The nature of massive transition galaxies in CANDELS, GAMA and cosmological simulations. *MNRAS*, 472:2054–2084, Dec. 2017. doi: 10.1093/mnras/stx2027.
- C. Papovich, S. L. Finkelstein, H. C. Ferguson, J. M. Lotz, and M. Giavalisco. The rising star formation histories of distant galaxies and implications for gas accretion with time. *MNRAS*, 412:1123–1136, Apr. 2011. doi: 10.1111/j.1365-2966.2010.17965.x.
- S. G. Patel, M. Fumagalli, M. Franx, P. G. van Dokkum, A. van der Wel, J. Leja, I. Labbé, G. Brammer, R. E. Skelton, I. Momcheva, K. E. Whitaker, B. Lundgren, A. Muzzin, R. F. Quadri, E. J. Nelson, D. A. Wake, and H.-W. Rix. The Structural Evolution of Milky-Way-like Star-forming Galaxies since $z \sim 1.3$. *ApJ*, 778:115, Dec. 2013. doi: 10.1088/0004-637X/778/2/115.
- L. Pozzetti, M. Bolzonella, E. Zucca, G. Zamorani, S. Lilly, A. Renzini, M. Moresco, M. Mignoli, P. Cassata, L. Tasca, F. Lamareille, C. Maier, B. Meneux, C. Halliday, P. Oesch, D. Vergani, K. Caputi, K. Kovač, A. Cimatti, O. Cucciati,

- A. Iovino, Y. Peng, M. Carollo, T. Contini, J.-P. Kneib, O. Le Fèvre, V. Mainieri, M. Scodreggio, S. Bardelli, A. Bongiorno, G. Coppa, S. de la Torre, L. de Ravel, P. Franzetti, B. Garilli, P. Kampczyk, C. Knobel, J.-F. Le Borgne, V. Le Brun, R. Pellò, E. Perez Montero, E. Ricciardelli, J. D. Silverman, M. Tanaka, L. Tresse, U. Abbas, D. Bottini, A. Cappi, L. Guzzo, A. M. Koekemoer, A. Leauthaud, D. Maccagni, C. Marinoni, H. J. McCracken, P. Memeo, C. Porciani, R. Scaramella, C. Scarlata, and N. Scoville. zCOSMOS - 10k-bright spectroscopic sample. The bimodality in the galaxy stellar mass function: exploring its evolution with redshift. *A&A*, 523:A13, Nov. 2010. doi: 10.1051/0004-6361/200913020.
- K. Rowlands, T. Heckman, V. Wild, N. L. Zakamska, V. Rodriguez-Gomez, J. Barrera-Ballesteros, J. Lotz, D. Thilker, B. H. Andrews, M. Boquien, J. Brinkmann, J. R. Brownstein, H.-C. Hwang, and R. Smethurst. SDSS-IV MaNGA: spatially resolved star formation histories and the connection to galaxy physical properties. *MNRAS*, 480:2544–2561, Oct. 2018. doi: 10.1093/mnras/sty1916.
- E. E. Salpeter. The Luminosity Function and Stellar Evolution. *ApJ*, 121:161, Jan. 1955. doi: 10.1086/145971.
- P. Sánchez-Blázquez, R. F. Peletier, J. Jiménez-Vicente, N. Cardiel, A. J. Cenarro, J. Falcón-Barroso, J. Gorgas, S. Selam, and A. Vazdekis. Medium-resolution Isaac Newton Telescope library of empirical spectra. *MNRAS*, 371:703–718, Sept. 2006. doi: 10.1111/j.1365-2966.2006.10699.x.
- K. Schawinski, S. Kaviraj, S. Khochfar, S.-J. Yoon, S. K. Yi, J.-M. Deharveng, A. Boselli, T. Barlow, T. Conrow, K. Forster, P. G. Friedman, D. C. Martin, P. Morrissey, S. Neff, D. Schiminovich, M. Seibert, T. Small, T. Wyder, L. Bianchi, J. Donas, T. Heckman, Y.-W. Lee, B. Madore, B. Milliard, R. M. Rich, and A. Szalay. The Effect of Environment on the Ultraviolet Color-Magnitude Relation of Early-Type Galaxies. *ApJS*, 173:512–523, Dec. 2007. doi: 10.1086/516631.
- R. P. Schiavon, S. M. Faber, N. Konidaris, G. Graves, C. N. A. Willmer, B. J. Weiner, A. L. Coil, M. C. Cooper, M. Davis, J. Harker, D. C. Koo, J. A. Newman, and R. Yan. The DEEP2 Galaxy Redshift Survey: Mean Ages and Metallicities of Red Field Galaxies at $z \sim 0.9$ from Stacked Keck DEIMOS Spectra. *ApJL*, 651:L93–L96, Nov. 2006. doi: 10.1086/509074.
- M. Schmidt. The Rate of Star Formation. *ApJ*, 129:243, Mar. 1959. doi: 10.1086/146614.
- V. Simha, D. H. Weinberg, C. Conroy, R. Dave, M. Fardal, N. Katz, and B. D. Oppenheimer. Parametrising Star Formation Histories. *arXiv e-prints*, Apr. 2014.
- J. S. Speagle, C. L. Steinhardt, P. L. Capak, and J. D. Silverman. A Highly Consistent Framework for the Evolution of the Star-Forming “Main Sequence” from $z \sim 0-6$. *ApJS*, 214:15, Oct. 2014. doi: 10.1088/0067-0049/214/2/15.

- J. Spilker, R. Bezanson, I. Barišić, E. Bell, C. d. P. Lagos, M. Maseda, A. Muzzin, C. Pacifici, D. Sobral, C. Straatman, A. van der Wel, P. van Dokkum, B. Weiner, K. Whitaker, C. C. Williams, and P.-F. Wu. Molecular Gas Contents and Scaling Relations for Massive, Passive Galaxies at Intermediate Redshifts from the LEGA-C Survey. *ApJ*, 860:103, June 2018. doi: 10.3847/1538-4357/aac438.
- C. C. Steidel, G. C. Rudie, A. L. Strom, M. Pettini, N. A. Reddy, A. E. Shapley, R. F. Trainor, D. K. Erb, M. L. Turner, N. P. Konidaris, K. R. Kulas, G. Mace, K. Matthews, and I. S. McLean. Strong Nebular Line Ratios in the Spectra of $z \sim 2$ -3 Star Forming Galaxies: First Results from KBSS-MOSFIRE. *ApJ*, 795:165, Nov. 2014. doi: 10.1088/0004-637X/795/2/165.
- C. M. S. Straatman, L. R. Spitler, R. F. Quadri, I. Labbé, K. Glazebrook, S. E. Persson, C. Papovich, K.-V. H. Tran, G. B. Brammer, M. Cowley, A. Tomczak, T. Nanayakkara, L. Alcorn, R. Allen, A. Broussard, P. van Dokkum, B. Forrest, J. van Houdt, G. G. Kacprzak, L. Kavinwanichakij, D. D. Kelson, J. Lee, P. J. McCarthy, N. Mehrrens, A. Monson, D. Murphy, G. Rees, V. Tilvi, and K. E. Whitaker. The FourStar Galaxy Evolution Survey (ZFOURGE): Ultraviolet to Far-infrared Catalogs, Medium-bandwidth Photometric Redshifts with Improved Accuracy, Stellar Masses, and Confirmation of Quiescent Galaxies to $z \sim 3.5$. *ApJ*, 830:51, Oct. 2016. doi: 10.3847/0004-637X/830/1/51.
- C. M. S. Straatman, A. van der Wel, R. Bezanson, C. Pacifici, A. Gallazzi, P.-F. Wu, K. Noeske, I. Barišić, E. F. Bell, G. B. Brammer, J. Calhau, P. Chauke, M. Franx, J. van Houdt, I. Labbé, M. V. Maseda, J. C. Muñoz-Mateos, A. Muzzin, J. van de Sande, D. Sobral, and J. S. Spilker. The Large Early Galaxy Astrophysics Census (LEGA-C) Data Release 2: Dynamical and Stellar Population Properties of $z \lesssim 1$ Galaxies in the COSMOS Field. *ApJS*, 239:27, Dec. 2018. doi: 10.3847/1538-4365/aac37a.
- I. Strateva, Ž. Ivezić, G. R. Knapp, V. K. Narayanan, M. A. Strauss, J. E. Gunn, R. H. Lupton, D. Schlegel, N. A. Bahcall, J. Brinkmann, R. J. Brunner, T. Budavári, I. Csabai, F. J. Castander, M. Doi, M. Fukugita, Z. Györy, M. Hamabe, G. Hennessy, T. Ichikawa, P. Z. Kunszt, D. Q. Lamb, T. A. McKay, S. Okamura, J. Racusin, M. Sekiguchi, D. P. Schneider, K. Shimasaku, and D. York. Color Separation of Galaxy Types in the Sloan Digital Sky Survey Imaging Data. *AJ*, 122:1861–1874, Oct. 2001. doi: 10.1086/323301.
- B. A. Terrazas, E. F. Bell, B. M. B. Henriques, S. D. M. White, A. Cattaneo, and J. Woo. Quiescence Correlates Strongly with Directly Measured Black Hole Mass in Central Galaxies. *ApJL*, 830:L12, Oct. 2016. doi: 10.3847/2041-8205/830/1/L12.
- D. Thomas, C. Maraston, R. Bender, and C. Mendes de Oliveira. The Epochs of Early-Type Galaxy Formation as a Function of Environment. *ApJ*, 621:673–694, Mar. 2005. doi: 10.1086/426932.

- D. Thomas, C. Maraston, K. Schawinski, M. Sarzi, and J. Silk. Environment and self-regulation in galaxy formation. *MNRAS*, 404:1775–1789, June 2010. doi: 10.1111/j.1365-2966.2010.16427.x.
- S. Toft, A. Gallazzi, A. Zirm, M. Wold, S. Zibetti, C. Grillo, and A. Man. Deep Absorption Line Studies of Quiescent Galaxies at $z \sim 2$: The Dynamical-mass-Size Relation and First Constraints on the Fundamental Plane. *ApJ*, 754:3, July 2012. doi: 10.1088/0004-637X/754/1/3.
- R. Tojeiro, A. F. Heavens, R. Jimenez, and B. Panter. Recovering galaxy star formation and metallicity histories from spectra using VESPA. *MNRAS*, 381: 1252–1266, Nov. 2007. doi: 10.1111/j.1365-2966.2007.12323.x.
- R. Tojeiro, S. Wilkins, A. F. Heavens, B. Panter, and R. Jimenez. A Public Catalog of Stellar Masses, Star Formation and Metallicity Histories, and Dust Content from the Sloan Digital Sky Survey using VESPA. *ApJS*, 185:1–19, Nov. 2009. doi: 10.1088/0067-0049/185/1/1.
- P. Torrey, S. Wellons, F. Machado, B. Griffen, D. Nelson, V. Rodriguez-Gomez, R. McKinnon, A. Pillepich, C.-P. Ma, M. Vogelsberger, V. Springel, and L. Hernquist. An analysis of the evolving comoving number density of galaxies in hydrodynamical simulations. *MNRAS*, 454:2770–2786, Dec. 2015. doi: 10.1093/mnras/stv1986.
- P. Torrey, S. Wellons, C.-P. Ma, P. F. Hopkins, and M. Vogelsberger. Forward and backward galaxy evolution in comoving cumulative number density space. *MNRAS*, 467:4872–4885, June 2017. doi: 10.1093/mnras/stx370.
- S. C. Trager, S. M. Faber, G. Worthey, and J. J. González. The Stellar Population Histories of Early-Type Galaxies. II. Controlling Parameters of the Stellar Populations. *AJ*, 120:165–188, July 2000. doi: 10.1086/301442.
- K.-V. H. Tran, M. Franx, G. D. Illingworth, P. van Dokkum, D. D. Kelson, and D. Magee. Field E+A Galaxies at Intermediate Redshifts ($0.3 < z < 1$). *ApJ*, 609:683–691, July 2004. doi: 10.1086/421237.
- T. Treu, R. S. Ellis, T. X. Liao, P. G. van Dokkum, P. Tozzi, A. Coil, J. Newman, M. C. Cooper, and M. Davis. The Assembly History of Field Spheroidals: Evolution of Mass-to-Light Ratios and Signatures of Recent Star Formation. *ApJ*, 633: 174–197, Nov. 2005. doi: 10.1086/444585.
- J. van de Sande, M. Kriek, M. Franx, P. G. van Dokkum, R. Bezanson, R. J. Bouwens, R. F. Quadri, H.-W. Rix, and R. E. Skelton. Stellar Kinematics of $z \sim 2$ Galaxies and the Inside-out Growth of Quiescent Galaxies. *ApJ*, 771:85, July 2013. doi: 10.1088/0004-637X/771/2/85.

- A. van der Wel, B. P. Holden, A. W. Zirm, M. Franx, A. Rettura, G. D. Illingworth, and H. C. Ford. Recent Structural Evolution of Early-Type Galaxies: Size Growth from $z = 1$ to $z = 0$. *ApJ*, 688:48-58, Nov. 2008. doi: 10.1086/592267.
- A. van der Wel, E. F. Bell, F. C. van den Bosch, A. Gallazzi, and H.-W. Rix. On the Size and Comoving Mass Density Evolution of Early-Type Galaxies. *ApJ*, 698:1232–1243, June 2009a. doi: 10.1088/0004-637X/698/2/1232.
- A. van der Wel, H.-W. Rix, B. P. Holden, E. F. Bell, and A. R. Robaina. Major Merging: The Way to Make a Massive, Passive Galaxy. *ApJL*, 706:L120–L123, Nov. 2009b. doi: 10.1088/0004-637X/706/1/L120.
- A. van der Wel, K. Noeske, R. Bezanson, C. Pacifici, A. Gallazzi, M. Franx, J. C. Muñoz-Mateos, E. F. Bell, G. Brammer, S. Charlot, P. Chauké, I. Labbé, M. V. Maseda, A. Muzzin, H.-W. Rix, D. Sobral, J. van de Sande, P. G. van Dokkum, V. Wild, and C. Wolf. The VLT LEGA-C Spectroscopic Survey: The Physics of Galaxies at a Lookback Time of 7 Gyr. *ApJS*, 223:29, Apr. 2016. doi: 10.3847/0067-0049/223/2/29.
- P. G. van Dokkum and G. Brammer. Hubble Space Telescope WFC3 Grism Spectroscopy and Imaging of a Growing Compact Galaxy at $z = 1.9$. *ApJL*, 718:L73–L77, Aug. 2010. doi: 10.1088/2041-8205/718/2/L73.
- P. G. van Dokkum and M. Franx. The Fundamental Plane in CL 0024 at $z = 0.4$: implications for the evolution of the mass-to-light ratio. *MNRAS*, 281:985–1000, Aug. 1996. doi: 10.1093/mnras/281.3.985.
- P. G. van Dokkum, K. E. Whitaker, G. Brammer, M. Franx, M. Kriek, I. Labbé, D. Marchesini, R. Quadri, R. Bezanson, G. D. Illingworth, A. Muzzin, G. Rudnick, T. Tal, and D. Wake. The Growth of Massive Galaxies Since $z = 2$. *ApJ*, 709:1018–1041, Feb. 2010. doi: 10.1088/0004-637X/709/2/1018.
- P. G. van Dokkum, J. Leja, E. J. Nelson, S. Patel, R. E. Skelton, I. Momcheva, G. Brammer, K. E. Whitaker, B. Lundgren, M. Fumagalli, C. Conroy, N. Förster Schreiber, M. Franx, M. Kriek, I. Labbé, D. Marchesini, H.-W. Rix, A. van der Wel, and S. Wuyts. The Assembly of Milky-Way-like Galaxies Since $z \sim 2.5$. *ApJL*, 771:L35, July 2013. doi: 10.1088/2041-8205/771/2/L35.
- P. G. van Dokkum, R. Bezanson, A. van der Wel, E. J. Nelson, I. Momcheva, R. E. Skelton, K. E. Whitaker, G. Brammer, C. Conroy, N. M. Förster Schreiber, M. Fumagalli, M. Kriek, I. Labbé, J. Leja, D. Marchesini, A. Muzzin, P. Oesch, and S. Wuyts. Dense Cores in Galaxies Out to $z = 2.5$ in SDSS, UltraVISTA, and the Five 3D-HST/CANDELS Fields. *ApJ*, 791:45, Aug. 2014. doi: 10.1088/0004-637X/791/1/45.
- M. Vogelsberger, S. Genel, V. Springel, P. Torrey, D. Sijacki, D. Xu, G. Snyder, S. Bird, D. Nelson, and L. Hernquist. Properties of galaxies reproduced by a hydrodynamic simulation. *Nature*, 509:177–182, May 2014a. doi: 10.1038/nature13316.

- M. Vogelsberger, S. Genel, V. Springel, P. Torrey, D. Sijacki, D. Xu, G. Snyder, D. Nelson, and L. Hernquist. Introducing the Illustris Project: simulating the coevolution of dark and visible matter in the Universe. *MNRAS*, 444:1518–1547, Oct. 2014b. doi: 10.1093/mnras/stu1536.
- D. A. Wake, P. G. van Dokkum, and M. Franx. Revealing Velocity Dispersion as the Best Indicator of a Galaxy’s Color, Compared to Stellar Mass, Surface Mass Density, or Morphology. *ApJL*, 751:L44, June 2012. doi: 10.1088/2041-8205/751/2/L44.
- D. R. Weisz, J. J. Dalcanton, B. F. Williams, K. M. Gilbert, E. D. Skillman, A. C. Seth, A. E. Dolphin, K. B. W. McQuinn, S. M. Gogarten, J. Holtzman, K. Rosema, A. Cole, I. D. Karachentsev, and D. Zaritsky. The ACS Nearby Galaxy Survey Treasury. VIII. The Global Star Formation Histories of 60 Dwarf Galaxies in the Local Volume. *ApJ*, 739:5, Sept. 2011. doi: 10.1088/0004-637X/739/1/5.
- S. Wellons and P. Torrey. An improved probabilistic approach for linking progenitor and descendant galaxy populations using comoving number density. *MNRAS*, 467:3887–3897, June 2017. doi: 10.1093/mnras/stx358.
- S. Wellons, P. Torrey, C.-P. Ma, V. Rodriguez-Gomez, A. Pillepich, D. Nelson, S. Genel, M. Vogelsberger, and L. Hernquist. The diverse evolutionary paths of simulated high- z massive, compact galaxies to $z = 0$. *MNRAS*, 456:1030–1048, Feb. 2016. doi: 10.1093/mnras/stv2738.
- P. Westera, T. Lejeune, R. Buser, F. Cuisinier, and G. Bruzual. A standard stellar library for evolutionary synthesis. III. Metallicity calibration. *A&A*, 381:524–538, Jan. 2002. doi: 10.1051/0004-6361:20011493.
- K. E. Whitaker, I. Labbé, P. G. van Dokkum, G. Brammer, M. Kriek, D. Marchesini, R. F. Quadri, M. Franx, A. Muzzin, R. J. Williams, R. Bezanson, G. D. Illingworth, K.-S. Lee, B. Lundgren, E. J. Nelson, G. Rudnick, T. Tal, and D. A. Wake. The NEWFIRM Medium-band Survey: Photometric Catalogs, Redshifts, and the Bimodal Color Distribution of Galaxies out to $z \sim 3$. *ApJ*, 735:86, July 2011. doi: 10.1088/0004-637X/735/2/86.
- K. E. Whitaker, P. G. van Dokkum, G. Brammer, and M. Franx. The Star Formation Mass Sequence Out to $z = 2.5$. *ApJL*, 754:L29, Aug. 2012. doi: 10.1088/2041-8205/754/2/L29.
- K. E. Whitaker, P. G. van Dokkum, G. Brammer, I. G. Momcheva, R. Skelton, M. Franx, M. Kriek, I. Labbé, M. Fumagalli, B. F. Lundgren, E. J. Nelson, S. G. Patel, and H.-W. Rix. Quiescent Galaxies in the 3D-HST Survey: Spectroscopic Confirmation of a Large Number of Galaxies with Relatively Old Stellar Populations at $z \sim 2$. *ApJL*, 770:L39, June 2013. doi: 10.1088/2041-8205/770/2/L39.

- D. M. Wilkinson, C. Maraston, D. Thomas, L. Coccato, R. Tojeiro, M. Cappellari, F. Belfiore, M. Bershad, M. Blanton, K. Bundy, S. Cales, B. Cherinka, N. Drory, E. Emsellem, H. Fu, D. Law, C. Li, R. Maiolino, K. Masters, C. Tremonti, D. Wake, E. Wang, A.-M. Weijmans, T. Xiao, R. Yan, K. Zhang, D. Bizyaev, J. Brinkmann, K. Kinemuchi, E. Malanushenko, V. Malanushenko, D. Oravetz, K. Pan, and A. Simmons. P-MaNGA: full spectral fitting and stellar population maps from prototype observations. *MNRAS*, 449:328–360, May 2015. doi: 10.1093/mnras/stv301.
- G. Worthey. Comprehensive stellar population models and the disentanglement of age and metallicity effects. *ApJS*, 95:107–149, Nov. 1994. doi: 10.1086/192096.
- P.-F. Wu, A. van der Wel, A. Gallazzi, R. Bezanson, C. Pacifici, C. Straatman, M. Franx, I. Barišić, E. F. Bell, G. B. Brammer, J. Calhau, P. Chauke, J. van Houdt, M. V. Maseda, A. Muzzin, H.-W. Rix, D. Sobral, J. Spilker, J. van de Sande, P. van Dokkum, and V. Wild. Stellar populations of over 1000 $z \sim 0.8$ galaxies from lega-c: Ages and star formation histories from dn4000 and $h\delta$. *ApJ*, 855(2):85, 2018.
- C. Yamauchi, M. Yagi, and T. Goto. E+A and companion galaxies - I. A catalogue and statistics. *MNRAS*, 390:383–398, Oct. 2008. doi: 10.1111/j.1365-2966.2008.13756.x.
- S. K. Yi, S.-J. Yoon, S. Kaviraj, J.-M. Deharveng, R. M. Rich, S. Salim, A. Boselli, Y.-W. Lee, C. H. Ree, Y.-J. Sohn, S.-C. Rey, J.-W. Lee, J. Rhee, L. Bianchi, Y.-I. Byun, J. Donas, P. G. Friedman, T. M. Heckman, P. Jelinsky, B. F. Madore, R. Malina, D. C. Martin, B. Milliard, P. Morrissey, S. Neff, D. Schiminovich, O. Siegmund, T. Small, A. S. Szalay, M. J. Jee, S.-W. Kim, T. Barlow, K. Forster, B. Welsh, and T. K. Wyder. Galaxy Evolution Explorer Ultraviolet Color-Magnitude Relations and Evidence of Recent Star Formation in Early-Type Galaxies. *ApJL*, 619:L111–L114, Jan. 2005. doi: 10.1086/422811.
- D. G. York, J. Adelman, J. E. Anderson, Jr., S. F. Anderson, J. Annis, N. A. Bahcall, J. A. Bakken, R. Barkhouser, S. Bastian, E. Berman, W. N. Boroski, S. Bracker, C. Briegel, J. W. Briggs, J. Brinkmann, R. Brunner, S. Burles, L. Carey, M. A. Carr, F. J. Castander, B. Chen, P. L. Colestock, A. J. Connolly, J. H. Crocker, I. Csabai, P. C. Czarapata, J. E. Davis, M. Doi, T. Dombeck, D. Eisenstein, N. Ellman, B. R. Elms, M. L. Evans, X. Fan, G. R. Federwitz, L. Fiscelli, S. Friedman, J. A. Frieman, M. Fukugita, B. Gillespie, J. E. Gunn, V. K. Gurbani, E. de Haas, M. Haldeman, F. H. Harris, J. Hayes, T. M. Heckman, G. S. Hennessy, R. B. Hindsley, S. Holm, D. J. Holmgren, C.-h. Huang, C. Hull, D. Husby, S.-I. Ichikawa, T. Ichikawa, Ž. Ivezić, S. Kent, R. S. J. Kim, E. Kinney, M. Klaene, A. N. Kleinman, S. Kleinman, G. R. Knapp, J. Korienek, R. G. Kron, P. Z. Kunzst, D. Q. Lamb, B. Lee, R. F. Leger, S. Limmongkol, C. Lindenmeyer, D. C. Long, C. Loomis, J. Loveday, R. Lucinio, R. H. Lupton, B. MacKinnon, E. J.

- Mannery, P. M. Mantsch, B. Margon, P. McGehee, T. A. McKay, A. Meiksin, A. Merelli, D. G. Monet, J. A. Munn, V. K. Narayanan, T. Nash, E. Neilsen, R. Neswold, H. J. Newberg, R. C. Nichol, T. Nicinski, M. Nonino, N. Okada, S. Okamura, J. P. Ostriker, R. Owen, A. G. Pauls, J. Peoples, R. L. Peterson, D. Petravick, J. R. Pier, A. Pope, R. Pordes, A. Prosapio, R. Rechenmacher, T. R. Quinn, G. T. Richards, M. W. Richmond, C. H. Rivetta, C. M. Rockosi, K. Ruthmansdorfer, D. Sandford, D. J. Schlegel, D. P. Schneider, M. Sekiguchi, G. Sergey, K. Shimasaku, W. A. Siegmund, S. Smee, J. A. Smith, S. Snedden, R. Stone, C. Stoughton, M. A. Strauss, C. Stubbs, M. SubbaRao, A. S. Szalay, I. Szapudi, G. P. Szokoly, A. R. Thakar, C. Tremonti, D. L. Tucker, A. Uomoto, D. Vanden Berk, M. S. Vogeley, P. Waddell, S.-i. Wang, M. Watanabe, D. H. Weinberg, B. Yanny, N. Yasuda, and SDSS Collaboration. The Sloan Digital Sky Survey: Technical Summary. *AJ*, 120:1579–1587, Sept. 2000. doi: 10.1086/301513.
- A. Zolotov, A. Dekel, N. Mandelker, D. Tweed, S. Inoue, C. DeGraf, D. Ceverino, J. R. Primack, G. Barro, and S. M. Faber. Compaction and quenching of high- z galaxies in cosmological simulations: blue and red nuggets. *MNRAS*, 450:2327–2353, July 2015. doi: 10.1093/mnras/stv740.